Soil - Structure Interaction in Cohesionless Soils due to Monotonic Loading

Master's Thesis
M.Sc. in Structural and Civil Engineering
Aalborg University
Spring 2012

Åsmund Sjelmo

AALBORG UNIVERSITY
STUDENT REPORT

Aalborg University
Department of Civil Engineering
Sohngårdsholmsvej 57
Phone: 96 35 97 31
Fax: 98 13 63 93
http://www.bsn.aau.dk

Title: Soil - Structure Interaction in Cohesionless Soils due to Monotonic Loading

Project period: 1. February - 14. June, spring 2012

Author:

Åsmund Sjelmo

Supervisor: Prof. Lars Bo Ibsen

Copies printed: 4

Numbers of pages: 27

Numbers of pages Appendix: 74

Submitted: 14. June 2012

Preface

This Master's Thesis, *"Soil - Structure Interaction in Cohesionless Soils due to Monotonic Loading"*, is prepared and completed as a part of the 4th and final semester on the M.Sc. in Structural and Civil Engineering at Aalborg University. The period of which this report is written is from the 1st of February to the 14th of June, under the inspiring supervision of Professor Lars Bo Ibsen.

The author further wishes to express gratitude for help and support received concerning laboratory assignments, which forms the core of this Master's Thesis. This especially, but not exclusively, apply to Research Assistant Linas Mikalauskas, whose competence regarding laboratory equipment and general technical knowledge were decisive for execution of the experiments. Furthermore, for good counsel when confronted with technical obstructions, Assistant Engineer Kurt S. Sørensen, and the rest of the staff at the Geotechnical Enginering Laboratory at AAU is sincerely acknowledged.
Finally, the author also want to acknowledge PhD Fellow Aligi Foglia for exciting academical discussions, reading corrections, and generally showing commitment to the project.

Reading Guide

The outcome of this Master Thesis is presented in a final report, which comprises three parts: Part I contains a introduction with aim of thesis, and an enclosed article. Part II concerns description of experiment, presented in a number of appendices, A-E. Part III display gained results from all tests, appendices F and G. Enclosed with the report is a CD-ROM, where the appertaining calculations, raw data and extensional documents are to find.

The appendices are numbered by letters. Figures, tables and equations are presented with consecutive numbers in each article/appendix. The article is printed with individual page numbering, while the page numbering of the appendices are consecutive with the rest of the report. Figure and table numeration refers to which chapter the desired figure or table is located in. The article hold a separate bibliography, while the references for the entire report is located at the end of Part III.

Sources are quoted by the Harvard method of bibliography with the name of the author and year of publication inserted in brackets after the text. Quoted sources from literature will appear e.g [Sawin et al., 2011].
The bibliography is sorted alphabetically by notices, under which information about the source type, i.e.; author, title, publisher or editor, year of publication, presentation number, ISBN, URL and date of download is stated.

Summary

There is a general understanding in the international community that the emission of greenhouse gases needs to be reduced. One of the ways of achieving this reduction is to increase the use of renewable energy sources, such as wind power.

As the market becomes more aware of the advantages of moving wind turbines offshore, new design procedures must be developed and improved to further reduce the gap in total expenses between onshore and offshore installations.
This Master's Thesis is motivated by the effort to optimize the design process for bucket foundations. It represents a preliminary basis for the study regarding undrained response of the bucket foundation in cohesionless soils, due to rapid/impulsive loading from the design wave. The current procedure in determining capacity in Ultimate Limit State, comprises calculation with both drained and undrained states, where the response causing lowest capacity is selected for design. For cohesionless soils, this will in most cases be the drained capacity, even though it may lead to an excessively conservative design.

Four small-scale tests on a monotonically loaded bucket foundation is conducted to evaluate the relationships between loading velocity and generation of negative pore pressures. The tests are performed at different loading velocities, increased by a factor 10 for each test, starting at 0.01 mm/s for test 1 and ending at 10 mm/s for test 4. Loading is applied by an hydraulic piston, which is coupled with a load cell that record the force mobilized to maintain the prescribed loading velocity. The bucket applied has a height/diameter ratio of 0.5. 8 transducers are installed on the bucket, which reads the pore pressure development during loading. Horizontal and vertical displacement transducers record movement of the bucket during the test, which will be analyzed in light of the generation of negative pore pressures.

The results presented indicates a strong correlation between loading velocity and generation of negative pore pressures. This has a clear effect on the mobilized loading, hence capacity, which is confirmed by the corresponding displacements and rotations.

To get a preliminary understanding of the responses encountered; undrained, partly drained, or drained, the drainage time, t_{90}, was both calculated and measured. The results were inconsistent, and the conclusion must be that the drainage during loading should be investigated numerically in further studies of the current subject.

Table of Contents

Part I

Main Report

Chapter 1

Introduction

As the energy consumption across the world continues to expand, the necessity for green energy is ever increasing. Promoting the benefits of, and investing in, renewable energy has until recently been led by western countries. This trend has been reversed, as developing countries in Asia and Africa progressively increases their capacity in production and installation of renewable energy sources during the last years economical recession in Europe [Sawin et al., 2011]. This tendency is not exclusively due to environmental considerations, but possesses deeper social economic roots, acknowledging that the green energy market generate new industries and jobs [EWEA, 2010], as well as reduces the dependency of fossil and/or nuclear energy sources. This trend is both encouraging and imperative, considering that the future growth in energy demand is anticipated to transpire from developing countries.

One of the favored sources of renewable energy in Europe has during the past 20 years been wind generated power. The European Wind Energy Association (EWEA) annually releases reports tracking the development in production of, naturally, wind energy. Numbers presented in Wilkes et al. [2012] states that (valid for Europe):

- 28.4 % of the total installed power capacity since 2000 comes from wind energy
- 21.4 % of the total installed power capacity in 2011 came from wind power
- Renewable power installations accounted for 71.3 % of new installations during 2011
- Annual installations of wind power have increased steadily over the last 17 years from 814 MW in 1995 to 9,616 MW in 2011, an annual average market growth of 15.6 %
- The wind capacity installed by the end of 2011 would, in a normal year, produce 204 TWh of electricity, representing 6.3 % of electricity consumption - up from 5.3 % the year before
- Europe is the world leader in offshore wind with a cumulative capacity of 2,844 MW spread across 39 offshore wind farms in nine European countries.
- EWEA has a target of 40 GW of offshore wind in the EU by 2020, implying an average annual market growth of 28 % over the coming 12 years. (2009)

The main capacity in wind generated power are still produced onshore, but the market becomes more an more aware of the advantages gained by offshore production. These advantages are mainly that the wind conditions are better offshore, making it possible to harvest more energy per turbine. Also, energy consumption and demand is normally higher in densely populated areas, where the possibilities of installing onshore farms are limited. An additional advantage of moving wind farms offshore is the visual aspect.

The main reason for hesitation regarding planning and construction of offshore wind farms has been related to the cost. Or with a longer perspective; investment. Offshore generated capacity is still considered to be $\approx 50\%$ more expensive than onshore capacity [Krohn et al., 2009], throughout the turbines lifetime. As the wind energy production

offshore still is quite new, there should be much to gain by developing and optimizing the current designprocesses. One of these designprocesses could be regarding the foundation, which accounts for $\approx 25\%$ of the total cost of an installed wind turbine.

1.1 Foundation concepts

Several different foundation concepts for marine and offshore wind turbines are available for design. Which to choose needs to be evaluated based on several factors, where total lifetime cost governs the final decision. The site, or location of wind farm, will to a large extent determine the type of foundation applied. In terms of soil conditions; is it clay, sand or organic soils? Stiff/dense or soft/loose? Layered or uniform? Other factors could be; water depth, transportation from production site to installation site, loading condition from waves, currents, and wind. The way all these factors influence each other will form a basis for design, and lead to selection of the most advantageous foundation alternative. Figure 1.1 illustrates different foundational alternatives (Fig. 1.1a) show two concepts in one figure), some more common than others. What the figure does not reveal is that these foundation alternatives are suitable for different water depths. For instance, the gravity and monopile foundations are traditionally favored at shallower water, while the tripod and jacket better suit deeper water.

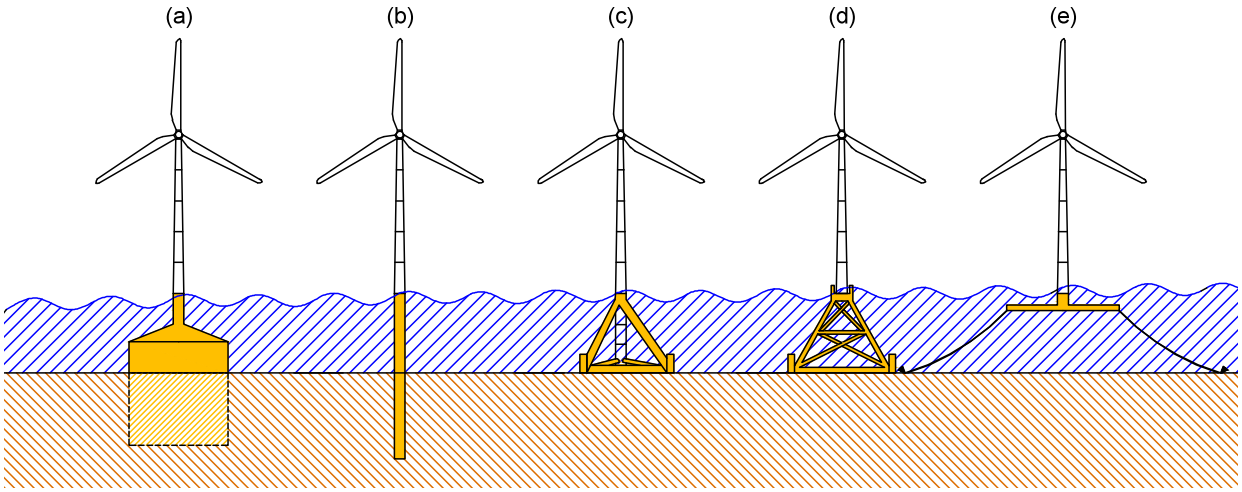

Figure 1.1: *Different foundation alternatives for offshore wind turbines. a) Gravity foundation above seabed and bucket foundation below. b) Monopile. c) Tripod. d) Jacket. e) Anchored foundation.*

The most common foundation concepts for offshore wind turbines have so far been the monopile and the gravity foundation. Monopiles are usually compiled of spliced hollow steel cylinders. They carry imposed loads by end bearing and shaft friction, and redistribute lateral loading to the surrounding soil. The strength properties of the upper soil layers will in many cases determine the pile length. The monopile is usually installed by ramming, and mainly installed in water depths up to 25 m.
Gravity foundations are usually large diameter concrete blocks that acts as counterweight to the imposed loads. The installation of a gravity foundations requires careful preparation of the seabed, which needs to be leveled and possibly preloaded and/or compacted [Lesny, 2010]. Also, caution must be displayed during lowering of the foundation onto the seabed, so to reduce the impact caused when the foundation touches the seabed. The range of application in terms of water depth are somewhat the same for the gravity foundation and the monopile.

The bucket foundation (suction bucket, suction caisson, monopod), has to this point mainly been applied as an-

chors for floating offshore installations. Even though, during the past decade extensive research has been directed towards documentation of the bucket foundations suitability as support for offshore wind turbines [Ibsen et al., 2005]. The motive for spending time and money on this research, is simply time and money; the suction bucket has the potential to generate lower total costs compared to the monopile and gravity foundation. This is reflected during several phases of the process, from constructing to operation.

Given the relatively uncomplicated design, monopiles are fairly inexpensive to produce, but still assumed to be more costly than buckets due to the large amount of steel used. Installation of monopile require heavy driving tools, which are expensive to rent/buy, and give cause to great oceanic disturbance/noise, agitating the nearby aquatic wildlife. Removal of monopile usually consists of cutting of the top part at a prescribed depth below the seabed, so to avoid unveiling due to erosion.
The gravity foundation cumulates a higher production cost compared to both monopile and bucket, due to the large amount of steel and concrete. Gravity foundations also require special production locations, such as dry or floating docks, as well as heavy vessels for transportation to location. They are quite sensitive to unfavorable weather conditions during installation, and, as mentioned, depend upon extensive preparations of the seabed. Removal is performed either by re-floating and transportation to decommissioning location, or alternatively they are dismantled on site.

For these reasons, the bucket foundation might become an highly competitive alternative as support structure for future offshore wind turbines. The corroborative arguments will be discussed in the following section.

1.2 Bucket Foundation

The bucket foundation combines the function of two foundational concepts; monopile, gravity foundation, cf. Figure 1.2.

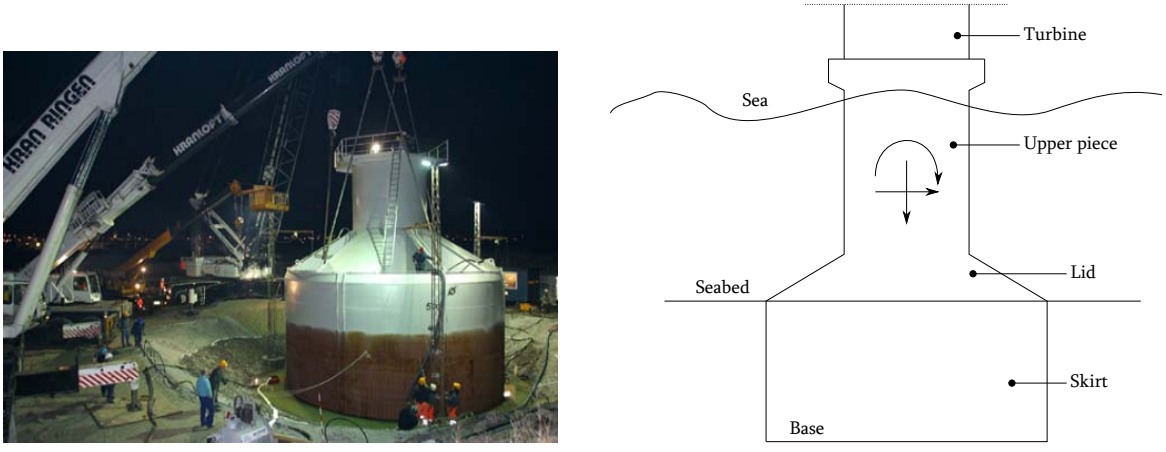

(a) (b)

Figure 1.2: *(a) Prototype bucket foundation installed at Frederikshavn. [www.hornsrev.dk]. (b) Conceptual illustration of bucket foundation.*

The bucket foundation is composed of three assembled parts; skirt, lid, and upper part. The skirt is completely submerged into the seabed, and gains the advantages of the gravity foundation and monopile as the immersed bucket takes possession of the encased soil. It is often reinforced by ring stiffeners, to overcome structural buckling chal-

lenges encountered during installation, and long term fatigue loading.
The function for the lid is to distribute the imposed loads from the upper piece/wind turbine, to the embedded bucket/skirt. Besides, the lid establishes a barrier around the encased soil which elongates the drainage path into the bucket. This is an important feature of the bucket foundation, as will be discussed later in the report. Also, the shape of the lid can be designed to reduce the need for scour protection.
The upper piece are simply a transition between the lower segments, skirt and lid, and wind turbine tower.

One of the benefits in favor of the bucket foundation relative to the monopile and gravity foundation is the installation process.
Installation of the bucket foundation occurs partly by self penetration and partly by suction, depending on the present soil conditions. The bucket is descended carefully onto the seabed, securing a smooth and even accession. Due to its submerged weight, the bucket will self-penetrate the soil until tip and friction resistance exceeds driving forces. Hereafter, suction is applied, causing water to flow from the outside, and into the bucket, cf. Figure 1.3. In non-cohesive soils, this leads to a reduction of both the tip resistance, and the frictional skirt resistance inside the bucket. Additionally, the differential water pressure across the base plate created by suction, haul the bucket further into the soil [Randolph and Gouvernec, 2011].
In cohesive soils, due to low permeability, penetration by suction is mainly provided by the hydrostatic pressure difference between inside and outside bucket.
Removal of the bucket foundation is achieved by inversing the suction process, which implies applying pressure between soil and lid. The excess pressure pushes the bucket up through the soil, where pontoons and floaters aids the ascension up to the water surface.

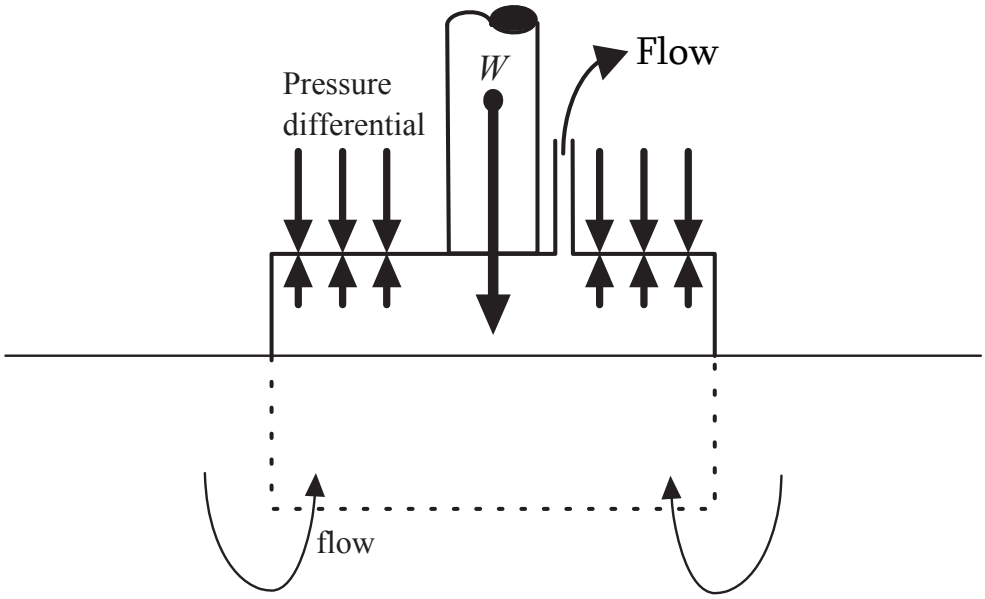

Figure 1.3: *Principe of suction assisted penetration. [Byrne and Houlsby, 2003]*

It should be stated that, for installation related purposes, the bucket favors some soil profiles better than other. Ideal conditions would be uniform soil profiles of either sand or clay. An exception to this is penetration through very stiff clay and very dense sands. In stiff clays, cracks/gaps along the skirt could develop, reducing the bucket-soil frictional capacity. Also, if the applied suction exceed the undrained shear strength, the encased clay plug may be detached in

the base area [Lesny, 2010].
The most apparent problem related to suction assisted penetration in non-cohesive soils is the formation of local flow channels along the bucket skirt, or so called *piping* [Ibsen and Thilsted, 2011], which in extreme cases lead to a global piping failure inside the bucket [Lesny, 2010].
Layered soils could also give cause to problems during penetration. This is particularly valid for sand layers overlaid with clay, a condition which would prohibit water to flow into the bucket, and hence fail to reduce the tip and frictional skirt resistance.

The concept of suction assisted penetration at shallow depths also give cause to restriction regarding applied under pressure. In non-cohesive soils, this limit is governed by piping. Houlsby and Byrne [2005a] suggest a maximum achievable suction assisted penetration depth equal to h/D $\approx$ 1, where h is the penetration depth, and D the bucket diameter. The mechanism governing suction limit in clay is identified as a *reversed bearing capacity problem*, which leads to a significantly higher limit; with h/D $\approx$ 3 for stiff clay, and 6 for soft normally consolidate clay [Houlsby and Byrne, 2005b].
Despite the above mentioned challenges, soil conditions rarely disqualifies the bucket foundation as a wind turbine support alternative. Both the monopile and gravity foundation has its restrictions regarding utilization as well.

Recalling the traditional application of the bucket foundation; deep water anchorage for floating installations, the loading regimes encountered at typical offshore wind turbine farms are quite different. The wind turbine itself is a fairly light structure. Depending on type of turbine, the vertical load/dead-weight could be somewhere around 4-6 MN, $\approx$ 400-600 tonnes. Critical loading are mainly imposed by sea; waves and current, as well as wind. Lesny [2010] states that total horizontal loading from wind and sea may surpass the vertical loads by a factor 1.5 at extreme conditions, while Houlsby et al. [2005] implies a factor 0.6. Considering that wind turbines are tall structures, and that the resulting horizontal loading acts relatively high above the foundation, it is quite safe to say the accumulating moment at base level are comprehensive. Houlsby et al. [2005] further claims that even though the total horizontal loading caused by wind is lower than those originated by waves, the resulting horizontal loading from wind might provide higher overturning moment due to a higher point of attack. This observation strongly depends on the water depth, since Lesny [2010] states that the inflicted hydrodynamic moments at base level can exceed the aerodynamic moments by a factor 2 or more.

Loading generated by waves can, for design purposes, be divided into two categories; 1) quasi-static forces induced by cyclic wave loading, and 2) monotonic, wave impact loading from breaking waves on topside structure [Ibsen and Lade, 1998]. The former are most relevant for long term performance studies of the Serviceability Limit State (SLS), while the latter provide the basis for determination of capacity in Ultimate Limit State (ULS).
The final design of a bucket foundation is usually governed by either considerations related to fatigue loading in SLS, or structural stiffness challenges affiliated with the installation process. Capacity in ULS rarely governs the design, but must be reviewed nonetheless, before dismissed as non-pertinent.

The procedure for determining ULS capacity for bucket foundations is one of the remaining obstacles that needs to be addressed before a final design process can be suggested, and hopefully approved and certified. ULS capacity due to braking waves in cohesive soil are naturally governed by the undrained shear strength. On the other hand, in non-cohesive soils, the ULS capacity is estimated assuming both drained and undrained condition, where the lowest of these two are selected for design. This will more or less always be the drained capacity. Intuitively, this should

not give cause to controversy, due to the fact that saturated non-cohesive soils for most engineering challenges acts drained. That being said, breaking waves causes impulsive loading, which could give rise to development of negative pore pressures inside the bucket.

1.3 Aim of Thesis

This thesis aspire to procure, through small scale testing of a bucket foundation, a consistent relationship between loading velocity and generation of negative pore pressures. The presented results should form a preliminary basis for further studies addressing the undrained response of the bucket foundation in cohesionless soils.

The main content of the thesis is presented in a enclosed article. This article gives a short summary of the test set-up and preparations, as well as an interpretation of results. A more elaborate description of the applied equipment and test procedures is presented in Part II of this report. Part III contains results gained from all test, and a enclosed CD-ROM include all raw data, as well as codes produced for interpretation of results.

Chapter 2

Soil - Structure Interaction in Cohesionless Soils due to Monotonic Loading

This chapter contains an article which presents the results gained from 4 monotonic loading test on a small scale bucket foundation. The aim of the test was to establish a consistent relationship between loading velocity and generation of negative pore pressures inside bucket. The tests were conducted in the Geotechnical Engineering Laboratory at Aalborg University.

Soil-Structure Interaction in Cohesionless Soils due to Monotonic Loading

Å. Sjelmo[1]; L. Mikalauskas[2]; L.B. Ibsen[3]; and A. Foglia[4]

Aalborg University, June 2012

Abstract

During the last decade, extensive research has been dedicated to document the suitability of the bucket as foundation for offshore wind turbines. Several issues still remain before an optimal design process can be introduced. One of these issues concerns the determination ULS capacity in frictional soils, related to loading caused by the design wave. Therefore, in the following article, the soil response due to monotonic loading will be investigated. This is achieved by conducting 4 monotonic loading tests on a small scale bucket foundation, with the loading velocity increasing by a factor 10 for each subsequent test. The aim of the performed tests is to identify the development of pore pressures inside the bucket during loading, and how this development relates to the loading velocity. At high rates of loading, the soil response is expected to approach an undrained condition. An undrained response will lead to a build up of negative pore pressure inside the bucket. Subsequently, the negative pore pressures results in suction, a so called *boot-effect*, which if present, will give a significant contribution to the capacity in ULS design.

1 Introduction

The bucket is a widely used foundation concept for marine and offshore installations. It's predominant area of application has so far been in relation to anchorage of floating installations and vessels, and additionally as foundation for a low number of platforms in the North-sea (Houlsby et al., 2005). Compared to alternative foundation concepts for offshore structures, the cost related to production and installation of a bucket is relatively low. Therefore, it is sought to expand the bucket foundations area of application.
During the last decade, extensive research concerning the buckets suitability as foundation for offshore wind turbines has been performed, both in terms of feasibility regarding the installation process and the in-service performance (Ibsen et al., 2005). In relation to determining the ULS capacity for the 50 or 100 year wave, the current procedure demands finding both the drained and undrained capacity, where the lowest is adopted for design. For cohesionless soils, this will in most cases be the drained capacity.

The soil encompassing a bucket foundation are exposed to a various set of loading. The environmental loads acting on any marine and offshore structure could arise from waves, wind, ice, earthquakes, etc. Wave loads are, for design purposes, divided in two sub-categories; 1) quasi-static forces induced by cyclic wave loading, and 2) monotonic, wave impact loading from breaking waves on topside structure (Ibsen and Lade, 1998).

The response of saturated soil due to monotonic loading is strongly dependent on the loading rate. For most engineering challenges, saturated cohesionless soils will behave drained. An exception to this statement is when the rate of loading occurs rapidly, such as the impact caused by breaking waves. A saturated soil exposed to rapid loading will offer more in resistance compared to slow loading. This increase in resistance is a contribution from the soils effort to redistribute pore pressures, interacting with the current drainage conditions.
Whether or not an undrained response will occur during loading of a bucket foundation, is mainly function a of three factors; skirt length and hence drainage path, s, permeability of soil, k, and wave period or loading velocity, v_l.

[1]Graduate Student, Dept. of Civil Engineering, Aalborg University, Denmark.
[2]Research Assistant, Dept. of Civil Engineering, Aalborg University, Denmark.
[3]Professor, Dept. of Civil Engineering, Aalborg University, Denmark.
[4]PhD Fellow, Dept. of Civil Engineering, Aalborg University, Denmark.

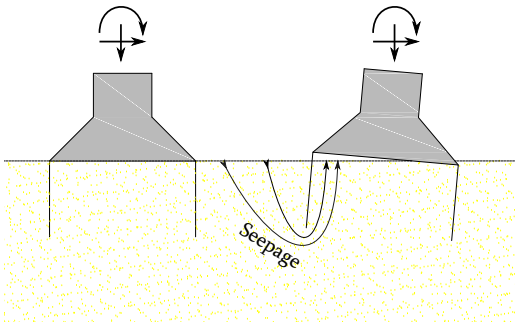

Figure 1: Generation of negative pore pressure inside bucket during loading.

$$\text{Undrained response} = f(s, k, v_l) \quad (1)$$

During a wave period, the bucket will experience rotation and to some degree an upward displacement, c.f. Fig. 1. Due to the relationship between the factors in Eq. 1, water cannot seep into the bucket fast enough to equalize the developing pressure difference, hence negative pore pressure starts to form inside the bucket. This effect creates a suction inside the bucket, which, in theory, would dramatically increase the capacity relative to a fully drained response.

To investigate this phenomenon further, a small scale model of a bucket, instrumented with pore pressure transducers, is exposed to monotonic loading at different loading velocities. To simulate the hydrostatic water pressure at 20 m of depth, the experiments are conducted inside a pressure tank.

This article presents the results obtained from four monotonic tests. The bucket is laterally loaded by a hydraulic piston, actuating the loading at an horizontal arm of 470 mm above the bucket lid, and a forced displacement equal to 3 times 40 mm. Loading velocities are increased by a factor 10 for each test, presenting the opportunity to investigate how the pore pressure, and capacity, develops at different loading velocities.

1.1 Undrained shear strength of sand

The mechanisms undergone prior to an undrained failure of a cohesionless soil are best understood by following the stress path of a CU-triaxial test.

Fig. 2 *a*) illustrate the stress path during a CU-triaxial test on Aalborg University Sand no. 1 at $D_r = 80$ %, as presented in Ibsen and Lade (1998). During compression, the stress path encounter various mechanisms which alter the response. These mechanisms are marked on the stress path, from the initial point O, to failure at D. From point O to A, the pore pressure increases to prevent the sample from compression. As q' approaches the characteristic line, $\delta\epsilon_V \Rightarrow 0$, and hence $\delta u \Rightarrow 0$. From A to B the sand wants to dilate, but is restricted by the generation of negative pore pressures. At point B, the positive hydrostatic pressure is consumed by the generated negative pore pressure. The sand then starts to dilate slowly, until cavity of the pore water occurs at point C, and the stress path hits the drained failure envelope at point D.
The line from point O to E illustrates the stress path for a CD-test. This line also illustrates the total stress path for the CU-test, which coincides with the effective stress path from a CD-test. From this particular type of sand, at this specific D_r, it is seen that the deviatoric stresses at failure in the CU-test are significantly higher than for the illustrated CD-test.

If it can be shown that impact loading from the design wave causes an undrained response, the capacity in ULS would become substantially higher compared to the drained capacity.

2 Scaling of model

Stating the correct scaling laws for the test setup is crucial in order to interpret model results, and later predict prototype responses. An applicable scaling concept is the laws of *similitude*, which states that a model is correctly scaled if a geometric, kinematic and dynamic similarity between model and prototype is present.

2.1 Dimensional analysis

The scaling framework of this study focuses on the seepage developing underneath a bucket foundation subjected to rapid lateral loading. The flow through a porous media is dominated by the permeability of the media, k, which for a given cohesionless soil depends on the relative density. Disregarding the anisotropy of the permeability, or better, assuming that to be similar in model and prototype, the veloc-

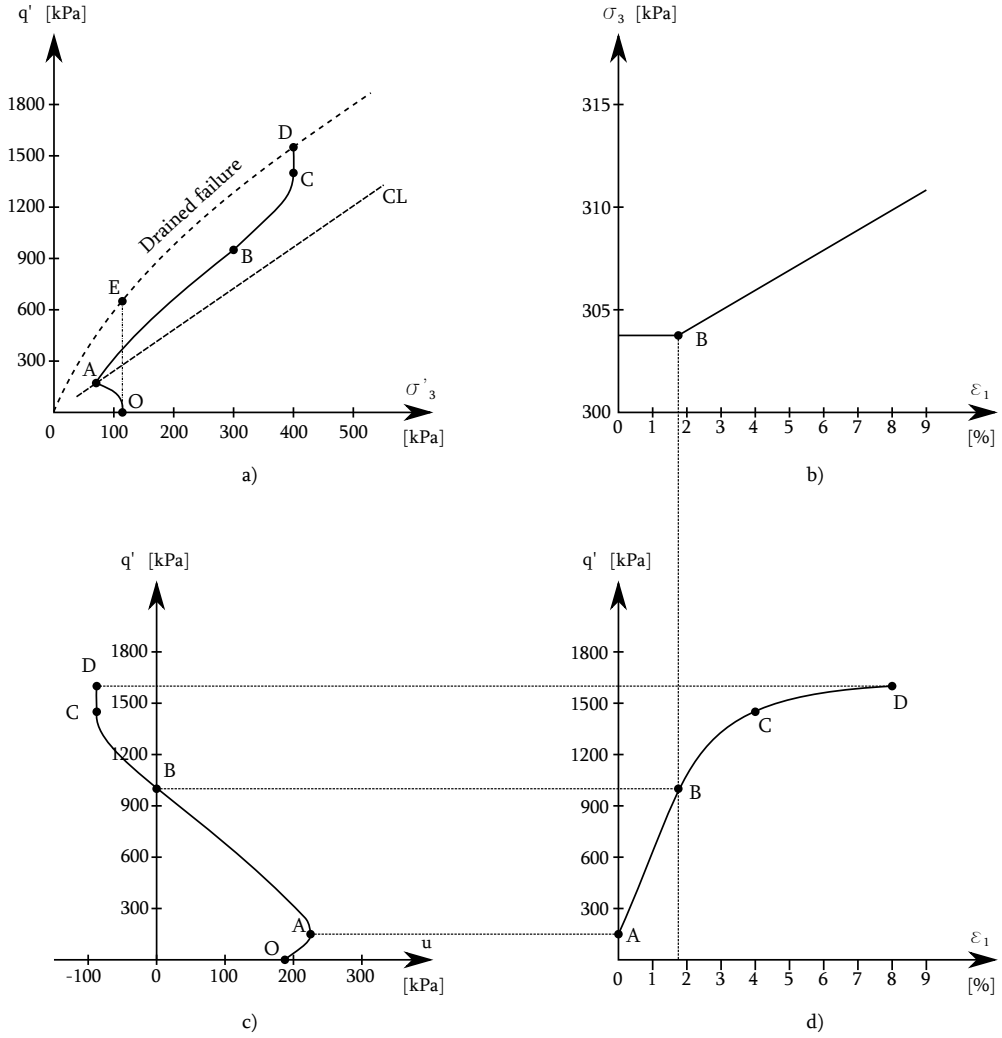

Figure 2: Results of a high deformation rate CU-triaxial test on Aalborg University Sand no. 1. (Ibsen and Lade, 1998)

ity of the water through the soil, v, can be expressed by Darcy's law:

$$v = k\frac{\delta p}{s} \tag{2}$$

Where δp is the pressure drop causing the flow, and s the drainage path length. These two variables of the problem are reasonably assumed to be respectively proportional to the time within which the loading occurs, t_L, and the skirt length of the bucket, h.

$$\delta p \propto t_L \tag{3}$$

$$s \propto h \tag{4}$$

Now by substituting Eqs. 3 and 4 in Eq. 2, the dimensionless group that must be satisfied for the small scale results to be scaled up to prototype scale is:

$$\left(k\frac{t_L}{h}\right)_{model} = \left(k\frac{t_L}{h}\right)_{prototype} \tag{5}$$

2.2 Scaling factors

By the laws of similitude, any geometrical or physical quantity of nature can be scaled down by applying Eq. 6.

$$X_{prototype} = \lambda_X \cdot X_{model} \tag{6}$$

Where the X denotes the dimension/unit, and λ an scaling factor. The following scaling factors are relevant for the bucket test (Pedersen and Kristensen, 2007):

λ_L, Length	λ_F, Force	λ_ρ, Density
λ_t, Time	λ_σ, Stress	λ_{μ_v}, Viscosity
λ_v, Velocity	λ_g, Gravity	λ_{k_i}, Permeability

Nonetheless, some restrictions in terms of scaling factors occur with the selected test set up. Scaling of λ_g would require that the test were performed inside a centrifuge. Correct scaling of λ_ρ and λ_{μ_v} would imply use of another fluid

Scale	Correct	Applied
Soil		
λ_L	λ_L	λ_L
λ_t	$\lambda_g^{-\frac{1}{2}} \cdot \lambda_L^{\frac{1}{2}}$	$\lambda_L^{\frac{1}{2}}$
λ_v	$\lambda_g^{\frac{1}{2}} \cdot \lambda_L^{\frac{1}{2}}$	$\lambda_L^{\frac{1}{2}}$
λ_F	$\lambda_\rho \cdot \lambda_g \cdot \lambda_L^3$	λ_L^3
λ_σ	$\lambda_\rho \cdot \lambda_g \cdot \lambda_L$	λ_L
Pore fluid		
λ_t	$\frac{\lambda_{\mu_v}}{\lambda_{k_i} \cdot \lambda_{\rho_v} \cdot \lambda_g} \cdot \lambda_L$	λ_L
λ_v	$\frac{\lambda_{k_i} \cdot \lambda_{\rho_v} \cdot \lambda_g}{\lambda_{\mu_v}}$	1

Table 1: Scaling factors for soil and pore fluid, after (Pedersen and Kristensen, 2007).

than water. Scaling of the sand would be extremely difficult, hence $\lambda_{k_i} = 1$. Therefore, all scaling factors are expressed by means of the length scale, λ_L c.f. Table 1. The results obtained during the following experiments have not been scaled up to prototype dimensions. In that context, it should be stated that Tab. 1 is merely a suggested set of scaling factors. Nevertheless, these factors could either be applied or modified in further stages of the current study.

3 Test setup

All tests are performed inside a pressure tank, located in the Geotechnical Engineering Laboratory at Aalborg University. The test setup consists of a pressuretank containing saturated sand, in which a small scale model of a bucket foundation is installed. The entire tank is located inside a loading frame, as seen in Fig. 3.

A highly permeable layer of gravel is deposited at the bottom of the tank, overlaid with a 0.6 m thick layer of Aalborg University Sand no. 1 which is separated from the gravel by a geotextile canvas. The bucket is equipped with 8 pore pressure transducers, located at different levels on the bucket, cf. Fig. 5. A vertical steel beam is situated ontop the embedded bucket, to transfer loading from piston to bucket. This steel beam will be referred to as the *tower*, which is assumed rigid in the interpretation of horizontal displacements.

Displacements during the tests are recorded by 5 transducers, 3 horizontal and 2 vertical. The location of these transducers and point of load application are shown in Fig. 6.

The lateral load was applied to the bucket employing a hydraulic piston, connected to the tower by use of a steel wire. The loading was performed as a forced displacement of the piston, 40 mm, over a given period of

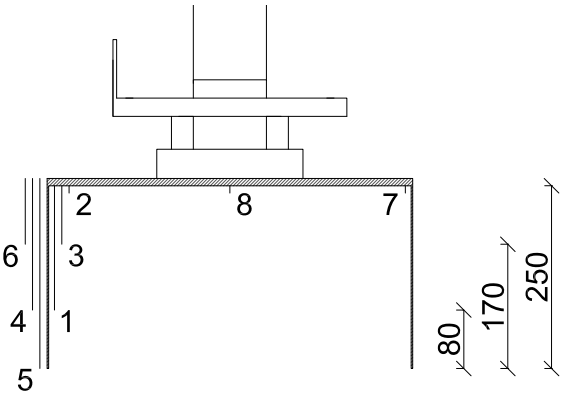

Figure 5: Location of pore pressure transducers on the bucket. Direction of loading towards right. All dimensions in [mm].

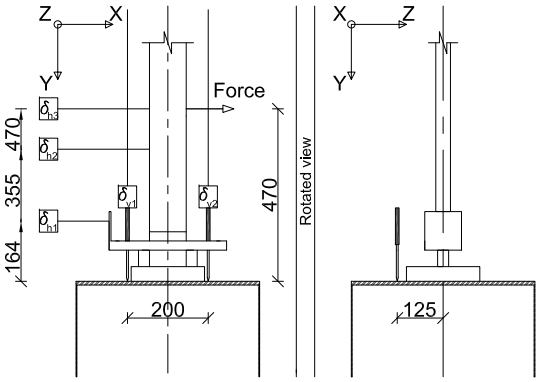

Figure 6: Location of vertical and horizontal displacement transducers, and loading. All dimensions in [mm].

time. A force transducer elongating the piston, records the pulling force, which varies regarding to displacement and loading velocity. Two different wires were used during the tests. The distance from the tower to the piston became too short for the first wire to be used in all loading sequences. The wire applied in the first loading sequence had a diameter of 5 mm, and should sustain loading up to $\approx$ 1600 kg. For loading sequence 2 and 3, a 3 mm wire were applied, which had a strength of $\approx$ 580 kg (Scanlifting, 2012).

The tests were conducted with an applied pressure equal to 2 bar, 200 kPa, to simulate the pore pressure conditions at 20 m depth.

3.1 Data collection and measuring system

The moment loading of the bucket are actuated by a hydraulic piston, M2000 PCS2, which originally has a displacement range of

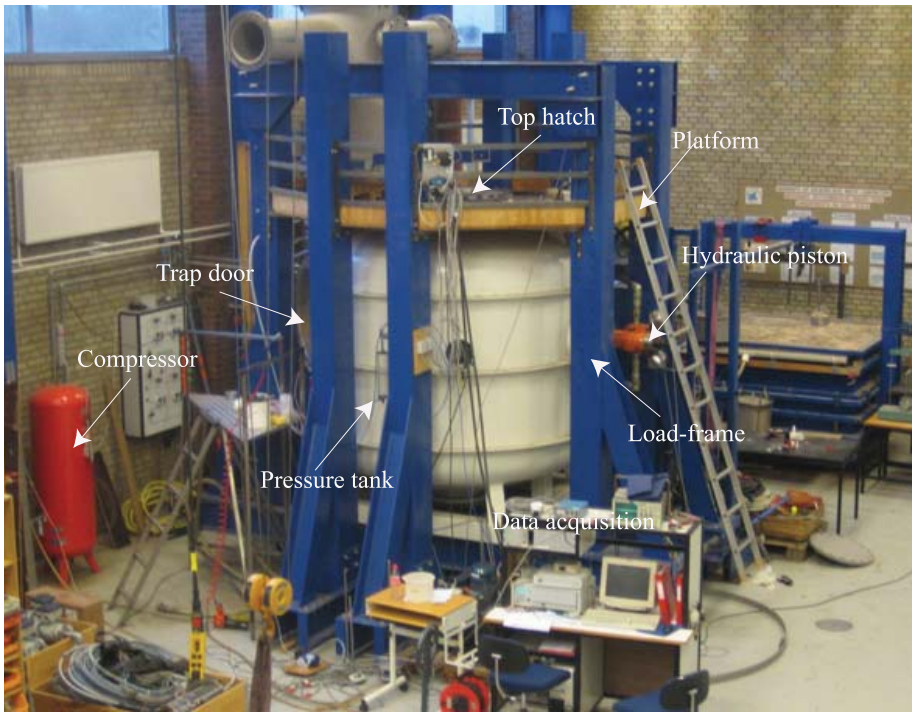

Figure 3: Pressuretank at AAU. (Sørensen et al., 2009)

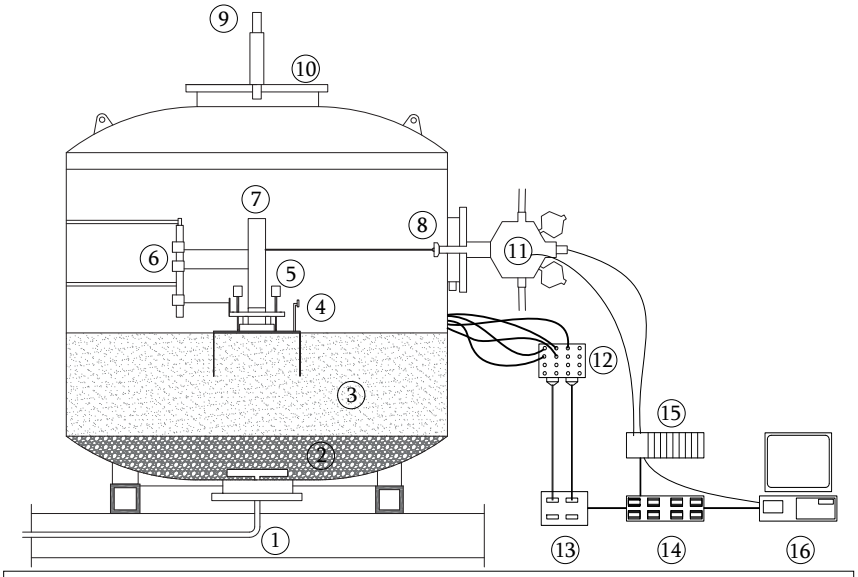

Figure 4: Complete test setup.

50 mm (Moog, 1998). Due to the suspension arrangement, the range is reduced to 40 mm, or if cyclic loading is desired; ±20 mm. The tests are performed as a monotonic lateral loading, allowing the piston to move 40 mm until it stops. Extending the hydraulic piston inside the tank is a pressure transducer, of the type HBM U2B 10 kN, which reads the force applied to sustain the prescribed loading velocity. A steel wire connects the bucket/tower to the piston, at an initial horizontal arm equal to 470 mm, relative to the bucket lid. Horizontal translation are measured at three levels, cf. Figure 6, by wire transducers of the type WS10-1000-R1K-L10 from ASM GmbH. To find vertical displacements, two linear variable differential transformers (LVDT), HBM WA/100mm, are placed on the bucket lid. The transducers are initially located on a line parallel to the loading direction, at the coordinates seen in Figure 6.

There are in total 14 gauges inside the tank during testing

- 8 pore pressure transducers
- 5 displacement transducers
- 1 force transducer

The output from these transducers are sent to a computer program, Catman 5.0, through an amplifier, MGCplus. Frequency of data sampling are 10 Hz for the first three test, and 25 Hz for the last test. The same frequencies are adapted for controlling the loading system through the hydraulic piston, 10 Hz for test 1, 2 and 3, and 25 Hz for test 4.

4 Test program

The tests were performed at 4 different velocities, subsequently increased with a factor 10; 0.01 mm/s, 0.1 mm/s, 1 mm/s, and 10 mm/s. For each test, the piston would move in total 120 mm, divided in three sequences of forced displacement equal to 40 mm, which is the maximum range of the piston. Between each test sequence at same velocity, the tank was opened, wire tightened, and piston reset to initial position.

The bucket used in the tests had the outer measurements D/h_{out} = 500 mm/260 mm. The bucket lid is 10 mm thick, giving an inner skirt length of h_{in} = 250 mm. See bucket geometry in Fig. 7.
The chosen test program is designed to investigate the build up of pore pressures during loading of the bucket. At the lowest rate of loading, the response is expected to be drained. However, as the velocity of loading increases, the response should gradually tend to become undrained. The test program is summarized in Tab. 2.

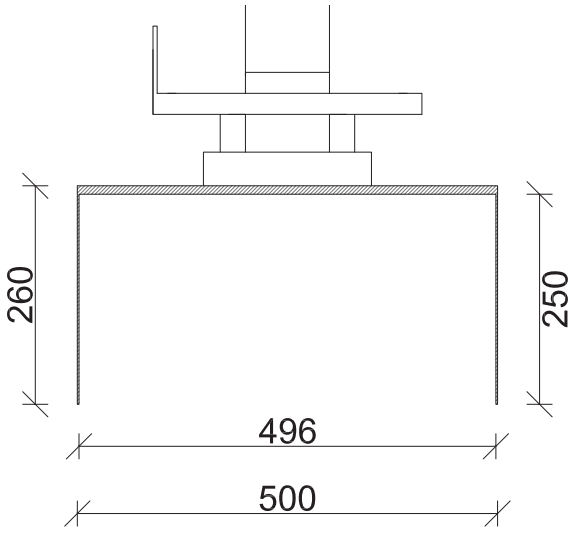

Figure 7: Bucket geometry. All dimensions in [mm].

Test no.	Displacement of piston [mm]	Duration of test [s]	Loading rate [mm/s]
Test 1	3·40	3·4000	0.01
Test 2	3·40	3·400	0.10
Test 3	3·40	3·40	1.00
Test 4	3·40	3·4	10.00

Table 2: Test program.

Two different buckets were available for testing; one half-bucket, where h/D = 1/2, and one full-bucket where h/D = 1. Both buckets contains the necessary equipment to read pore pressures. In the following article, the test results for the half-bucket are presented. In further studies of the current topic, it is planned to perform tests on the full bucket as well, both monotonic and cyclic.

5 Soil Conditions

The sand type used inside the pressure tank is Aalborg University Sand no. 1, which is a uniform, industrially prepared quartz-sand. The grain-size distribution can be seen in Fig. 8.
Aalborg University Sand no. 1 has been used in a series of experiments at AAU over the past 20 years. Therefore, its properties are well documented. Tab. 3 states the material properties of the sand, as presented in Ibsen et al. (2009).

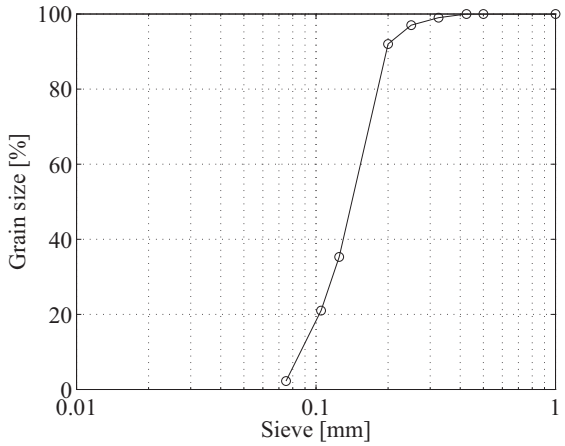

Figure 8: Grain size distribution of Aalborg University Sand no. 1, from Sørensen et al. (2009).

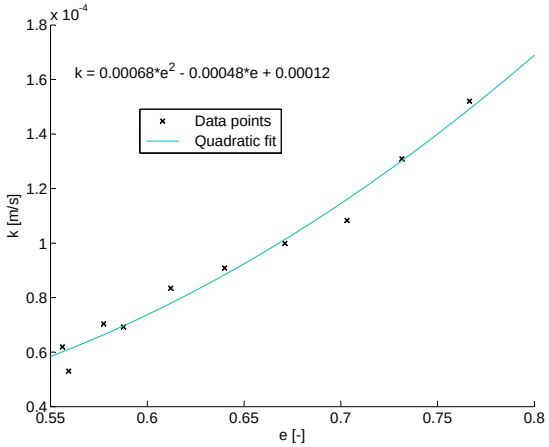

Figure 9: Permeability of Aalborg University Sand no. 1.

Property	Value	Unit
Specific grain density, d_s	2.64	[-]
Maximum void ratio, e_{max}	0.858	[-]
Minimum void ratio, e_{min}	0.549	[-]
Mean grain size, d_{50}	0.14	[mm]
Uniformity coeff., $C_U = \frac{d_{60}}{d_{10}}$	1.74	[-]

Table 3: Material properties of Aalborg University Sand no. 1.

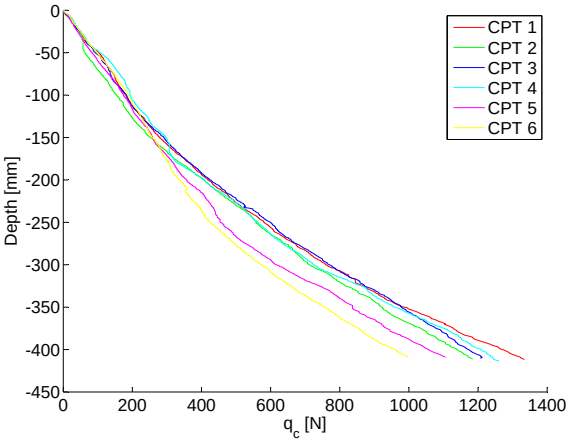

Figure 10: CPT from test 1.

5.1 Permeability

Despite the fact that Aalborg University Sand no. 1 has been used frequently at AAU, no documentation of its permeability has been registered. Since the generation of pore pressures during loading strongly depends on the coherent drainage properties, the permeability, k, were found by means of a falling head apparatus, for sand samples at different relative densities. Fig. 9 show the relationship between void ratio, e, and permeability, k.
This was also done for sand retrieved from the test site in Frederikshavn (Ibsen et al., 2005), so to create a framework for future comparison between model and prototype. A detailed description of the procedure for determining the permeability, along with corresponding results, are presented in Sjelmo (2012).

5.2 Preparation of Sand

During the tests, the sand becomes greatly disturbed. Therefore, to ensure homogeneous conditions, the sand is vibrated after a recommended pattern before each test. The vibration procedure is based on the experiments presented in Fisker and Kromann (2004).

The entire set up inside the tank is removed after each test. Then, water is let into the tank, with an upward gradient of 0.9 which causes the sand to loosen, followed by the first round of vibration. Water is let in a second time, under the same gradient, followed by a second round of vibration. Six Cone Penetration Tests (CPT) were performed prior to each test to control whether or not the vibrated sand had gained a tolerable homogeneity. A plot of the tip resistance, q_c, versus depth for test 1 is shown in Fig. 10.
The CPTs are carried out following a predetermined pattern. Four CPTs are conducted 500 mm from center tank, while CPT 5 and 6 is performed 200 mm from center tank perpendicular to the loading direction, as seen in Fig. 11. It should be noted that these coordinates are somewhat approximate. CPT locations will be adjusted with respect to the commenced vibration pattern.
The results from CPTs are further used to find the compaction/relative density of the embed-

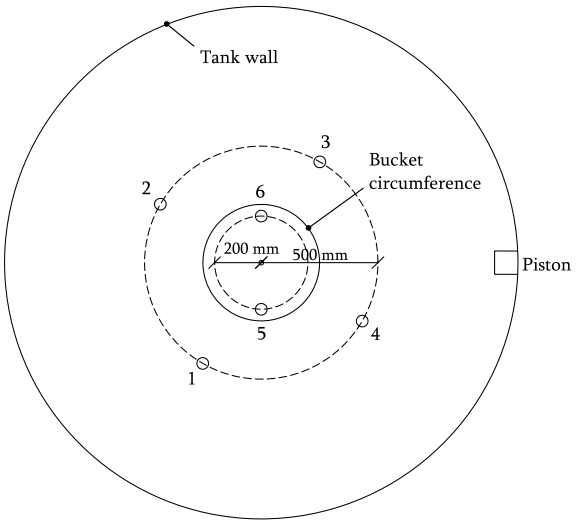

Figure 11: Approximate coordinates for CPTs.

ded sand. By extensive triaxial testing of Aalborg University Sand no. 1, Ibsen et al. (2009) derived several empirical relationships between different soil properties. Eqs. 7 to 12 summarizes the iterational procedure performed to find the soil properties presented in Tab. 4, which contain derived values for relative density, D_r, the internal angle of internal friction, ϕ_{tr}, the dilation angle, ψ_{tr}, and the submerged unit weight of the sand γ'.

$$\phi_{tr} = 0.152 \cdot D_r + 27.39 \cdot {\sigma'_3}^{-0.2807} + 23.21 \quad (7)$$

$$\psi_{tr} = 0.195 \cdot D_r + 14.86 \cdot {\sigma'_3}^{-0.09764} - 9.946 \quad (8)$$

$$\gamma' = \frac{d_s - 1}{1 + e} - \gamma_w \quad (9)$$

$$\sigma'_1 = \gamma' \cdot x \quad (10)$$

$$D_r = c_2 \cdot \frac{\sigma'^{\,c_3}_1}{q_c^{c_1}} \quad (11)$$

$$D_r = \frac{e_{max} - e}{e_{max} - e_{min}} \cdot 100 \quad (12)$$

Where $\gamma_w = 10.0\ kN/m^3$ is the unit weight of water, σ'_1 is the vertical effective stresses in MPa. $c_1 = 0.75$, $c_2 = 5.14$, $c_3 = -0.42$, are fitting constants applied in Eq. 11, unique for Aalborg University Sand no. 1, and the utilized CPT equipment. e is the actual void ratio of the deposit.

Test No.	D_r [%]	ϕ_{tr} [°]	ψ_{tr} [°]	γ' $[kN/m^3]$
Test 1	83.81	46.78	10.26	10.26
Test 2	89.52	47.81	10.37	10.37
Test 3	89.25	47.76	10.37	10.37
Test 4	85.66	47.12	10.29	10.29

Table 4: Properties derived from CPTs prior to each test.

5.3 Uncertainties regarding soil properties

The hydraulic piston applied to install the bucket does not allow alteration of the penetration velocity. Therefore, during installation, pressure tends to build up in the pore water, inside the bucket. The bucket is equipped with one valve located on the top lid, which is the only way, save under the skirt and through the sand, the excess pore pressure can dissipate. The build up of pressure during penetration can therefore lead to a minor loosening of the sand outside the bucket. This effect is minimized by performing the installation in small steps, allowing the excess pressure inside the bucket to dissipate between each step of penetration.

To be able to perform CPTs at different locations inside the tank, a triangular suspension arm was mounted to the centered piston located ontop the tank, cf. Fig. 4. Due to a somewhat weak connection between the CPT device, suspension arm, and piston, the whole setup tended to give in or bend upward as the penetration commenced. Even though no accurate measurement of the error was conducted, the vertical displacement of the CPT device during penetration is assumed to be approximately 10-15 mm. This means that q_c, and hence other derived parameters, could be somewhat underestimated.

6 Results

Four monotonic loading tests of a small scale bucket foundation, cf. Tab. 2, were executed to investigate the relationship between loading velocity and build up of (negative) pore pressures. Negative pore pressures inside the bucket develop when the rate of loading surpasses the rate of drainage. This condition would cause the bucket to resist any movement by suction, which again would lead to an increase the ultimate capacity, as shown in Sec. 1.1.
As mentioned in Sec. 4, the loading are ap-

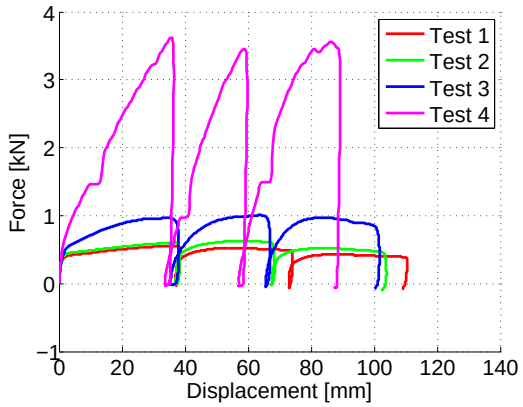

Figure 12: Force - Displacement.

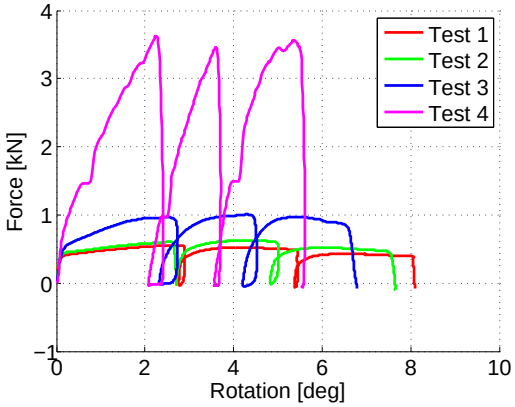

Figure 13: Force - Rotation.

plied as sequences of forced displacement. For each sequence, the piston can move 40 mm. Information of particular interest are the pore pressure development, as well as the magnitude of loading for each velocity, and how these results relates to rotation and displacement.

6.1 Development of loading

Three loading and unloading sequences are performed for each loading velocity, v_l. Fig. 12 indicates that in test 1-3 the bucket reaches failure after $\approx$ 2-3 mm horizontal displacement, and that the ultimate capacity is surpassed. This is not the case for test 4 (at v_l = 10 mm/s), where the peak in capacity remain unrevealed due to the fact that the piston cannot move further than 40 mm per sequence. Even though, it is seen that the capacity increases dramatically from v_l= 1 mm/s to v_l= 10 mm/s.
Fig. 12 also show that the largest lateral deflections occur at the lowest rate of loading. It should be noted that the displacement in Fig. 12 are the measured displacement of the top horizontal transducer, which is fixed to the tower. As the loading commences, the bucket starts to rotate as well as displace in horizontal and vertical direction. This leads to a minor error in the measurements of exact horizontal displacements. An error which is disregarded in the current plot.

In Fig. 13 the force is presented relative to the rotation of the bucket. The rotations agrees with the displacements in Fig. 12, by implying the largest rotations at the lowest rate of loading.
The rotation is determined based on output from the vertical displacement transducers which, unlike the horizontal transducers, are installed separately from the bucket and tower. As the loading commences the vertical transducers will slide along the bucket lid, while the distance between them are constant. Therefore, the presented rotations, as calculated by Eq. 13, should be accurate.

$$\Theta = \arctan\left(\frac{\delta_{v1} - \delta_{v2}}{200\ mm}\right) \tag{13}$$

Where δ_{v1} and δ_{v2} is the recorded vertical displacements, as presented in Fig. 6.

6.2 Pore pressure development

Figs. 14 to 21 show the development of pore pressures during the first loading sequence for all 4 tests. The intensity of the colored lines indicate which load step the present pore pressures corresponds to, where white/no color symbolizes initial conditions and darkest color indicate peak load. The red and blue lines indicate inside and outside pore pressure development, respectively.
The bucket skirt or lid is illustrated with a black line. Both inside and outside pore pressures are plotted on the same side, to avoid confusion with the operational sign on the x-axis. The number of load steps illustrated have been limited to 50, to be able to see a clear trend in the development of pore pressures. The values gained from pressure transducer no. 5, located outside the bucket at skirt tip, are assumed to also represent the conditions at inside skirt at same depth. Since no pressure transducer are located at the top bucket bucket skirt, it is assumed to be zero at all time, which is a fair assumption. It should also be stated that the hydrostatic pressure is removed from the plotted results, to better illustrate the resulting differences between each test.

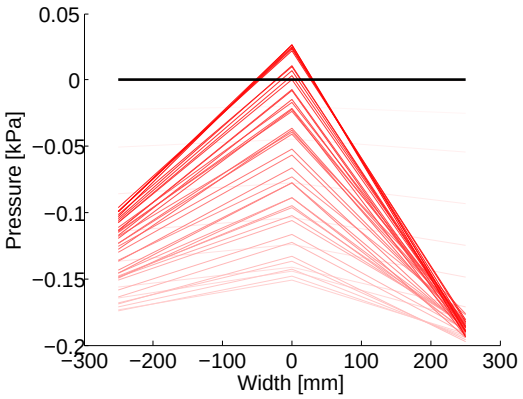

Figure 14: Pore pressure development under lid, test 1.

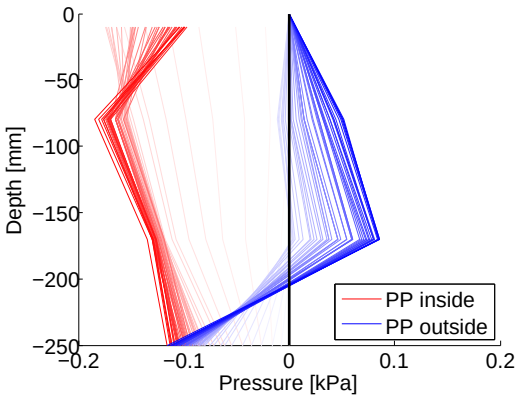

Figure 15: Pore pressure development along skirt, test 1.

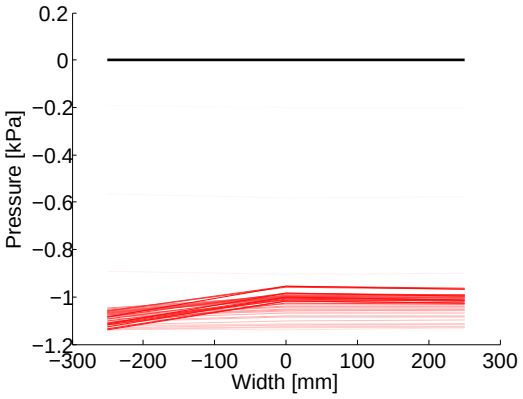

Figure 16: Pore pressure development under lid, test 2.

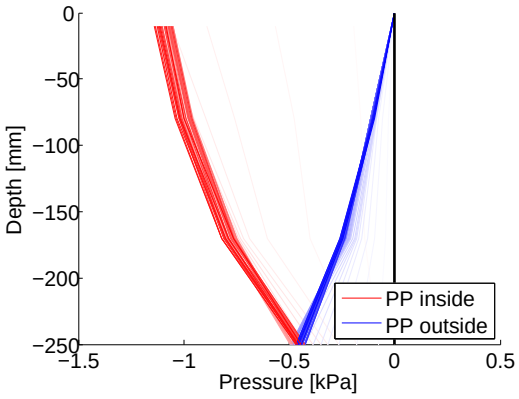

Figure 17: Pore pressure development along skirt, test 2.

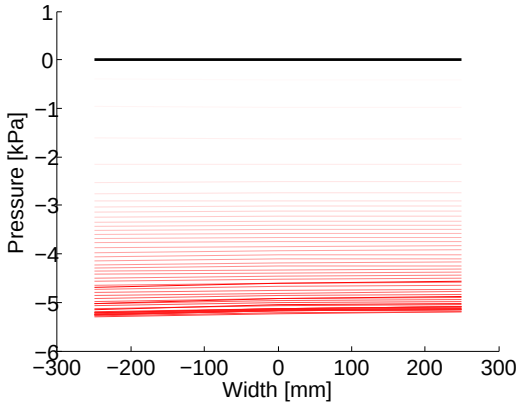

Figure 18: Pore pressure development under lid, test 3.

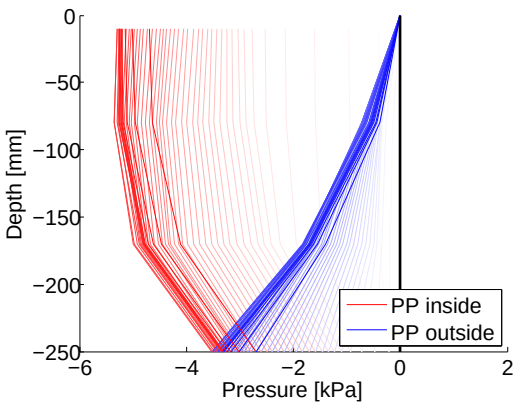

Figure 19: Pore pressure development along skirt, test 3.

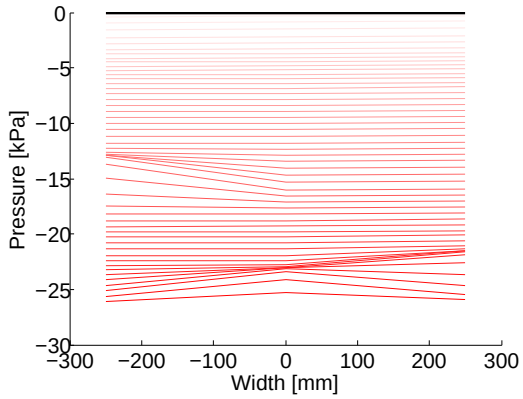

Figure 20: Pore pressure development under lid, test 4.

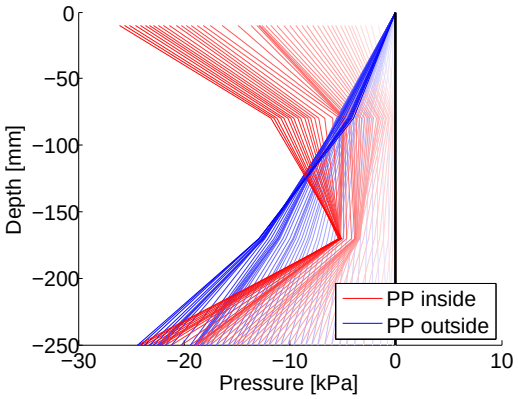

Figure 21: Pore pressure development along skirt, test 4.

The pore pressures building up in test 1 are marginal and inconclusive, as expected. In test 2 a clearer tendency is displayed for the pore pressure development, although the values are relatively small. As seen in Figs. 12 and 13, altering v_l from 0.01 mm/s to 0.1 mm/s has little or no effect on the capacity.
In test 3 the negative pore pressure continues to increase, which leads to a clear leap in capacity compared to test 1 and 2.

In test 4, Figs. 20 and 21, the negative pore pressures continues to develop. Also, in contrast to the previous tests, the development of negative pore pressures under the bucket lid does not seem to stagnate. This is due to the fact that the failure load is not reached during the loading sequence, as seen in Figs. 12 and 13. Still, the capacity increases by a factor ≈ 7 compared with test no. 1 and 2.
The pore pressures on the skirt inside the bucket, display a fold or drop at $\approx$ h/2. At this velocity a lag, or delay, might develop in pore pressure generation due to the time dependent behavior of viscous materials. The mechanisms leading to this result will be investigated further, but are unavailable at this stage.

6.3 Rotation and displacement

The cumulative displacements and rotations are displayed in Figs. 22 to 24, and include all three loading and unloading sequences. Both vertical and horizontal displacements differ with respect to point on/along bucket. Therefore, Fig. 22 and 23 refers to the resulting displacement of bucket lid center.

The three plots illustrating normalized time vs. displacements and rotations, show a shifted behavior of test 1. This is due to the fact that test 2-4 had an unloading time equal to the loading time, whereas test 1 had an unloading time that was 10 times faster than the loading time. The trends for test 1 displayed in Figs. 22 to 24 should therefore be steeper, which must be kept in mind when interpreting results.

The vertical displacement of bucket center in Fig. 22 seems consistent with previous findings, i.e. the build up of negative pore pressure under bucket lid, which reduces the vertical movement by suction. Therefore, the difference in vertical displacement, for all tests, during the first loading sequence is quite notable. During the second and third loading sequence, the vertical displacements in test 3 and 4 tends to flat out, while test 1 and 2 show a steeper tendency. This can be reviewed in light of the rotation point, cf. Fig. 25, which moves during loading, but tends to stabilize as the peak load is reached. The point of rotation for test 3 and 4 are significantly deeper and more centered than for test 1 and 2.

The horizontal displacements in Fig. 23 show a quite similar development throughout the loading for all tests. The exception would be test no 4, which display a drop in displacement during unloading after sequence 2 and 3. This could be because the bucket is pulled back by the remaining negative pore pressures during unloading.
Fig. 24 show the normalized time vs. rotations, which indicates a gradually separation regarding the rotation between the performed tests. The difference between test 1 and 4,

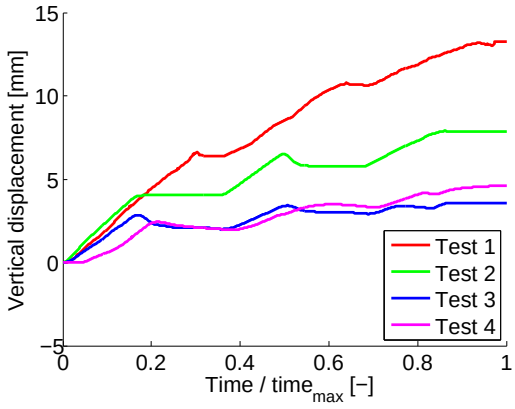

Figure 22: Normalized vertical displacement of bucket center for all tests.

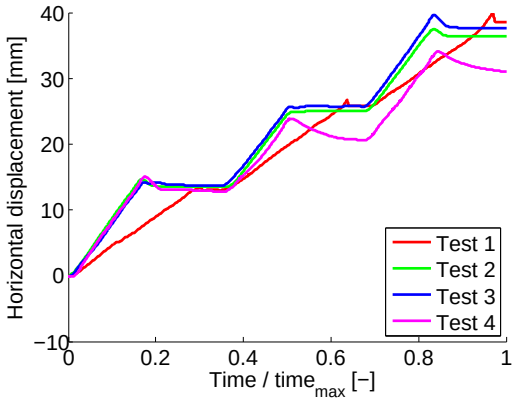

Figure 23: Normalized horizontal displacement of bucket center for all tests.

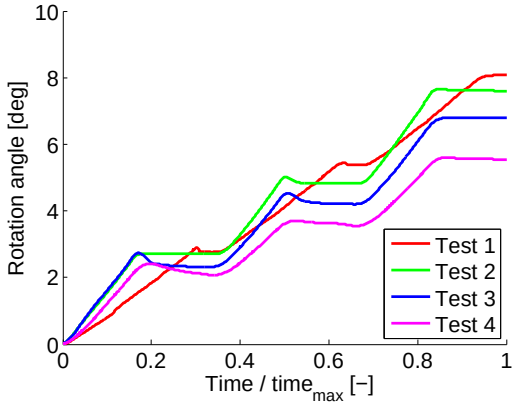

Figure 24: Normalized rotation of bucket for all tests.

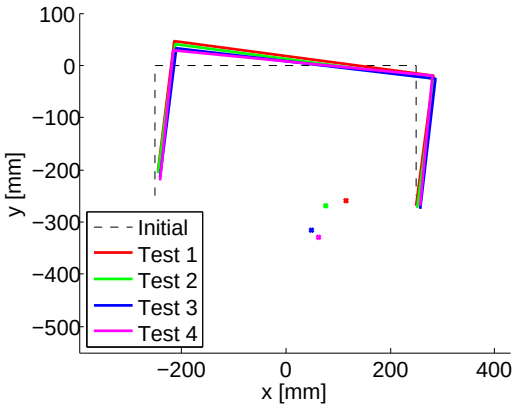

Figure 25: Final point of rotation for all tests.

are 2-2.5° at the end of unloading after load sequence three.

7 Drainage conditions

The drainage properties greatly influences the capacity of a bucket foundation exposed to monotonic loading. All movements of the bucket are dependent on redistribution of pore pressures, and hence the permeability of the soil, k. To get a better understanding of the type of response during testing; undrained, partly drained or drained, an estimation of the seepage time, t, are calculated.

The seepage time for dissipation of 90% of the pore pressure, t_{90}, is determined based the assumtions valid for Terzaghis one-dimensional consolidation theory. This is expressed by the coefficeint of vertical consolidation, c_v, which contains the material properties governing the consolidation process. t_{90} is hence calculated as presented in Eq. 14.

$$t_{90} = \frac{T \cdot s^2}{c_v} \tag{14}$$

Where s is the seepage length in m, and T a dimensionless time factor dependent on the percentage of pressure dissipation.

Eq. 15 to 18 give the correct input for Eq. 14.

$$c_v = \frac{k \cdot E_{oed}}{\gamma_w} \tag{15}$$

$$E_{oed} = \frac{E_{50}(1-\nu)}{(1+\nu)(1-2\nu)} \tag{16}$$

$$E_{50} = \frac{E_0(2-R_f)}{(2} \tag{17}$$

Where E_{oed} is the oedometer modulus, E_{50} the secant modulus, R_f the failure ratio equal to 0.9 (Plaxis, 2010), γ_w the unit weight

of water, ν Poisson's ratio, and E_0 initial/tangential modulus. E_0 were experimentally determined by a light falling weight deflectometer, PRIMA 100 LWD. The procedure involves releasing a predetermined weight from a chosen height onto the sand surface. The deflectometer then reads force and vertical displacement, rearranges this into stresses and strains, and calculates a resulting E_0. The test were performed at four different locations inside the tank. The applied E_0-value in Eq. 16 are an average of these four test.
For an optimal determination of E_0, the LWD manual advise numerous drops of the weight from different levels. This could not be performed due to the low height between sealing and sand surface inside the pressure tank.
The determination of seepage length, s, is in accordance to Ibsen and Thilsted (2011), cf. Eq. 18

$$s = h\left(2.86 - arctan\left[4.1\left(\frac{h}{D}\right)^{0.8}\right]\left(\frac{\pi}{2.62}\right)\right) \tag{18}$$

Where h is the embedded height of the skirt and D the bucket diameter. Tab. 5 summarizes the values which are involved in the process of determining t_{90}.

ν, [-]	0.25
E_0, [MPa]	40.2
h, [m]	0.25
D, [m]	0.5
k_v, $[m/s]$	$6.926{\cdot}10^{-5}$
γ_w, $[kN/m^3]$	10
T, [-]	0.85

Table 5: Values applied in the process of determining t_{90}.

The value of k_v corresponds to the measured hydraulic conductivity for Baskarp sand No. 15 at D_r = 88 %. By applying the values in Tab. 5, and calculating Eq. 18 to 14, t_{90} were found to be 0.6 s, which is a significanly lower value than expected.

To verify the result gained in Eq. 14, a test was performed in the pressure tank. A full bucket, h/D = 1, was installed in the sand. Then suction was applied at the pore pressure transducer located at center bucket, no. 8, 500 mm above skirt tip. After a build up of approx 15 kPa of underpressure, suction was removed, followed by a measurement t_{90}, cf. Fig. 26. It could be discussed whether or not the drainage will transpire equally for the measured stationary case, and for when the bucket is loaded, but as a preliminary

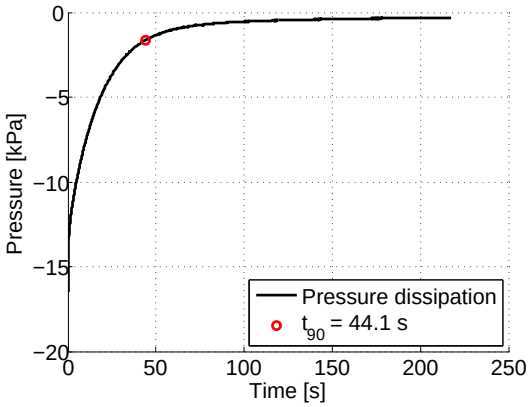

Figure 26: Measurement of t_{90} for full bucket.

indication this method should be sufficient.
Assuming homogeneous soil conditions, and that s_{full}=2·s_{half}, the relationship between t_{90} for the half and full bucket are

$$t_{90_{full}} = \frac{T \cdot s_{full}^2}{c_v} = \frac{T \cdot 4s_{half}^2}{c_v}$$
$$\rightsquigarrow t_{90_{half}} = \frac{t_{90_{full}}}{4}$$

Which gives a $t_{90_{half}} \approx 11$ s, which intuitively sounds more appropriate than 0.6 s, as calculated using the values presented in Tab. 5.

A preliminary assumption with respect to the type of response, would be that test 4 are partly drained. This can be assumed based on the loading time, 4 s, and the observed t_{90}, which was found to be 11 s for the half bucket. Therefore, the response can hardly be completely drained or undrained.

8 Conclusion

This article presents the results gained from 4 monotonic loading tests on a small scale bucket foundation, conducted at AAU. All tests were performed inside a pressure tank at 2 bar, to simulate the hydrostatic pressure at 20 m depth. The applied bucket had an outer diameter of 500 mm, and an inside skirt height equal to 250 mm.
The loading was applied in three sequences with an forced displacement equal to 40 mm, over a given time frame. The rate of loading was increased by a factor 10 for each test, starting at 0.01 mm/s for test 1, and ending at 10 mm/s for test 4.
8 pressure transducers were installed on the bucket to record the pore pressure development during loading. Horizontal and vertical displacement transducers measured the movement of the bucket during loading,

and a load cell registered the required force applied to maintain prescribed load velocity.

The results presented in this article show a strong correlation between the applied loading velocity and the responding build-up of negative pore pressures. In terms of capacity and pore pressure development, the first two tests experienced only minor differences. Test 3 displayed some higher values, but it was first after the step up in velocity from test 3 to 4 that the increase in capacity became significant. Due to the range limitations of the hydraulic piston, 40 mm, test 4 did not reach peak load. Still, the load displayed for test 4 were ≈ 7 times higher than failure load for test 1 and 2, and ≈ 3.5 relative to test 3.

Displacements and rotations of the bucket measured throughout the tests were in compliance with the developed pore pressures. An increase in negative pore pressures creates higher suction, which again restrains the bucket in terms of movement. Thus, there is a clear tendency of reduction in movement as the loading velocity increases.

To get a preliminary understanding of the response encountered in test 4, a one dimensional consolidation analysis was performed. This resulted in an unexpectedly low drainage time of 0.6 s. Therefore, a simple physical test was conducted on a installed full-bucket. Suction was applied and removed at pressure transducer 8, center bucket, followed by a measurement of the drainage time t_{90}. The measured time were recalculated to represent the half-bucket, which gave a $t_{90} \approx 11$ s. The deviation between calculated and measured t_{90} could be due to a rather crude method of determining the modulus of the soil, which provided a result that might be overestimated. Also, some uncertainties were associated with the method determining the seepage length, which has a significant influence on the calculated drainage time.
Therefore, in further studies of the current topic, it is recommended to perform a numerical drainage analysis, and compare these results against direct measurements of the drainage time prior to the loading, and also the observed drainage time during unloading of bucket.
This could lead to the finding of a limit for the loading velocity, which causes an undrained response.

8.1 Reflections and future studies

All in all, the tests were performed without any significant complications, and the results seems very reliable. Nonetheless, some changes regarding the test procedure should be considered before further work are conducted. The CPT suspension arrangement inside the tank could be modified to minimize the upward deflection, which influence the recorded q_c measurements, and hence other parameters derived from q_c.
Change of equipment regarding bucket installation should also be evaluated. The piston applied had a constant velocity, which was relatively high, so to reduce the build-up of excess pore pressure during penetration, the installation was performed stepwise. The best solution would be to use a device which is able to conduct the installation at a slower velocity.
Due to the multi-directional movement of the bucket, the wire transducers set to record horizontal movement created a unnecessary complicated framework for interpretation of displacements. It should be investigated whether or not applying a LVDT for measurements of horizontal movement could simplify the required calculation process.

Further work related to the undrained response of the bucket foundation in ULS design will include tests performed both monotonically and cyclically, on the half and full bucket. A new hydraulic piston are in the process of being acquired for AAU, which has an significantly longer range in terms of movement. This piston could make it possible to run high velocity experiments to failure due to cavitation.

References

Fisker and Kromann, **2004**. L.B. Fisker and K. Kromann. *Cyklisk Belastning af Bøttefundament i Tryktank*. Speciale ved AAU, 2004.

Houlsby, Ibsen, and Byrne, **2005**. G.T. Houlsby, L.B. Ibsen, and B.W. Byrne. *Suction caissons for wind turbines*. Frontiers in Offshore Geotechnics: ISFOG 2005, Taylor & and Francis Group, London, ISBN 978-0-415-58480-7, 75–93, 2005.

Ibsen and Lade, **1998**. L.B. Ibsen and P.V. Lade. *The Strength and Deformation*

Characteristics of Sand Beneath Vertical Breakwaters Subjected to Wave Loading. AAU Geotechnical Engineering Papers, Soil Mechanics Paper No 23(ISSN 1398-6465 R 9805), 1998.

Ibsen and Thilsted, **2011**. L.B. Ibsen and C.L. Thilsted. *Numerical study of piping limits for suction installation of offshore skirted foundations and anchors in layered sand*. Frontiers in Offshore Geotechnics II, ISBN 978-0-415-58480-7, 421–426, 2011.

Ibsen, Liingaard, and Nielsen, **2005**. L.B. Ibsen, M. Liingaard, and S.A. Nielsen. *Bucket Foundations, a status*. Conference Proceedings Copenhagen Offshore Wind 2005, 2005.

Ibsen, Hanson, Hjort, and Thaarup, **2009**. L.B. Ibsen, M. Hanson, T. Hjort, and M. Thaarup. *MC - Parameter Calibration for Baskarp Sand No. 15*. DCE Technical Report No. 62.(ISSN 1901-726X), 2009.

Moog, **1998**. Moog. *Programmable Servo Control for Hydraulic and Electric Drives*. 1998.

Pedersen and Kristensen, **2007**. T.S. Pedersen and L.K. Kristensen. *Bøttefundamenters styrke og deformationsegenskaber ved cyclisk belastning*. Speciale ved AAU, 2007.

Plaxis, **2010**. Plaxis. *Plaxis: Material Models Manual*. 2010.

Scanlifting, **2012**. Scanlifting. *Standard stålwire, 7X7 galv. stålwire*. URL: `http://www.scanlifting.dk/Produkt.aspx?p=440`, 2012. Accessed: 05/06/2012.

Sjelmo, **2012**. Å. Sjelmo. *Evaluation of the undrained behavior of cohesionless soils under monotonic loading*. Master Thesis at AAU, 2012.

Sørensen, Møller, Brødbaek, Augustsen, and Ibsen, **2009**. S. P. H. Sørensen, M. Møller, K.T. Brødbaek, A.H. Augustsen, and L.B. Ibsen. *Evaluation of Load-Displacement Relationships for Non-Slender Monopiles in Sand*. DCE Technical Report No. 79(ISSN 1901-726X), 2009.

Appendices

Part II

Description of Experiments

Appendix **A**

Description of Pressuretank

To perform monotonic loading tests on a bucket foundation under pressure, a tank is prepared in the laboratory at Aalborg University. When the tank is sealed, a pressure of 2 bar is applied to the system, simulating the hydrostatic pressure at 20 meter depth. The geometry, construction and function of the tank is described herein.

A.1 Dimensions of Pressuretank

The pressuretank has a cylindrical cross-section with an outer diameter of of 2.2 meter, as seen in Figure A.1.

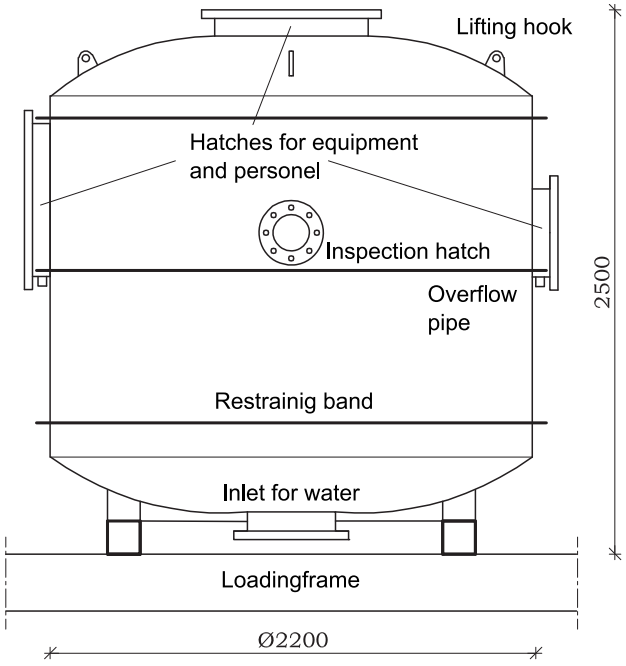

Figure A.1: *Dimensions of pressuretank.*

Figure A.2: *Image of pressuretank with loadframe.*

The tank is placed within a loadframe, which again is placed ontop a foundation, installed separately from the remaining floor in the laboratory hall. In Figure A.2, the pressuretank and loadframe are shown.

A.1.1 Water supply

The tank is connected to a water container with a volume of 1,2 m^3. The water container is placed somewhat higher than the tank, to be able to create a pressure gradient while saturating the sand inside the tank. The water pressure is controlled by a vault. The principle of letting water in and out of the tank are illustrated in Figure A.3.

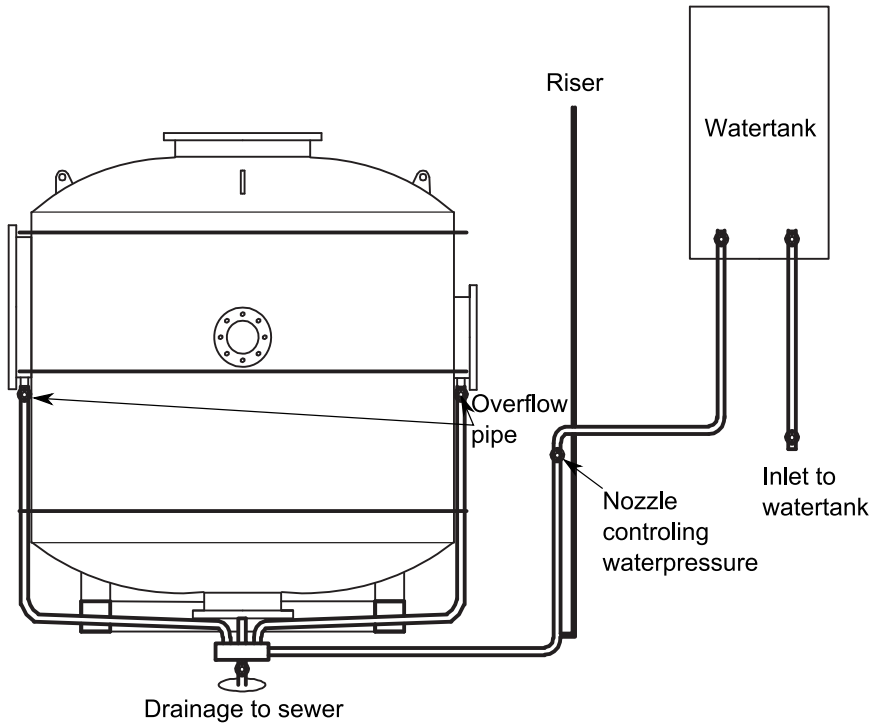

Figure A.3: *Illustration of the system providing water inside tank.*

A modified shower head is located at the bottom of the tank, which distributes water evenly in a horizontal direction. Three overflow pipes are placed inside the tank, which together with the shower head could be used to lead water out of the tank.

A.1.2 Outlet for measurement devices

At the other side of the largest entrance the outlet for the pressure, displacement, and loading transducers are located, as shown in Figure A.4.

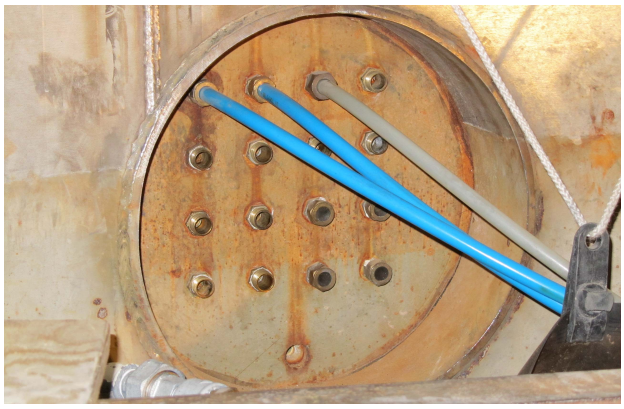

(a) Inside tank

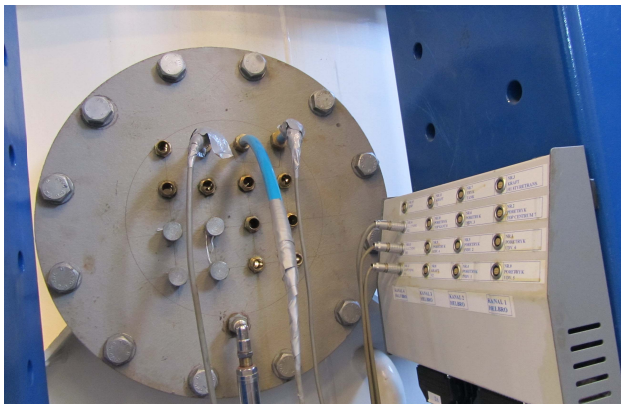

(b) Outside tank

Figure A.4: *Outlet for transducers.*

In total, 14 wires are led out through the tank. The wires collects the signal from

- 5 displacement transducers, 2 vertical and 3 horizontal
- 8 porepressure transducers
- 1 load transducer

All wires are inlaid in a flexible rubber hose. The hoses are pushed through the outlet shown in Figure A.4, and sealed with partially closed nut inlaid with a rubber o-ring, to reduce leakage when pressure is applied.

A.1.3 Applying pressure

Pressure inside the tank is generated by an external compressed air container which is connected to the tank. Figure A.5 show the compressed air container, along with the buffer tank which both are a part of the system allowing pressure to be applied inside the tank.

(a) Compressed air container, connected to the pressuretank.

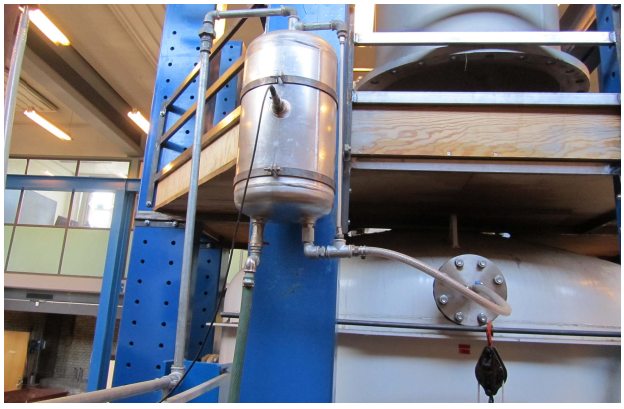

(b) Buffertank, and inlet to pressuretank.

Figure A.5: *Setup for applying and controlling pressure inside tank.*

It is difficult to seal the tank completely. So to compensate for the occurring leakage, a regulation nozzle can be adjusted to continuously add enough air to keep the desired pressure inside the tank. Figure A.6 illustrates the mechanisms controlling airflow into the tank.

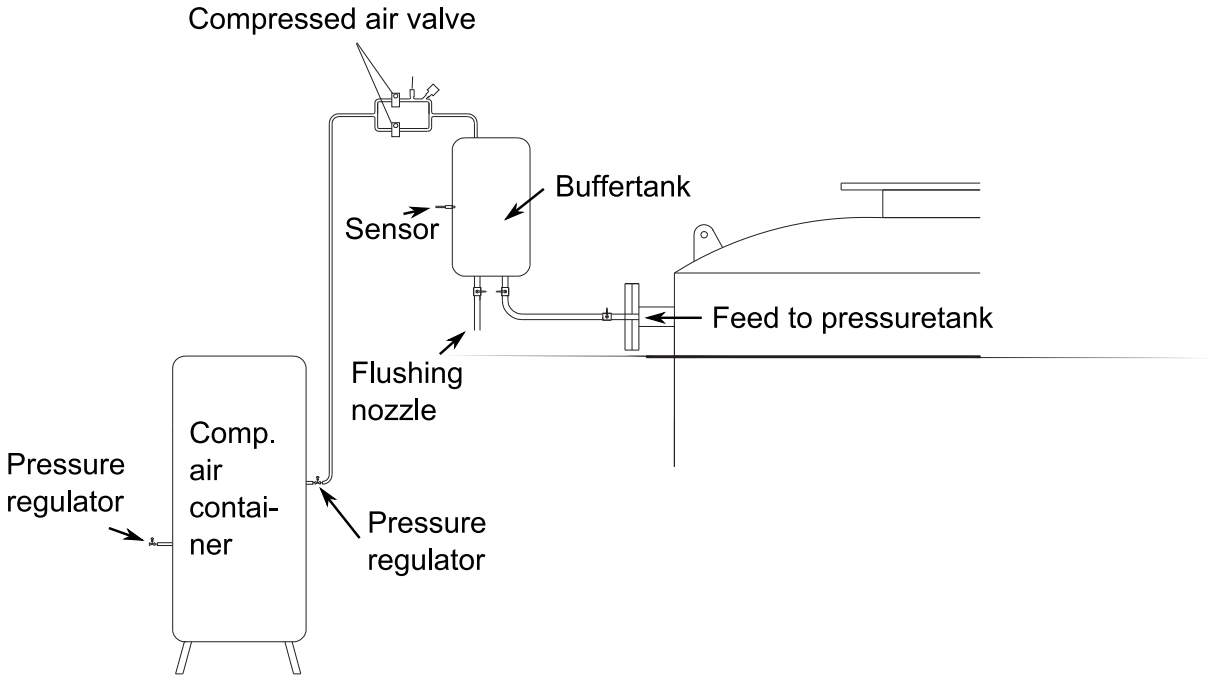

Figure A.6: *Illustration of the pressurized air system.*

Appendix **B**

Preparation of sand

In the following chapter, the procedure for preparation of the sand are described. The method applied are designed to ensure a homogeneous compaction of the sand, to make the test conditions as equal as possible.

B.1 Preparation of material inside pressure tank

The soil inside the tank is divided in two layers that serves different purposes. A layer of gravel is placed in the bottom of the tank, while above, sand is embedded, which is the soil in direct contact with the test object. Figure B.1 is an illustration of the soil layering. In he following section the layering of the soil is described.

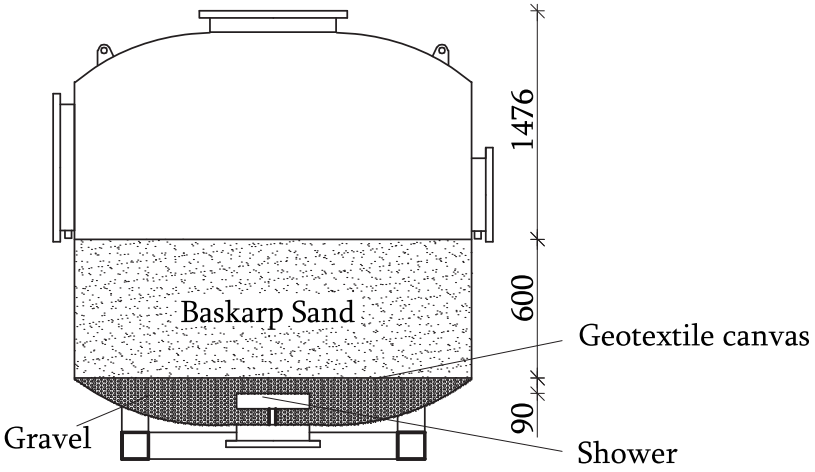

Figure B.1: *Gravel and sand inside tank, all dimesions in [mm].*

Gravel

The layer of gravel, which is approximately 30 cm at center tank, acts as a water distributor, leading water evenly throughout the bottom and creating a uniform water pressure at the transition between gravel and sand. The gravel is classified as described below:

- Product designation: Rock 4/8 class M
- Product description: Raw materials from old sea deposited beach ridges
- Location of production: Vigsø quarry, Hanstholm, Denmark.

Geotextile canvas

A geotextile canvas is placed ontop the gravel. The canvas prevents sand from falling through the gravel, and allow the gravel to maintain its main function; distributing water evenly throughout the tank cross section. The canvas is fixed to the pressuretank using a strip of silicone along the tank circumference.

Sand

The sand layer inside the tank is 60 cm deep, and is the actual deposit in which the model is installed. The sand used in the tank is Aalborg University Sand no. 1, which is a graded sand from Sweden. The larger grains are rounded, while the smaller grains are angular. The main part of the sand consist of quartz, but there are also traces of feldspar and Biotit. Aalborg University Sand no. 1 is classified by the following parameters [J.R Hedegaard, 1993]:

- Specific gravity: $d_s = 2.64$
- Void ratio in loosest state: $e_{max} = 0.858$
- Void ratio in densest state: $e_{min} = 0.549$
- 50% - fractile: $d_{50} = 0.14$ mm
- Coefficient of uniformity: $C_u = \frac{d_{60}}{d_{10}} = 1.78$

B.2 Procedure for embedding of sand

Homogeneous conditions in both horizontal and vertical direction is initially sought when preparing the sand inside the tank. A homogeneous deposit provides several advantages; the sand is modeled as only one layer in numerical calculations. Furthermore, scaling effects between different model sizes, and also previously performed tests at same density, could be compared.

B.2.1 Vibration of sand

For vibration of the sand inside the tank, a circular deck with holes in a desired pattern for vibration is produced. The circular deck consists of four elements, to be able to get the plate in and out of the tank, as seen in Figure B.2. The holes are spread out over the entire plate, in a grid with 20 cm between each hole, as seen in Figure B.3.

(a) Deck and rod vibrator inside pressuretank.

(b) Rod during vibration.

Figure B.2: *Equipment used for vibration of sand.*

To vibrate the sand, the rod is lowered through the holes in the deck, and into the sand, until the tip of the rod is approximately 1-2 cm over the geotextile canvas. It is important to keep the rod as perpendicular as possible relative to the sand surface. When the rod is at its designated depth it should be pulled slowly up through the sand, making sure that the sand is vibrated equally, and that no air pockets are formed.

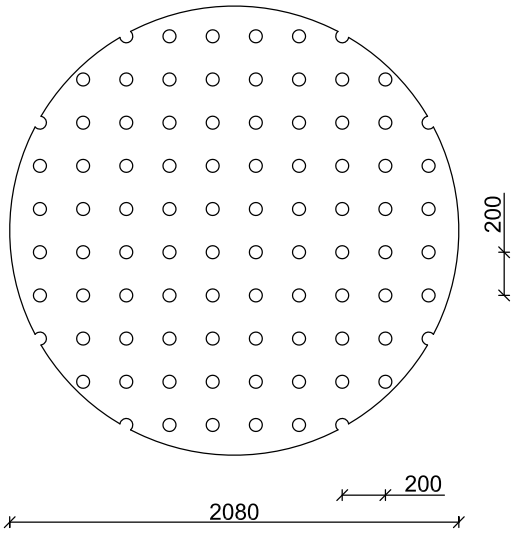

Figure B.3: *Sketch of deck with holes for vibration. All dimesions in [mm].*

The preferred procedure for preparing the sand is found from a series of tests, where different patterns of vibrations with the resulting void ratio are compared. The results of these tests are presented in [Fisker and Kromann, 2004]. After a test is run in the pressure tank, the sand is disturbed, and needs to be vibrated again to gain proper homogeneity. The recommended procedure to gain a homogeneous and dense sand are presented herein.

- The sand is leveled using the equipment described in B.2.3.
- The sand should be completely covered by the water, or else the rod vibrator will pull air into the sand. A suitable level of water is approximately 6 cm above the sand surface.
- The sand is loosened for $\approx$ 5 minutes, by applying water through the bottom shower as discussed in section B.2.2.
- The sand is vibrated one time, after the established pattern, see Figure B.4. First the holes marked by $\triangle$ are vibrated, followed by vibration of the holes marked with $\square$.

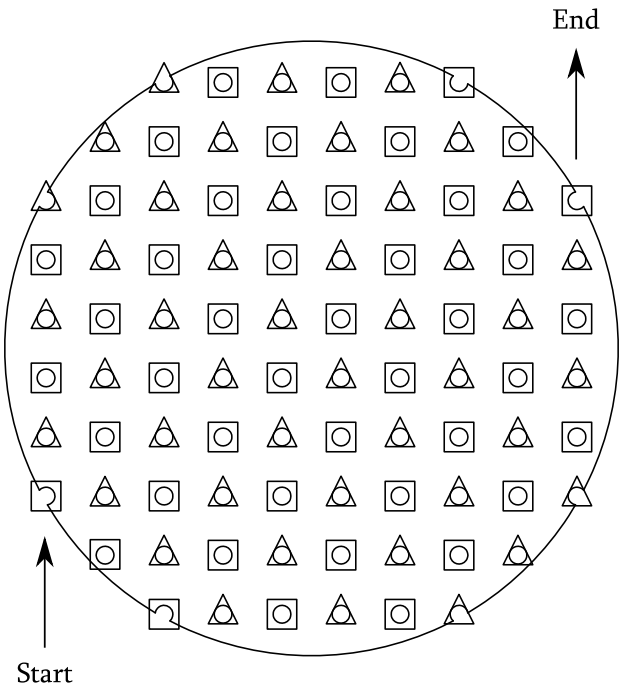

Figure B.4: *Illustration of the vibration pattern.*

- The sand is loosened again for 5 minutes.
- The vibration procedure is repeated once more.
- When the vibration is finished, water is let out from the tank until the water surface is below the surface of the sand. This is done slowly, with a small back-pressure, which ensures uniform drainage throughout the sand and gravel, so that the sand maintain full saturation after the process is completed.
- The sand surface is leveled.
- Water is led back into the tank, until the water surface coincides with that of the sand.
- Thereafter, to get the desired water level inside the tank, water is filled slowly from the top. This is done by placing a steel plate, $\approx 0.25\ m^2$, ontop the sand, on which a hose is fixed, so to avoid disturbance of the sand surface, see Figure B.5.
- The prepared sand is ready for testing.

Figure B.5: *Hose connected to plate which is used to fill the tank with water after the sand is vibrated and leveled.*

B.2.2 Loosening of sand

Before vibrating the sand, the sand needs to be Loosened. This is done by letting water in from the tank, mentioned in A.1.1, through the shower and into the soil. The water must be enter the soil under a suitable velocity. If the loosening take place with a to high hydraulic gradient, flow channels could develop, and hence reduce the soil strength. Based on experiments performed earlier at the Foundational laboratory at Aalborg University (Larsen & Ibsen, 2003), the applied hydraulic gradient, i, during the process is equal to 0.91. The hydraulic gradient, i, describes the reduction in energy, or head loss, per unit length:

$$i = \frac{\delta h}{l} \tag{B.1}$$

where

i	Gradient [-]
δh	Loss of energy between two randomly chosen heights/sections [m]
l	Length of sample [m]

Applying the upward gradient through the sand from the bottom of the tank is performed before each round of vibration.

B.2.3 Leveling the sand

To gain a completely flat and horizontal surface of the sand after vibration, a customized leveling device is used. The device is installed at the top of the tank, and is adjustable in height, so to fit different levels of sand. See Figure B.6 for illustration of the leveling device. At the tip of the device, there is a rotating head, where a thin steel board is attached. When the right height is set, the board is connected to the rotating head, and then spinned around until the sand surface is plane.

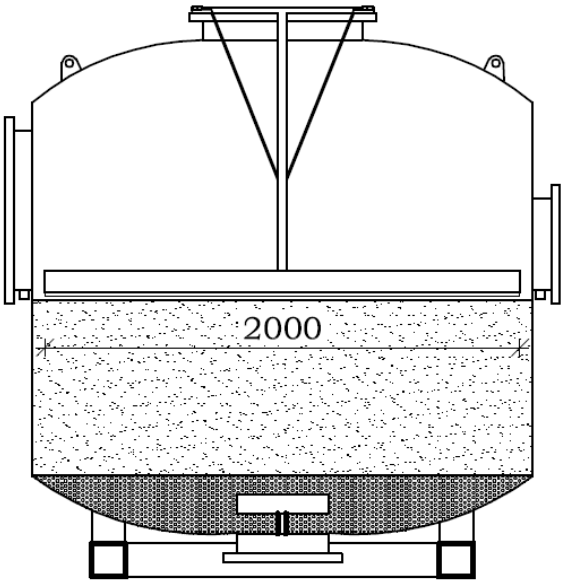

Figure B.6: *Illustration of leveler installed in the pressure tank. All dimensions in [mm].*

Appendix **C**

CPT Testing in Pressuretank

To determine the homogeneity, strength, and density of the sand inside the tank, CPT's are performed. The CPT, or ***Cone Penetration Test****, measures the tip resistance exerted on the cone from the soil during penetration. The output could be used to determine a series of soil properties, by various empirical relationships.*

C.1 Equipment used for CPT

The strength of the sand is determined based on CPT's. The applied equipment consists of a CPT probe, a hydraulic piston, and an suspension device allowing tests performed at desired location inside the tank. The CPT probe has a length of 600 mm and a diameter of 15 mm. Furthermore, the probe is designed for a maximum resistance equal to 2 kN.

The first step to perform a CPT is to install the hydraulic piston ontop the pressure tank. Then the suspension device, a triangular arm, is attached beneath the piston, inside the tank. The CPT probe is thereafter assembled to the arm. The arm is free to be rotated 360 degrees inside the tank, and at the same time the probe could be moved anywhere along the arm in a radial direction from the tank center, to approx 15 cm from the tank wall. When the desired coordinate of the CPT is located, the probe can be fixed to that position, as seen in Figure C.1. While penetration of the probe, the depth is continuously measured using a wire transducer of the type W510-1000-R1K-L10 1000 mm, as shown in Figure C.1.

(a) Setup inside tank.

(b) Wire transducer, at the top of the tank.

Figure C.1: *Complete CPT setup.*

C.2 Calibration of CPT equipmen

The output from the CPT's are millivolt, mV. To transfer mV to kN, the equipment needs to be calibrated. This is done assembling the CPT probe to a stable frame, and loading it with various known weights. The results from the calibration can be seen in Figure C.2.

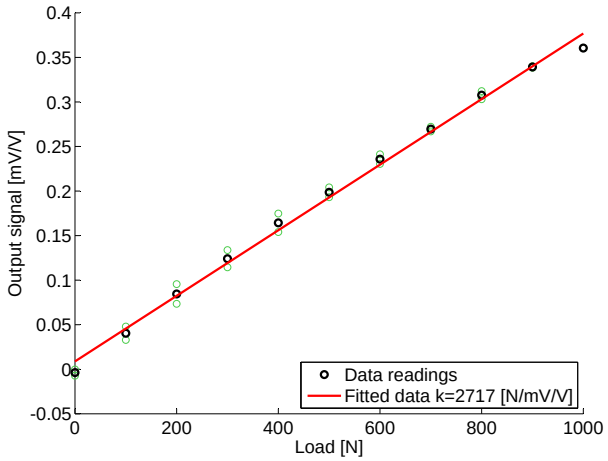

Figure C.2: *Fitted relationship between output in mV/V and N for calibration of CPT equipment.*

C.3 Interpretation of CPT data

Besides determining the homogeneity of the deposit, the output from the CPTs are also used to determine several strength and stiffness parameters, which in turn could be used as input in numerical modeling. The parameters found are those presented in Table C.3. The methods applied to derive these values are described in Ibsen et al. [2009]; where results from triaxial tests were investigated to find a relationship between D_r, ϕ_{tr} and the confining pressure, σ'_3, as shown in Equation C.1. D_r and σ'_3 could also be used to find the dilatation angle, ψ_{tr}, as seen in Equation C.2.

$$\phi_{tr} = 0.152 \cdot D_r + 27.39 \cdot \sigma'^{\,-0.2807}_3 + 23.21 \tag{C.1}$$

$$\psi_{tr} = 0.195 \cdot D_r + 14.86 \cdot \sigma'^{\,-0.09764}_3 - 9.946 \tag{C.2}$$

Where σ'_3 are found by $K_0 = (1 - sin\phi_{tr})$.
Equations C.3 to C.6 summarizes the iterative process of finding the relative density, D_r.

$$\gamma' = \frac{d_s - 1}{1 + e} - \gamma_w \tag{C.3}$$

$$\sigma'_1 = \gamma' \cdot x \tag{C.4}$$

$$D_r = c_2 \cdot \frac{\sigma'^{\,c_3}_1}{q_c^{c_1}} \tag{C.5}$$

$$D_r = \frac{e_{max} - e}{e_{max} - e_{min}} \cdot 100 \tag{C.6}$$

Where γ' is the submerged unit weight of the sand in kN/m^3, and γ_w = 10.0 kN/m^3 is the unit weight of water. σ'_1 is the vertical effective stresses in MPa. c_1 = 0.75, c_2 = 5.14, c_3 = -0.42, are fitting constants applied in Equation C.5, unique for Aalborg University Sand no. 1, and the used CPT equipment. e is the actual void ratio of the deposit.

The methods presented in Ibsen et al. [2009] also allows for determining stiffness parameters of the sand, such as the tangential and secant stiffness, E_0 and E_{50}, cf. Equations C.7 and C.8.

$$E_{50} = (0.6322 \cdot D_r^{2.507} + 10920) \cdot (\frac{c \cdot cos\phi_{tr} + \sigma_3' \cdot sin\phi_{tr}}{c \cdot cos\phi_{tr} + \sigma_3'^{ref} \cdot sin\phi_{tr}}) \tag{C.7}$$

$$E_0 = \frac{2 \cdot E_{50}}{2 - R_f} \tag{C.8}$$

Where $\sigma_3'^{ref}$ is a reference pressure equal to 100 kPa, and R_f a failure ratio, normally set to 0.9.
The determination of E_{50} and E_0 based on CPT results at low effective stresses, are associated with significant uncertainties. Therefore, these values are not presented in the current report.

By calculating Equation C.3 to C.6, and setting the convergence tolerance value of e equal to 10^{-4}, e and hence D_r are found after 4-5 iterations.
The resulting D_r and ϕ_{tr} for the conducted 4 tests are presented in Table C.3.

Test No.	D_r	ϕ_{tr}	ψ_{tr}	γ'	K_0
	[%]	[°]	[°]	kN/m^3	[−]
1	83.81	46.80	17.16	10.26	0.27
2	89.52	47.81	18.33	10.37	0.26
3	89.25	47.76	18.27	10.37	0.25
4	85.66	47.12	17.54	10.29	0.26

C.4 Sources of Error During CPT

A problem encountered during CPT runs is that the suspension arm tends to bend upwards as the penetration resistance increases. The further out on the arm the CPT probe is located, the more the arm tends to bend. The stiffness of the arm itself is sufficient. The weakness of the entire setup lies within the connection between the rod from the piston, and the suspension arm.

This error leads to a small deviation between the measured penetration depth and the actual penetration depth, due to the fact that the wire transducer is connected to the piston rod at the center of the tank. A deviation between actual and measured penetration depth, could also, to some degree, influence the measured q_c, which in turn would influence the resulting D_r and ϕ_{tr}.

Still, an accurate measurement of the deviation is not performed, but is approximately 10 mm when the CPT-probe are located far out on the suspension arm.

Appendix **D**

Bucket tests

Four monotonic loading experiments are performed on the bucket foundation at different velocities. The bucket is 250 mm high, and has a diameter of 500 mm. Eight pressure transducers are located on the bucket, reading the pore pressure build-up during the tests. The current chapter contains a description of the equipment used both inside the tank during testing, and the equipment applied to process the recorded signals.

D.1 Equipment for Bucket Test

The test setup for the bucket foundation involves a great deal of laboratory equipment. An illustration of the test set up are presented in Figure D.1.

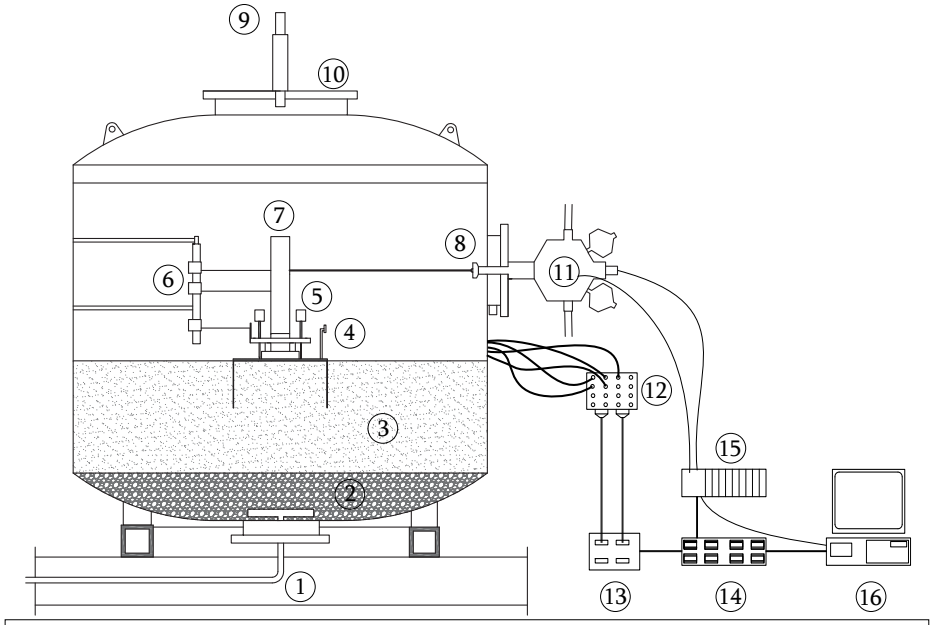

Figure D.1: *Illustration of test setup.*

The following chapter describes the equipment used during testing, and the chosen test program.

D.1.1 Model of Bucket

The bucket applied in the tests were equipped with eight pressure transducers, HBM P3MBA 5 bar, located at various positions to measure the development of pore pressures during loading. Three of the transducers are located beneath the bucket lid, in an centered line parallel to the loading direction. The remaining transducers are also installed approximately along this line, down along the rear part of the skirt, cf. Figure D.2

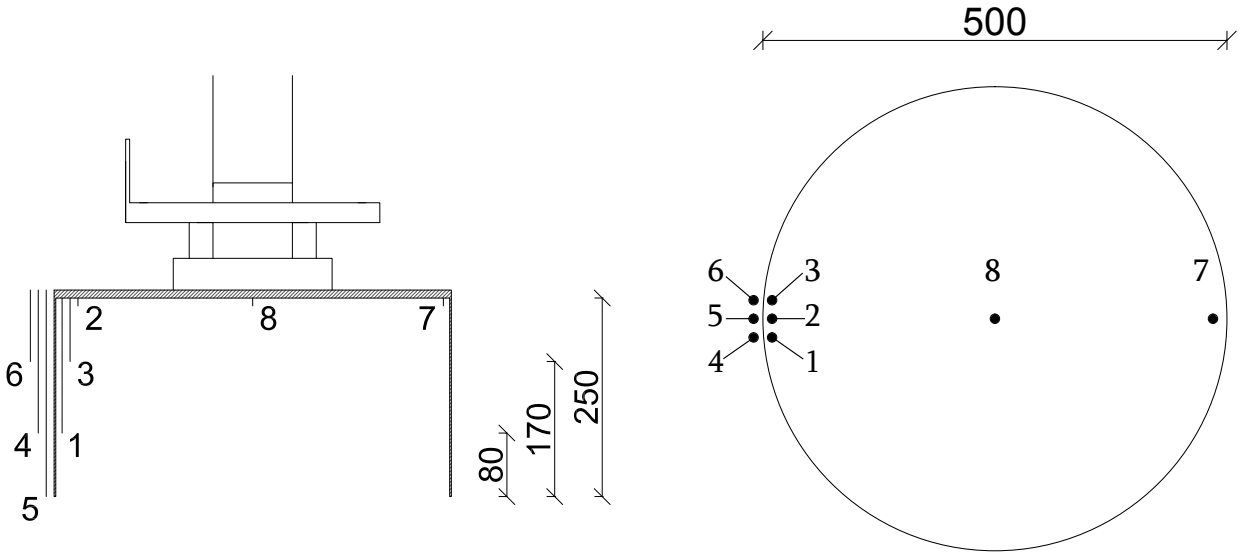

(a) (b)

Figure D.2: *Location of pore pressure transducers, with loading direction towards right. All dimensions in [mm].*

The location of the transducers, along with the serial number and corresponding calibration factors are listed in Table D.1. Bucket geometry are described in Table D.2. The listed calibration factors are those presented from the manufacturer. Hence, no new calibration of the pressure transducers are performed.

Serial no.	Location	Calibration factor $[mV/V]$	Height over skirt tip [mm]
1566930	1 Inside	1.997	80
1566934	2 Inside	1.989	250
1532184	3 Inside	1.998	170
1660087	4 Outside	1.995	80
1660074	5 Outside	1.995	0
1660076	6 Outside	1.994	170
1575930	7 Inside	1.992	250
1660089	8 Inside	1.995	250

Table D.1: *Location of pore pressure transducers.*

Description	Dimension [mm]
Outer diameter, D_{out}	500
Inner diameter, D_{in}	496
Outer skirt height, l_{out}	260
Inner skirt height, l_{in}	250
Skirt thickness, t_{skirt}	2
Top lid thickness, t_{lid}	10

Table D.2: *Geometrical properties of bucket model.*

D.1.2 Loading, Measurements and Data Collection

The information regarding all tests is collected by in total 15 transducers; 8 pore pressure transducers, 3 horizontal displacement transducers, 2 vertical displacement transducers, and 1 load transducer, which are located inside tank, cf. Figure D.3.

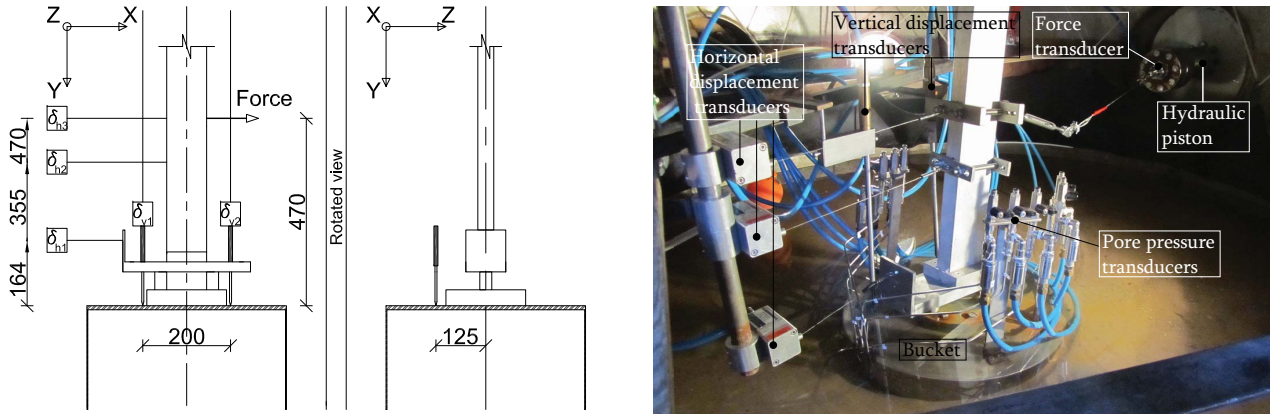

(a) (b)

Figure D.3: *Setup inside tank. All dimensions in [mm].*

The last transducer is connected directly on the tank, below the outlet cover as seen in Figure A.1.2, and reads the pressure level inside the tank throughout the test. A description of all transducers applied in the tests are presented in Table D.3.

Transducer type	Number	Description
Pore pressure	8	HBM P3MBA 5 bar
Tank pressure	1	HBM P6A 10 bar
Horizontal disp.	3	WS10-1000-R1K-L10
Vertical disp.	2	HBM WA/100mm
Load	1	HBM U2B 10 kN

Table D.3: *Number and description of applied transducers.*

All of the cables, which are connected to the transducers inside the tank, are led through the tank to a signal assemblance box. The signal assemblance box contains 16 channels, which the cables are plugged into. The signals are then sent through a distribution box and further to a signal amplifier, MGC plus, and ends up as an output file in Catman 5.0, cf. Figure D.4 and overall illustration of set-up in Figure D.1.

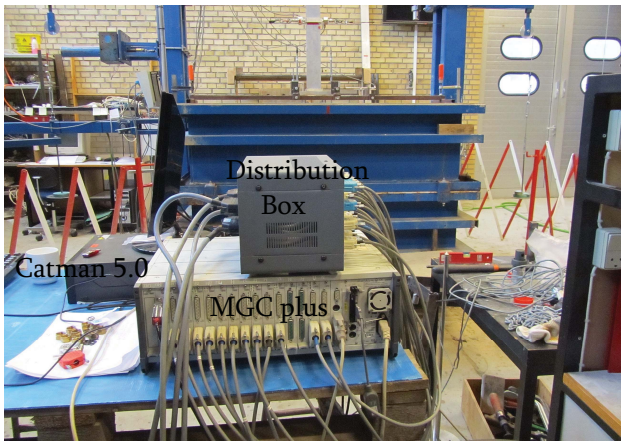

(a) Distribution box, MGC plus and Catman 5.0.

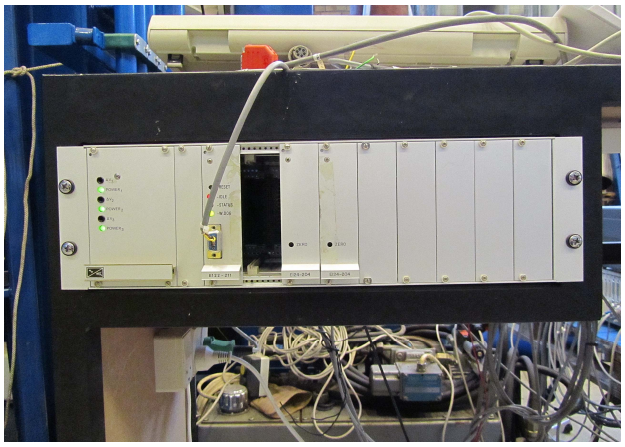

(b) PSC-rack.

Figure D.4: *Data setup, processing signals from tests.*

The loading of the bucket inside the pressure tank are performed by a hydraulic piston, M2000 PCS2. The actuated movement of the piston are controlled through Catman 5.0, where both the data sampling and signal feed frequencies are controlled.
For each test, different input files were generated to initiate piston movement and uploaded to the PSC-rack, cf. Figure D.4. The input files contained a positioning map, or code, which needed to fit the total loading time and signal feed frequency. Table D.4 summarizes the frequencies applied in the tests.

Test No.	Signal feed frequency [Hz]	Sampling frequency [Hz]	Test duration [s]	Displacement [mm]
1	10	10	4000	40
2	10	10	400	40
3	10	10	40	40
4	25	25	4	40

Table D.4: *Sample and feed frequencies for all tests*

Altering the signal feed from 10 to 25 Hz implies updating the piston position 25 times per second, instead of 10 times per second. It should be noted that a minor lag was experienced in test 4 at 25 Hz. To get a more elaborate description of the signal processing, the reader is advised to confer the work presented in Pedersen and Kristensen [2007].

D.2 Test Program

Four monotonic loading tests are performed on the bucket foundation model to examine how the pore pressures develop during loading. The loading is applied as a forced translation of the tower, which is attached by a steel wire to the hydraulic piston, at an horizontal arm equal to 470 mm above bucket lid, cf. Figure D.1.2.

Test no.	Displacement per sequence [mm]	Number of sequences [-]	Loading time [s]	Unloading time [s]
1	40	3	4000	400
2	40	3	400	400
3	40	3	40	40
4	40	3	4	4

Table D.5: *Program for performed tests.*

Table D.5 display the chosen test program. Note that the "Displacement" column refers to horizontal movement of piston, and not bucket. The displacement of 40 mm is limited by the piston. It cannot move any longer. Hence, to see how the soil response would effect the mobilized force at large displacements, the loading was commenced in 3 sequences, providing a total displacement of 120 mm for the piston.
Note that the unloading time for test 1 is 10 times faster than the loading time, while the other tests had the same time for loading and unloading. An illustration of the test program is shown in Figure D.5.

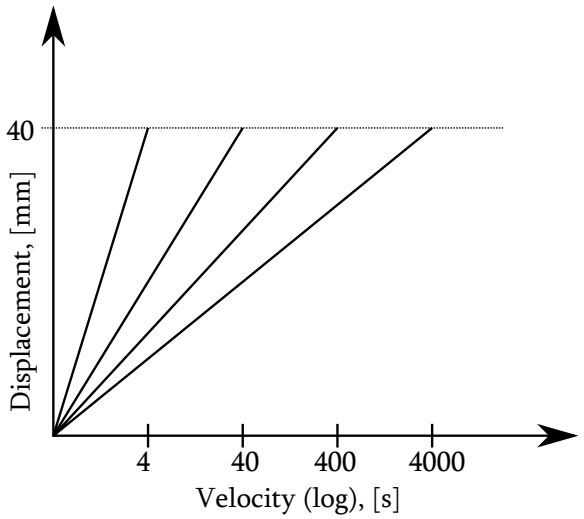

Figure D.5: *Loading velocities for all tests.*

D.3 Interpretation of displacements

This section contains a brief description of the trigonometrical considerations assessed to calculate the correct horizontal, vertical and rotational movements during loading of bucket.

An illustration of the test setup is shown in Figure D.6. Vertical displacement transducers are located at $y1$, $y2$ and $y3$. Their readings are represented by δ_{h1}, δ_{h2} and δ_{h3} respectively. Horizontal displacement transducers are located at $x1$ and $x2$ and their readings are represented by δ_{v1} and δ_{v2} respectively. C is a reference point where displacements and rotation are obtained, located at the center of the bucket lid.

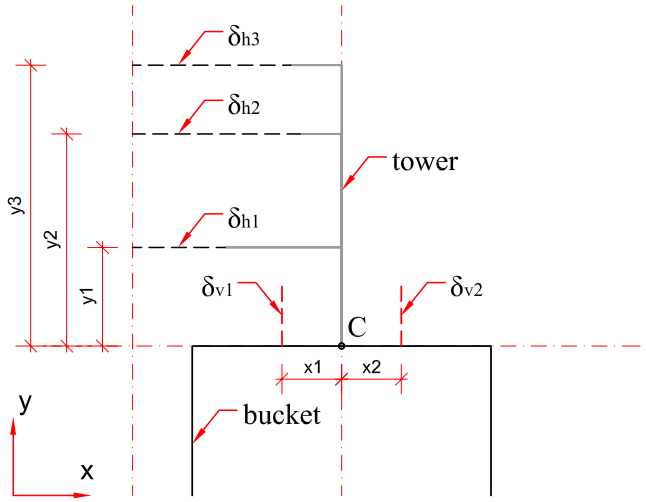

Figure D.6: *Scheme of the test setup.*

It could with fair accuracy be assumed that the bucket model experience movement in three degrees of freedom (DOF) during loading: Movement in horizontal, u, and vertical, w, directions, and rotation, θ, cf. Figure D.7.

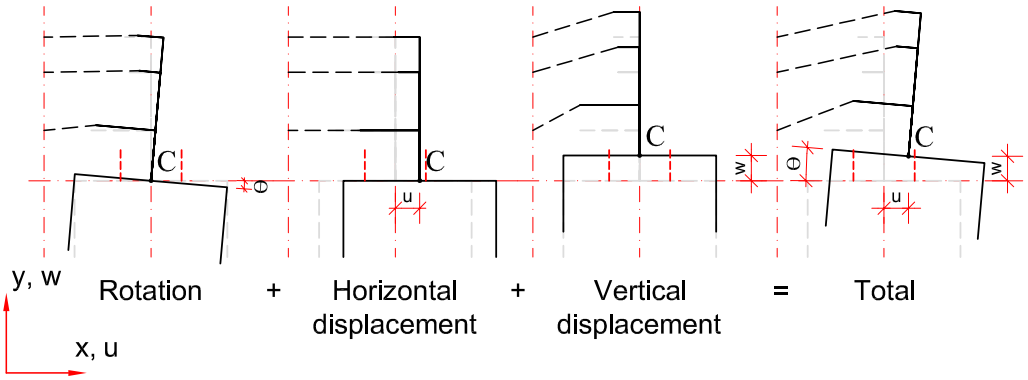

Figure D.7: *Strategy for finding the correct horizontal and vertical displacement of bucket.*

From Figure D.7 it can bet seen that each of DOF has its own contribution to final horizontal displacement, cf. Figure D.8. $\delta_{h\,ini}$ is the reading in the initial stage of the test, $\delta_{h\,rot\,x}$ and $\delta_{h\,rot\,y}$ are the contribution in x and y directions due to the rotation, $\delta_{h\,u}$ and $\delta_{h\,v}$ are the contributions of translation of the bucket in x and y directions respectively, δ_h is the wire length when the bucket is moved in all DOF.

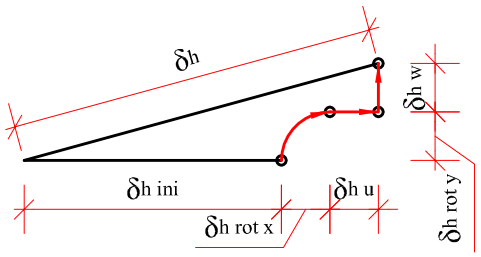

Figure D.8: *Wire position changes due to the movement of the bucket.*

Following relationship can be designed:

$$\delta_h = \sqrt{\left(\delta_{h\,ini} + \delta_{h\,rot\,x} + \delta_{h\,u}\right)^2 + \left(\delta_{h\,rot\,y} + \delta_{h\,w}\right)^2} \tag{D.1}$$

Rotation angle is obtained from vertical displacement transducer readings by the following equation:

$$\Theta = \arctan\left(\frac{\delta_{v1} - \delta_{v2}}{x1 + x2}\right) \tag{D.2}$$

Wire elongation in x and y directions due to a rotation are obtained:

$$\delta_{h\,rot\,x} = x_{ini} - \left(x_{ini} \cdot \cos(\Theta) - y_{ini} \cdot \sin(\Theta)\right) \tag{D.3}$$

$$\delta_{h\,rot\,y} = x_{ini} - \left(x_{ini} \cdot \sin(\Theta) + y_{ini} \cdot \cos(\Theta)\right) \tag{D.4}$$

Where x_{ini} and y_{ini} are the initial coordinates of the point. $\delta_{h\,u}$ and $\delta_{h\,w}$ are obtained from Equation D.1 by an iterational procedure. For the first iteration $\delta_{h\,w}$ is set to 0 and $\delta_{h\,u}$ is obtained. Then the value is inserted into Equation D.1 and a new value for $\delta_{h\,w}$ is obtained, which is used in the next iteration. This procedure is continued until the difference of $\delta_{h\,w}$ values in two last iterations is smaller than 0.0001.

When position and rotation of the bucket is known for all three test sequences, the point of rotation can be obtained, cf. Figure D.9.

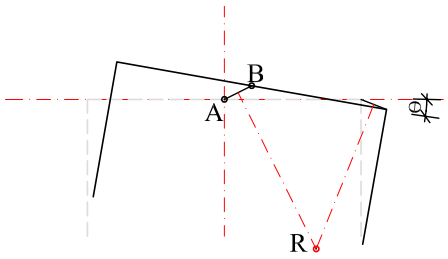

Figure D.9: *Scheme for obtaining the rotation point.*

Point A represents the initial position of the bucket, point B represents position after displacement and point R is the point of rotation, which is obtained by solving the following matrix for R_x and R_y.

$$\begin{bmatrix} B_x \\ B_y \\ 1 \end{bmatrix} = \begin{bmatrix} r_{00} & r_{01} & R_x - r_{00} \cdot R_x - r_{01} \cdot R_y \\ r_{10} & r_{11} & R_y - r_{10} \cdot R_x - r_{11} \cdot R_y \\ 0 & 0 & 1 \end{bmatrix} \cdot \begin{bmatrix} A_x \\ A_y \\ 1 \end{bmatrix}$$

where

$$r_{00} = \cos(\theta) \tag{D.5}$$

$$r_{01} = -\sin(\theta) \tag{D.6}$$

$$r_{10} = \sin(\theta) \tag{D.7}$$

$$r_{11} = \cos(\theta) \tag{D.8}$$

Appendix **E**

Permeability testing

When performing monotonic loading experiments in the pressure tank, the corresponding pore pressure build up are measured. How this pore pressure builds up is dependent on loading velocity as well as the permeability, K, of the soil. Therefore, several permeability tests are performed on Aalborg University Sand no. 1, which is the same sand as inside the pressure tank. The permeability of Frederikshavn sand 103-47 will also be determined. The permeability tests are performed at different void ratios, e, so to find an approximate relationship between K and e. The permeability is found using the falling head procedure.

E.1 Types of sand

The permeability of two types of sand will be investigated.

- Frederikshavnersand 103-47
- Aalborg University Sand no. 1

In the following section, the relevant basic sand properties will be presented, such as

- Grain size distribution
- Specific gravity, d_s
- Maximum and minimum void ratio, e_{max} and e_{min}
- Mean grain size, d_{50}
- Uniformity coefficient, $C_U = \frac{d_{60}}{d_{10}}$

E.1.1 Aalborg University Sand no. 1

Aalborg University Sand no. 1 is a graded sand from the Baskarp quarry in Sweden. The larger grains are rounded, while the smaller grains are angular. The main part of the sand consist of quartz, but there are also traces of feldspar and Biotit. Although Aalborg University Sand no. 1 is regularly used in various geotechnical projects at AAU, there exists no studies of its permeability. See Table E.1 for the classification properties of Aalborg University Sand no. 1.

Property	Value
Specific gravity, d_s	2.644
Void ratio in looses state, e_{max}	0.858
Void ratio in densest state, e_{min}	0.549
Mean grain size, d_{50}	0.14 mm
Uniformity coefficient, $C_U = \frac{d_{60}}{d_{10}}$	1.78

Table E.1: *Classification properties for Aalborg University Sand no. 1.*

The grain size distribution is presented in Figure E.1.

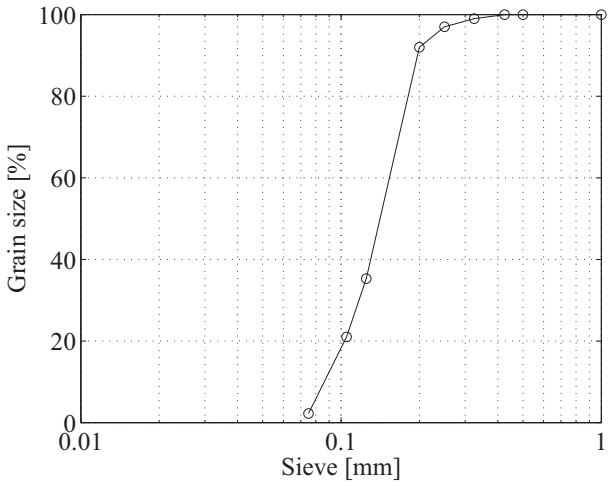

Figure E.1: *Plot of grain-size distribution for Aalborg University Sand no. 1. [Ibsen et al., 2009]*

E.1.2 Frederikshavn sand 103-47

No classification data for the Frederikshavn sand were available, so before the permeability tests could be executed, some basic properties needed to be found. This includes determining the grain size distribution, $e_{min} - e_{max}$, and specific gravity, d_s.
The Gotechnical Engineering Laboratory at AAU, GELAAU, has developed a series of guides for classifying various geotechnical properties. All properties for Frederikshavn sand 103-47, which are listed in Table E.2, were found following these guidelines.

Property	Value
Specific gravity, d_s	2.64
Void ratio in looses state, e_{max}	0.969
Void ratio in densest state, e_{min}	0.621
Mean grain size, d_{50}	0.158 mm
Uniformity coefficient, $C_U = \frac{d_{60}}{d_{10}}$	1.74

Table E.2: *Classification properties for Frederikshavn sand 103-47.*

Grainsize distribution

The guideline presenting the procedure for determining the grainsize distribution are based on the standard DS/CEN ISO/TS 17892-4.

The grainsize distribution are determined based on three samples of approximately 100 grams each. After the first test, it was seen that the weightlimit for one of the sieves, 0.125 mm, were surpassed. Therefore, due to the uniformity of the sand, the samples were divided in half. Also, three additional sieves were included in the following tests, 0.212, 0.18 and 0.09 mm. The plot from the grain size distribution are shown in Figure E.2.

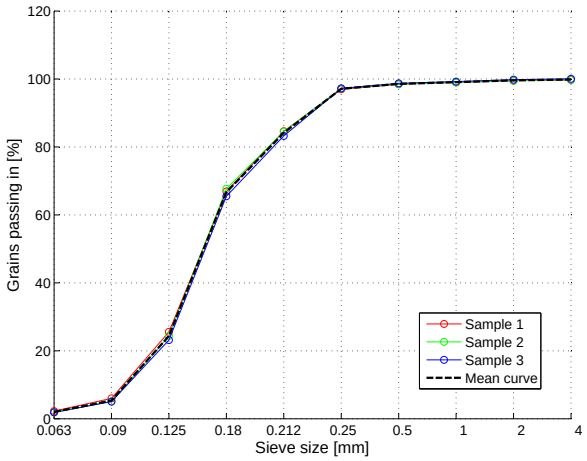

Figure E.2: *Plot of grain-size distribution of Frederikshavn sand 103-47, three samples combined.*

The applied sieves for fine screening were; 4, 2, 1, 0.5, 0.25, 0.212*, 0.18*, 0.125, 0.09*, and 0.063 mm, where * denotes the non-standard sieves. The average fines content for the three samples are 2 %. The remnants in sieves with 4, 2 and 1 mm, mainly consisted of shells.

Dense and loose state, e_{min} - e_{max}

To determine a relative density, D_r, of the sand, it is necessary to find the loosest and densest state of the material. It should be mentioned that e_{min} and e_{max}, and especially e_{min}, are not absolute values. Meaning that the sand could occur in denser states than that found from laboratory experiments. This would be the apparent reason for reaching an D_r of 101.5% while building in a sample for one of the permeability tests presented in Appendix G.3.

The apparent void ratio, e, is calculated as shown in Equation E.1.

$$e = \frac{d_s \cdot \rho_w \cdot V}{M_{Sand}} - 1 \tag{E.1}$$

where

d_s	Specific gravity, 2,64 [-]
ρ_w	Density of water, 1 $[g/cm^3]$
V	Volume of material, $[cm^3]$
M_{Sand}	Mass of sand, [g]

Four experiments were performed to determine e_{max}. The results are presented in Table E.3.

	M_{cyl}	$M_{cyl+sand}$	M_{sand}	V	e
	[g]	[g]	[g]	$[cm^3]$	[-]
Test 1	239.13	332.82	93.69	70.07	0.974
Test 2	239.13	333.13	94.00	70.07	0.968
Test 3	239.13	332.97	93.84	70.07	0.971
Test 4	239.13	333.33	94.20	70.07	0.964
Mean	239.13	333.06	93.93	70.07	0.969

Table E.3: *Loosest state of Frederikshavn sand 103-47.*

Three experiments were performed to determine e_{min}. The results are presented in E.4.

	M_{cyl}	$M_{cyl+sand}$	M_{sand}	V	h	e
	[g]	[g]	[g]	$[cm^3]$	[mm]	[-]
Test 1	239.13	347.77	108.64	6.68	66.87	0.625
Test 2	239.13	348.17	109.04	6.68	66.87	0.619
Test 3	239.13	348.06	108.93	6.68	66.87	0.621
Mean	239.13	348.00	108.87	6.68	66.87	0.621

Table E.4: *Densest state of Frederikshavn sand 103-47.*

Specific gravity, d_s

The specific gravity, or particle density, is determined based on the pycnometer method. The guideline produced bye the GELAAU are based on the standard DS/CEN ISO/TS 17892-3. In the guideline it is stated that:

> *For soil without organic content, d_s is expected to vary from 2.65 for clean quartz sand to 2.85 for certain clay minerals. For soil containing especially heavy or light minerals, d_s can adopt values outside of this area.*

This statement is in good agreement with the results presented in Table E.2, where the relatively low d_s-value are due to the presence of shells.

The guideline further defines the specific gravity as:

$$d_s = \frac{\text{Weight of a given volume of soil grains}}{\text{Weight of the same volume deonised water at 4 °C}}$$

or

$$d_s = \frac{W_s}{V_s \cdot \rho_w} \tag{E.2}$$

where

W_s Weight of dry grain material, [g]

V_s Volume of dry grain material, $[cm^3]$

ρ_w Density of deonised water at 4 °C, = 1 g/cm^3

E.2 Falling Head Procedure

To determine the permeability of both AAU sand no 1 and Frederikshavn sand, the falling head method is applied. A setup of the test are illustrated in Figure E.3.

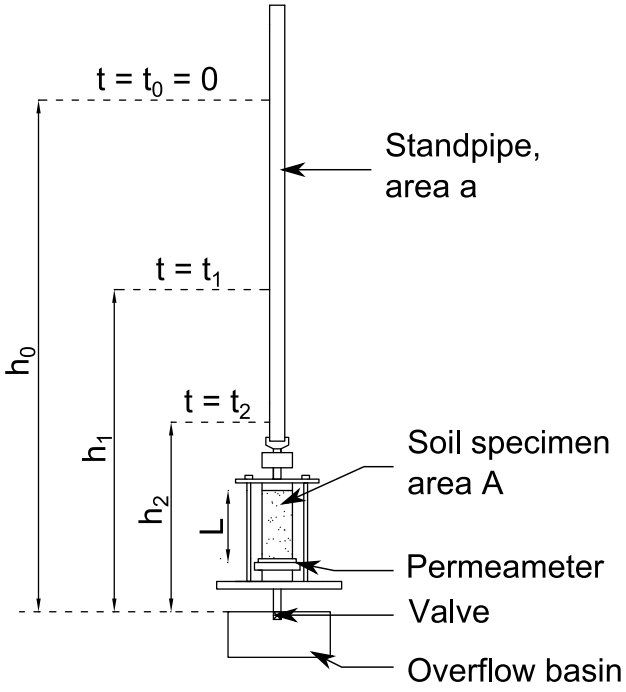

Figure E.3: *Illustration of the falling head test set up.*

The setup consists of basically three parts; the permeameter, an overflow basin, and a standpipe. A soil specimen is built into a cylinder which is placed inside the permeameter device, and saturated under a suitable gradient, depending on the density of the sample.

Water is led through the specimen, and further up the standpipe to a chosen point of reference, which is the initial starting point for all tests. The initial startingpoint for these performed tests are 220 cm above the reference level (overflow basin, see Figure E.3), or 20 cm above h_0, which is at 200 cm above reference level. h_0 denotes the initial hydraulic head, while h_2 denotes the final hydraulic head.
The water level at reference level is held constant, due to an overflow arrangement. The experiment starts when the valve beneath the permeameter are opened.

The corresponding flow time between h_0 and h_1 are denoted t_1, and h_1 - h_2 are denoted t_2.

During the test, the flow time between h_0, h_1 and h_2 are measured. The test is repeated until a reproducible value of t_2 is obtained. Using the obtained flow times, t_1 and t_2, along with measured temperatures, the hydraulic conductivity and permeability can be found using fairly simple analytical relationships, presented in Section E.4.

E.3 Preparation of specimen

First a relative density, D_r, is chosen for the specimen. Using e_{min} - e_{max} and d_s, the approximate weight of the sand could be calculated. The sand is then built into the plexiglass cylinder, with height of 200 mm and a diameter of 70 mm. The specimen is then placed in the permeameter. Vacuum is applied, draining the air from the sample, at the same time as de-aired and de-ionised water is led through the bottom filter and up through sand under a small gradient. As the water slowly rises in the specimen, the air left inside the sand are flushed out through the top filter. As the water rises above the top filter, the sand should be fully saturated.

E.4 Applied theory

The flow of water through pores and voids in soil masses could in most cases be considered laminar. If the flow is laminar, the relationship between flow velocity, v, and hydraulic gradient, i, are linear. This relationship is expressed in E.3, which is called Darcy's law.

$$v = ki \tag{E.3}$$

Where i is the ratio of head loss h per unit length l, as seen in Equation E.4

$$i = \frac{h}{l} \tag{E.4}$$

Furthermore, considering a laminar and quasi static flow, the discharge from the standpipe should be equal to the amount of water passing through the specimen per unit time. Therefore, the hydraulic conductivity, and hence permeability, could with reasonable accuracy be described with the continuity equation and Darcy's law [W.P. Lund, 1998].
At the time t, the continuity equation is given as:

$$-\frac{dh}{dt} \cdot a = A \cdot v \tag{E.5}$$

where

a	Area of standpipe
A	Area of specimen
v	Flow velocity through soil specimen

By solving Equation E.5 with the boundary conditions illustrated in Figure E.3, $h = h_0$, and $t = t_0 = 0$, are the following relationships found

$$ln(h) = \frac{A \cdot k_T}{a \cdot L} \cdot t + ln(h_0) \tag{E.6}$$

or

$$k_T = \frac{a \cdot L}{A \cdot t} \cdot ln\left(\frac{h_0}{h}\right) \tag{E.7}$$

Where k_T is the hydraulic conductivity at temperature T. k_T are dependent not only of the soil matrix, but also of the fluid property. To remove the dependency of fluid flow properties, the kinematic viscosity, ν, are introduced through the permeability, K, as seen in Equation E.8.

$$K = k_T \cdot \frac{\nu_T}{g} \tag{E.8}$$

Where ν_T is the kinematic viscosity of the present fluid at a given temperature, T, in °C.

Measurements from the intermediate level, t_1 at h_1, could be used to control whether or not the water flow through the specimen can be considered a quasi-static process.
h_1 is set to the height where the corresponding flow time, t_1, is half of the total flowtime, t_{tot}. The total flowtime can be found rearranging E.6, and inserting the valid boundary conditions; $h = h_2$ for $t = t_{tot}$. Inserting these variables into Equation E.6, yields

$$t_{tot} = \frac{a \cdot L}{A \cdot k_T} \cdot ln\left(\frac{h_0}{h_2}\right) \tag{E.9}$$

Completing the argument above, h_1 is found by inserting $t_1 = t_{tot}/2$ into E.9, so that

$$h_1 = \sqrt{h_0 \cdot h_2} \tag{E.10}$$

If the measurements during the experiments show that $t_1 \simeq t_2$, the assumption of quasi-static conditions are valid.

E.5 Results

All in all, 18 tests were performed; 10 tests on AAU sand 1 and 8 tests on the Frederikshavn sand. Table E.5 show the results from the tests on AAU sand 1, while Table E.6 show the results from the tests performed on Frederikshavn sand.

Void ratio, e	Permeability, K
[-]	$[10^{-12}m^2]$
0.556	5.816
0.559	5.122
0.578	6.590
0.588	6.598
0.612	7.570
0.640	8.289
0.671	9.551
0.703	10.922
0.732	12.367
0.767	14.488

Table E.5: *Results from permeability tests on Aalborg University Sand no. 1.*

Void ratio, e	Permeability, K
[-]	$[10^{-12}m^2]$
0.616	7.076
0.650	8.532
0.670	8.973
0.691	10.405
0.719	11.372
0.736	12.414
0.753	12.696
0.773	14.325

Table E.6: *Results from permeability tests on Frederikshavn sand 103-47.*

The results from Table E.5 and E.6 are ploted in Figure E.4 and E.5. The the results are fitted to a polynomial line,with the following relationship between the permeability, K, and void ratio, e;

$$K_{AAU1} = 7.075 \cdot 10^{-11} \cdot e^2 - 5.218 \cdot 10^{-11} \cdot e + 1.277 \cdot 10^{-11} \tag{E.11}$$

For AAU sand 1, and;

$$K_{fred} = 5.584 \cdot 10^{-11} \cdot e^2 - 3.277 \cdot 10^{-11} \cdot e + 6.113 \cdot 10^{-12} \tag{E.12}$$

For Frederikshavn sand.

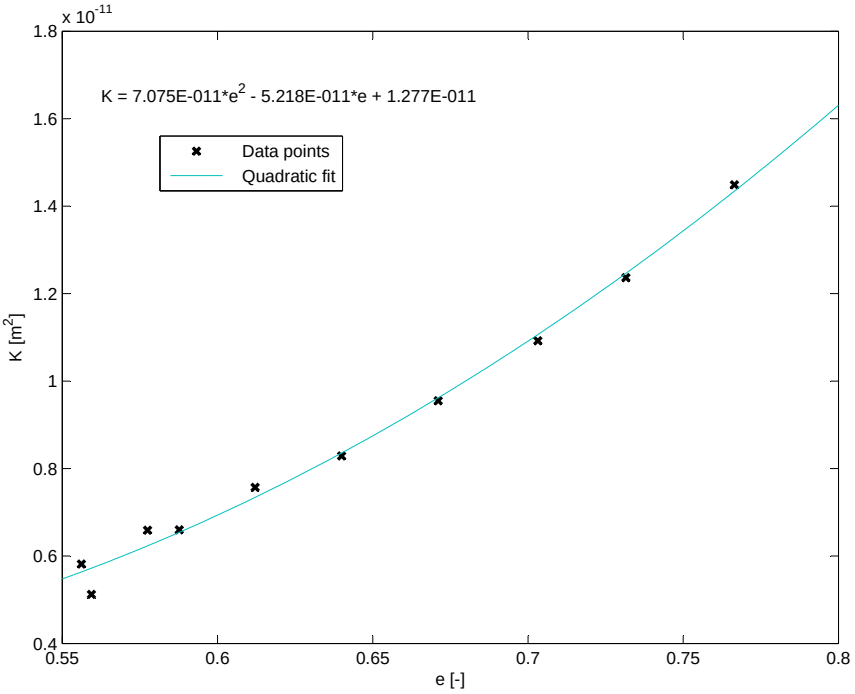

Figure E.4: *Plot of permeability results of Aalborg University Sand no. 1.*

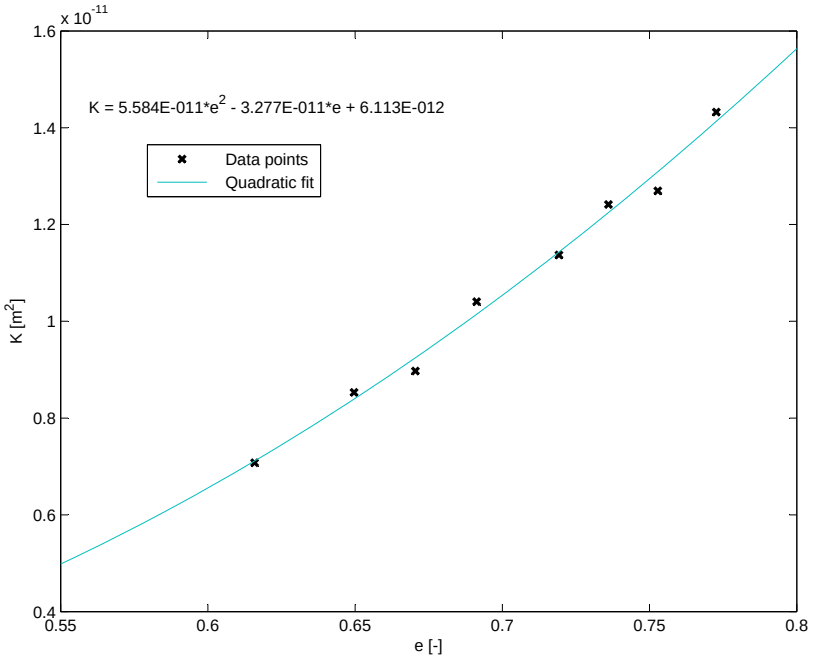

Figure E.5: *Plot of permeability results of Frederikshavn sand 103-47.*

Part III

Test Results

Appendix **F**

Results from Bucket Tests

Four monotonic loading tests have been conducted inside the pressure tank at GELAAU. A selection of the results gained from these tests are presented herein.

F.1 Test 1

Monotonic Loading		**Test 1**
Sand:	Hydrostatic pressure in tank:	Date:
Aalborg University sand no. 1	2 bar	18.05.2012
Test ID:	Displacement per sequence:	Performed by:
Monotonicbucket01	40 mm	ÅS & LM
Bucket diameter:	Number of sequences:	
500 mm	3	
Skirt height:	Time per sequence:	
250 mm	4000 s	

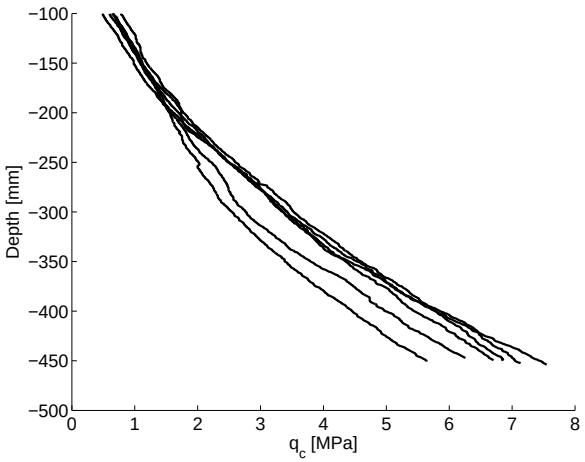

Figure F.1: *q_c versus depth for test 1.*

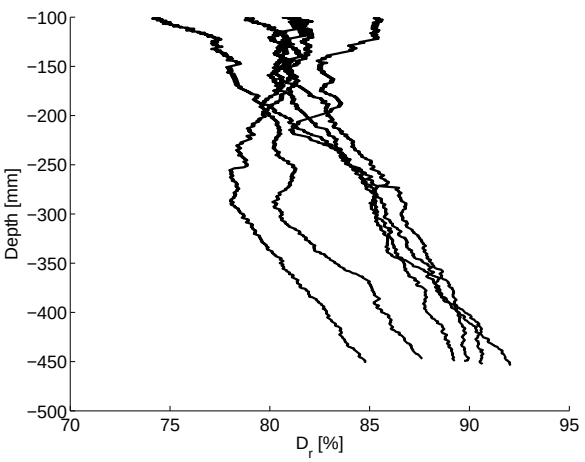

Figure F.2: *D_r versus depth for test 1*

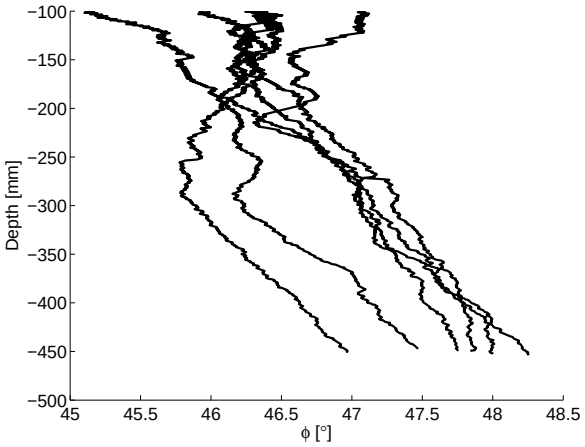

Figure F.3: ϕ *versus depth for test 1.*

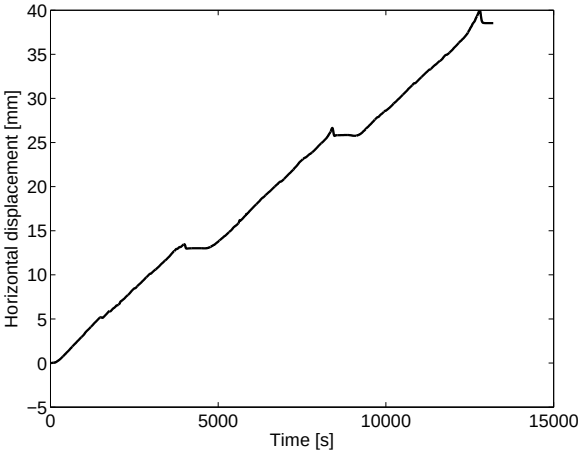

Figure F.4: *Horizontal displacement of center bucket lid versus time for test 1.*

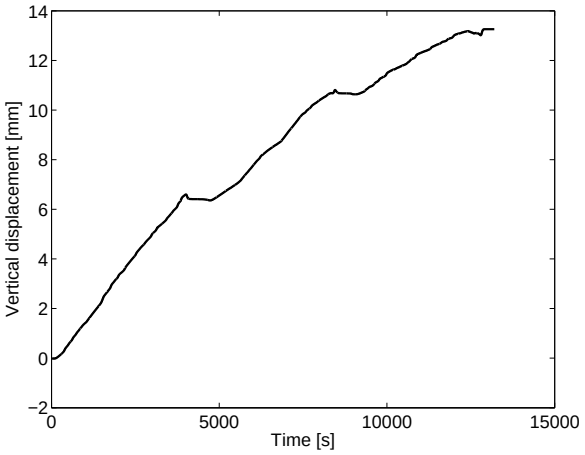

Figure F.5: *Vertical displacement of center bucket lid versus time for test 1*

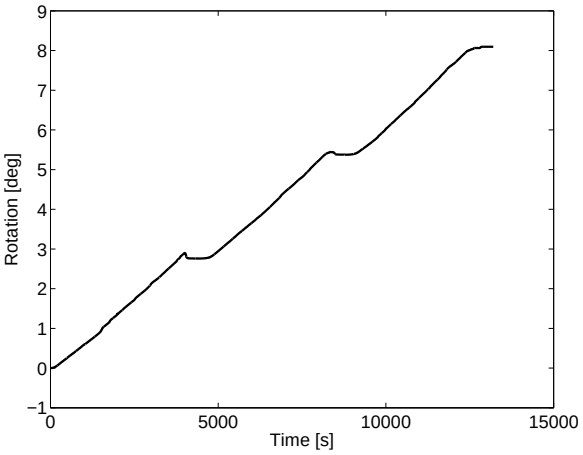

Figure F.6: *Rotation of bucket versus time for test 1.*

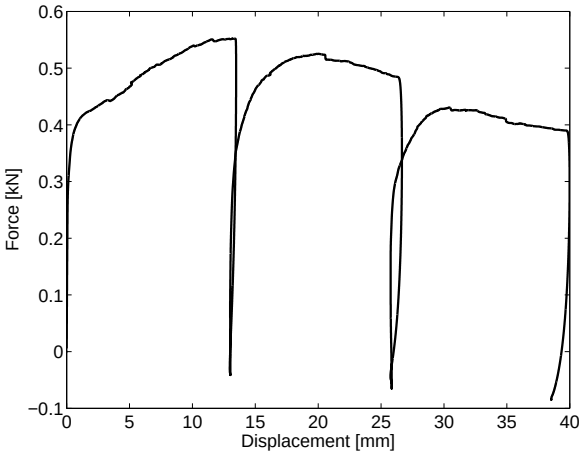

Figure F.7: *Force - displacement (top horizontal transducer) for test 1*

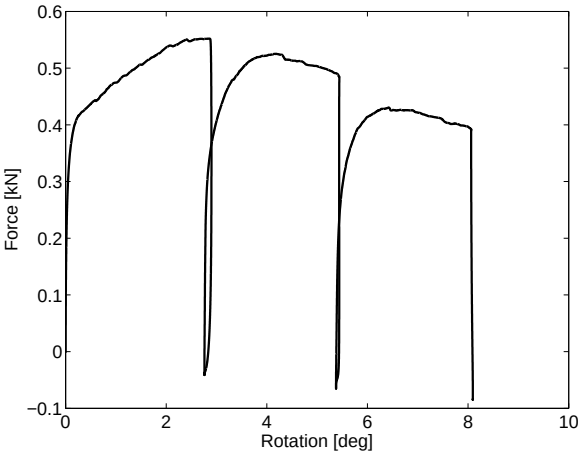

Figure F.8: *Force - Rotation of bucket for test 1.*

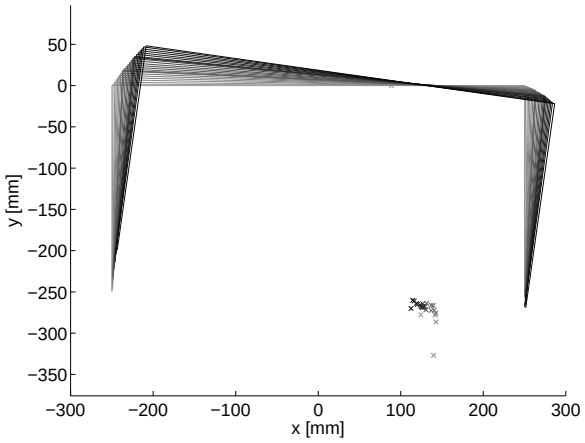

Figure F.9: *Development of rotation point for test 1.*

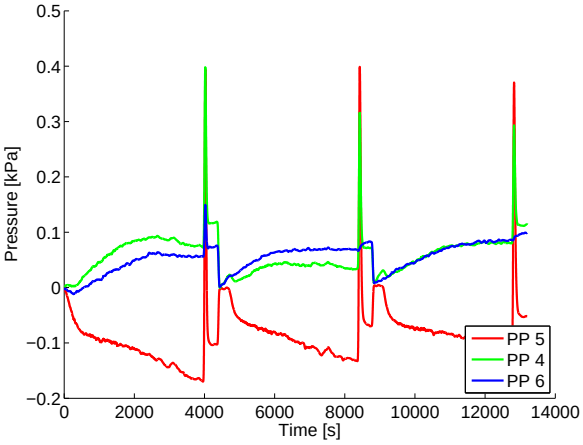

Figure F.10: *Pore pressures outside bucket skirt, test 1.*

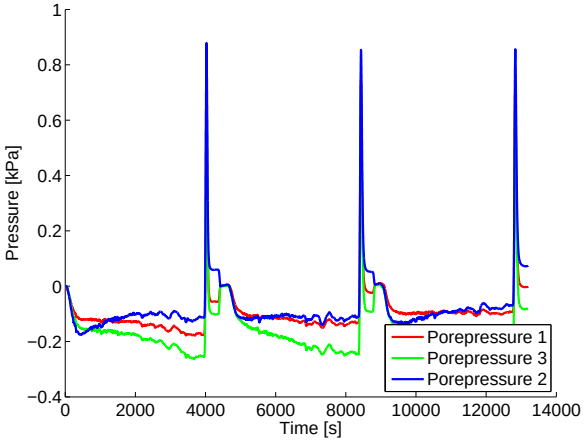

Figure F.11: *Pore pressures inside bucket skirt, test 1.*

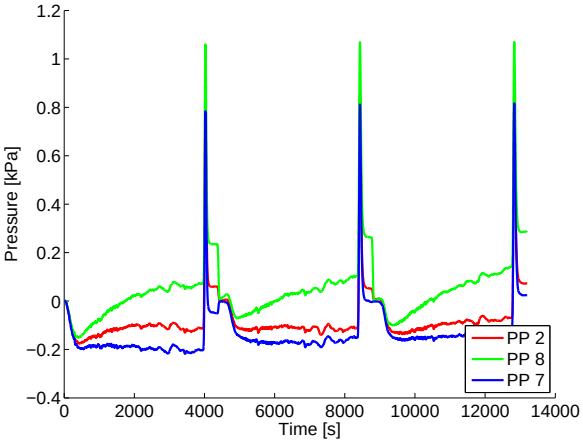

Figure F.12: *Pore pressures under bucket lid, test 1.*

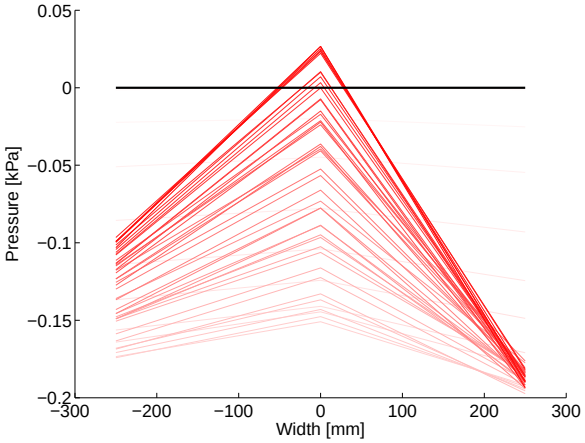

Figure F.13: *Pore pressure development under bucket lid, test 1.*

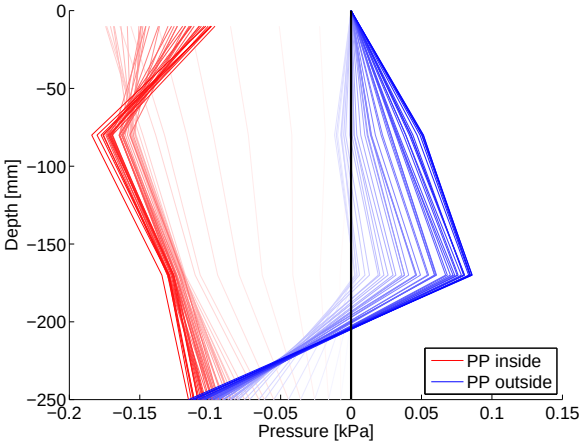

Figure F.14: *Pore pressure development along bucket skirt, test 1.*

F.2 Test 2

Monotonic Loading		**Test 2**
Sand:	Hydrostatic pressure in tank:	Date:
Aalborg University sand no. 1	2 bar	30.04.2012
Test ID:	Displacement per sequence:	Performed by:
Monotonicbucket02	40 mm	ÅS & LM
Bucket diameter:	Number of sequences:	
500 mm	3	
Skirt height:	Time per sequence:	
250 mm	400 s	

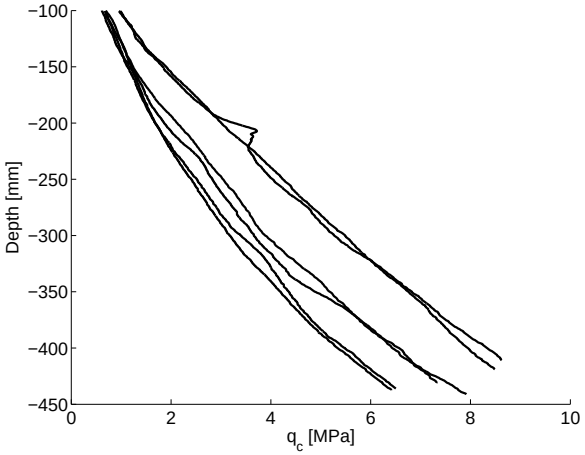

Figure F.15: *q_c versus depth for test 2.*

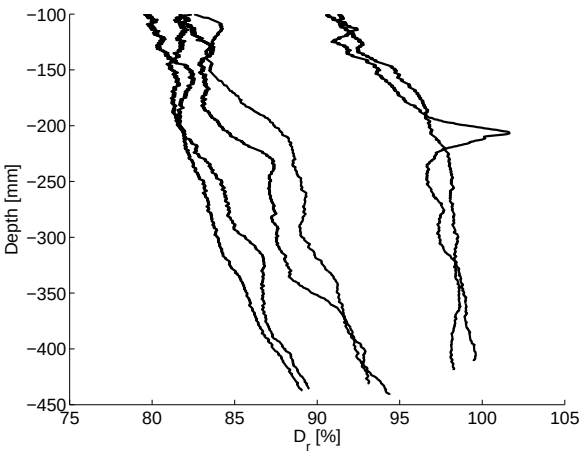

Figure F.16: *D_r versus depth for test 2*

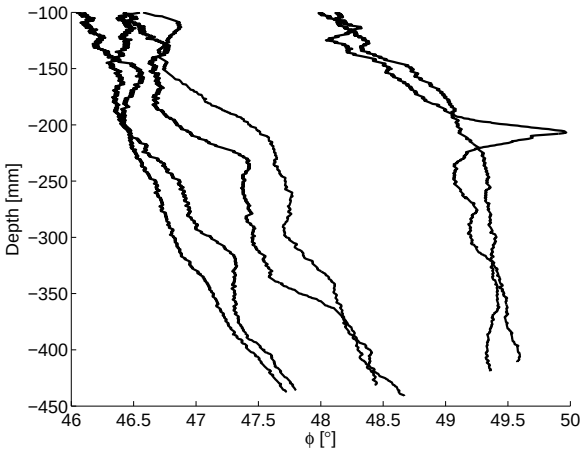

Figure F.17: *ϕ versus depth for test 2.*

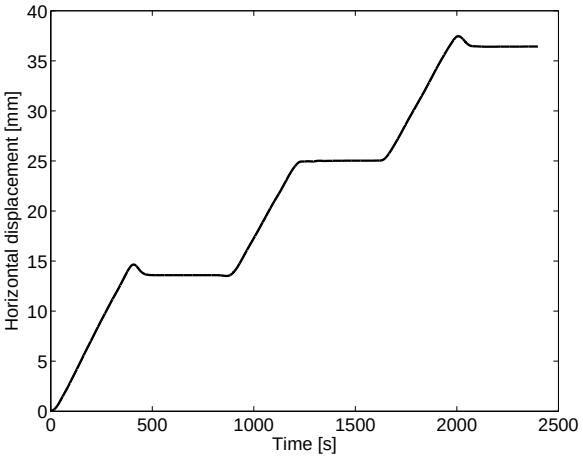

Figure F.18: *Horizontal displacement of center bucket lid versus time for test 2.*

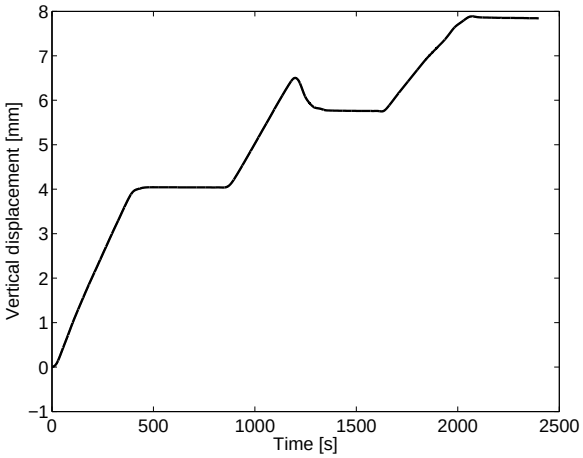

Figure F.19: *Vertical displacement of center bucket lid versus time for test 2*

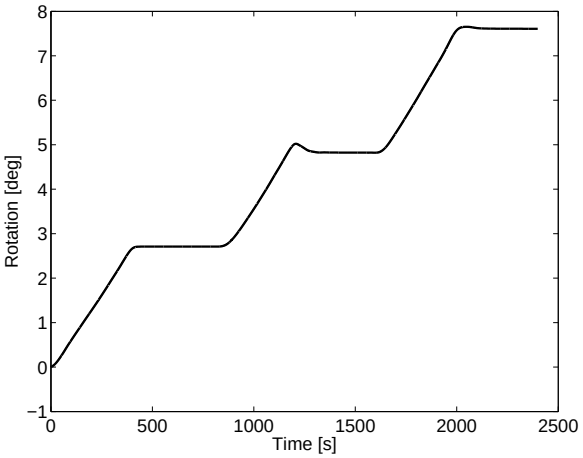

Figure F.20: *Rotation of bucket versus time for test 2.*

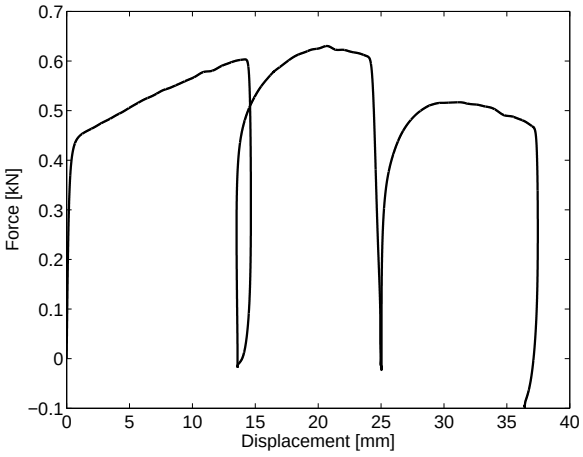

Figure F.21: *Force - displacement (top horizontal transducer) for test 2*

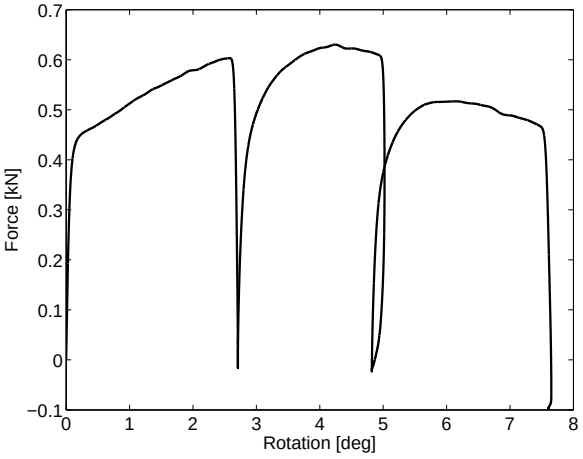

Figure F.22: *Force - Rotation of bucket for test 2.*

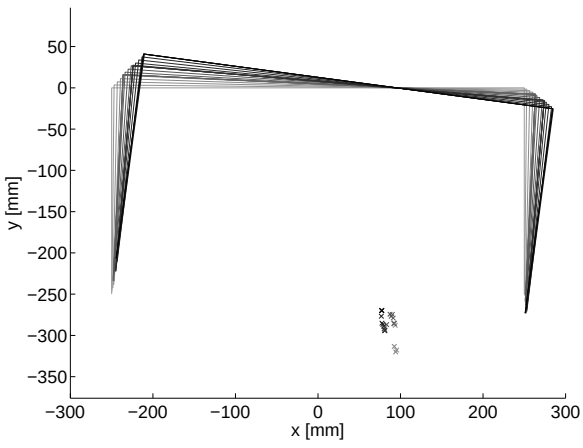

Figure F.23: *Development of rotation point for test 2.*

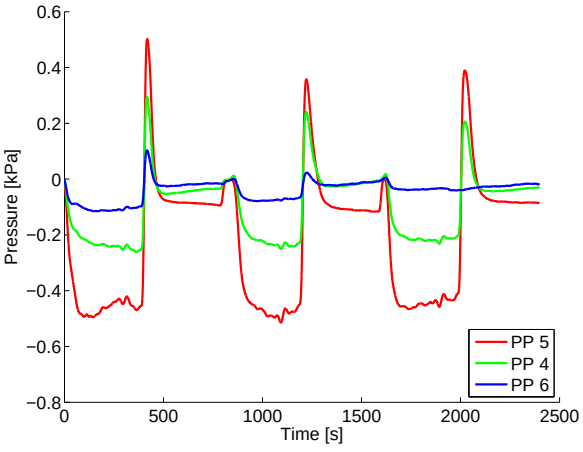

Figure F.24: *Pore pressures outside bucket skirt, test 2.*

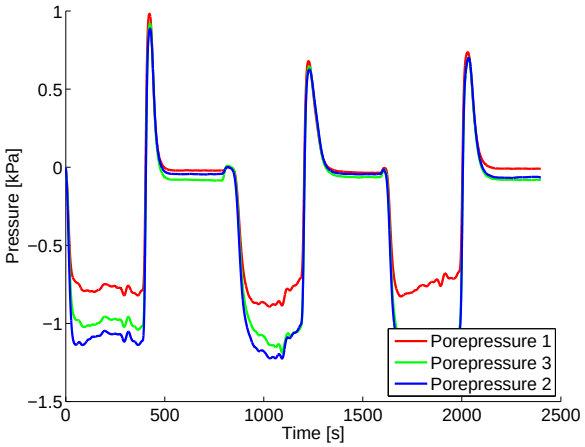

Figure F.25: *Pore pressures inside bucket skirt, test 2.*

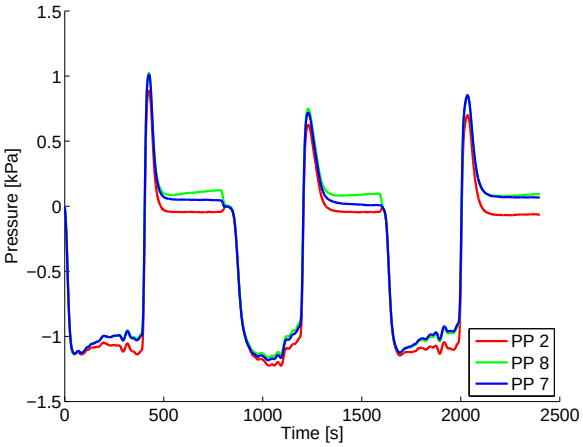

Figure F.26: *Pore pressures under bucket lid, test 2.*

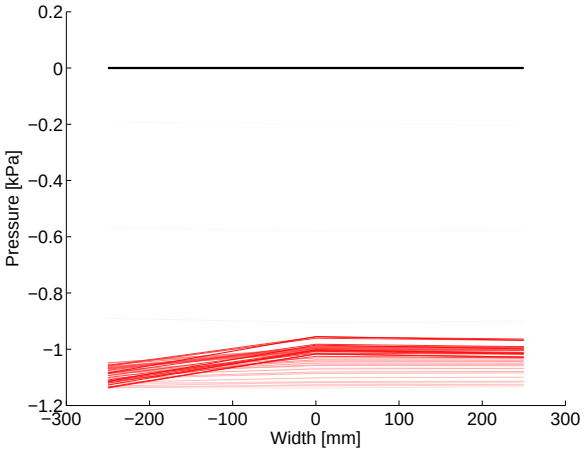

Figure F.27: *Pore pressure development under bucket lid, test 2.*

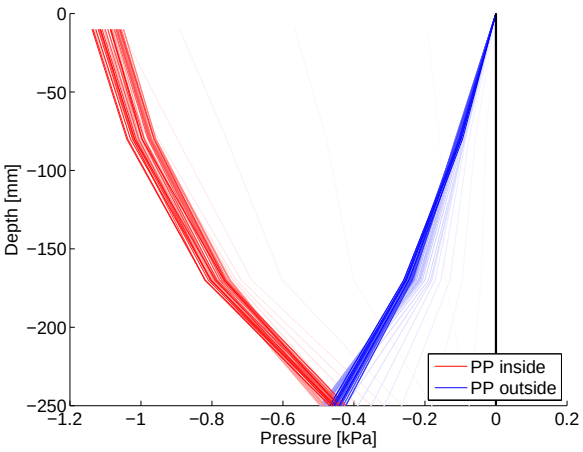

Figure F.28: *Pore pressure development along bucket skirt, test 2.*

F.3 Test 3

Monotonic Loading		**Test 3**
Sand:	Hydrostatic pressure in tank:	Date:
Aalborg University sand no. 1	2 bar	03.05.2012
Test ID:	Displacement per sequence:	Performed by:
Monotonicbucket03	40 mm	ÅS & LM
Bucket diameter:	Number of sequences:	
500 mm	3	
Skirt height:	Time per sequence:	
250 mm	40 s	

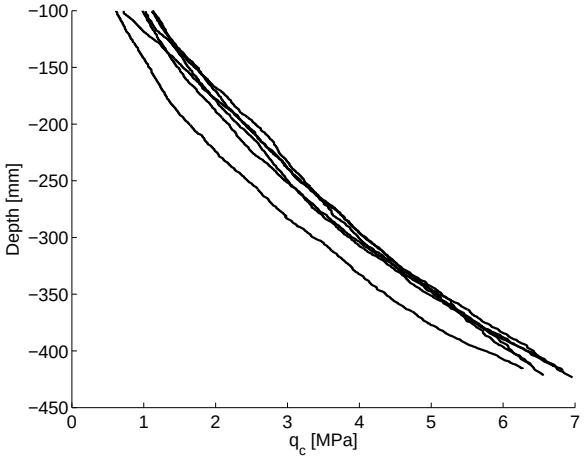

Figure F.29: *q_c versus depth for test 3.*

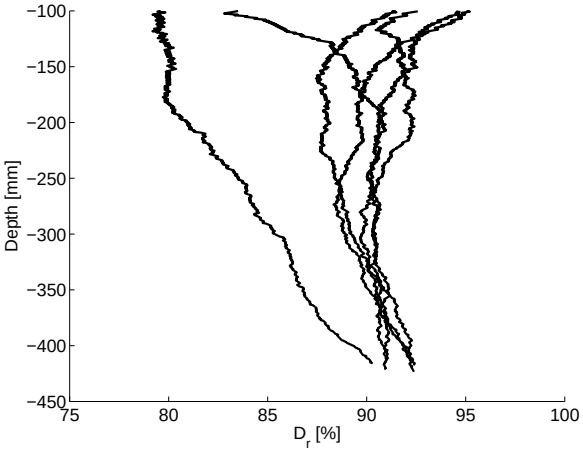

Figure F.30: *D_r versus depth for test 3*

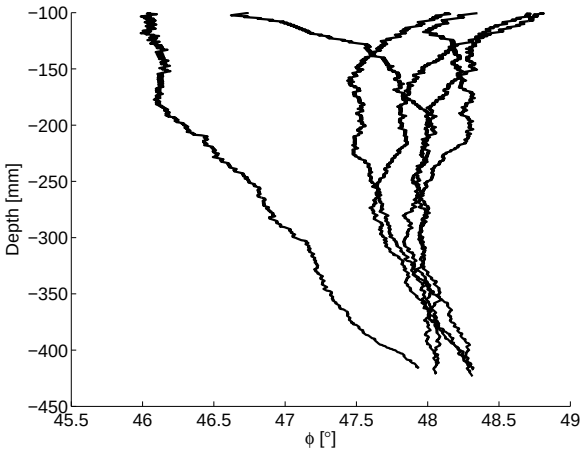

Figure F.31: *ϕ versus depth for test 3.*

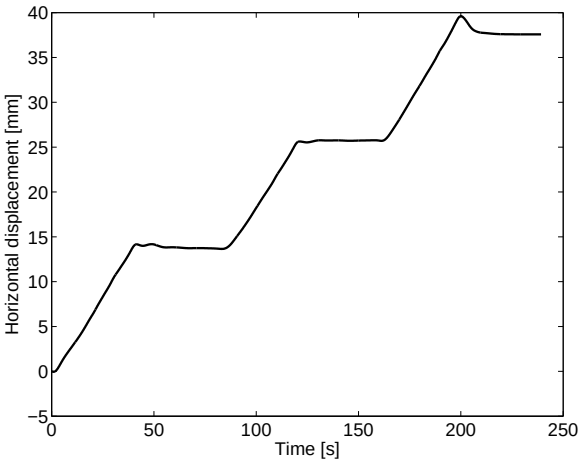

Figure F.32: *Horizontal displacement of center bucket lid versus time for test 3.*

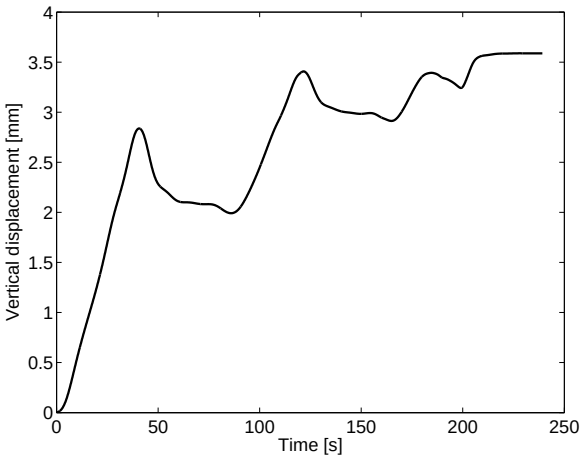

Figure F.33: *Vertical displacement of center bucket lid versus time for test 3.*

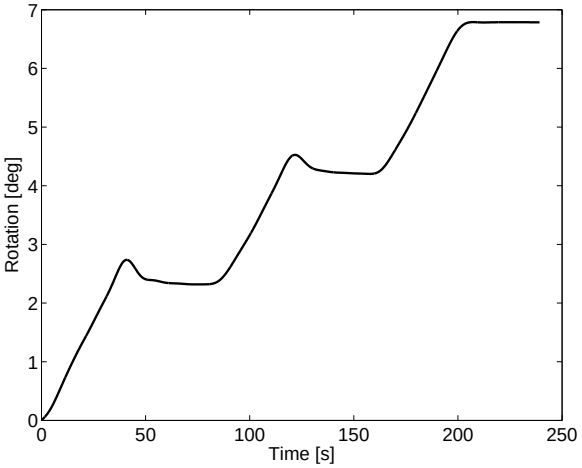

Figure F.34: *Rotation of bucket versus time for test 3.*

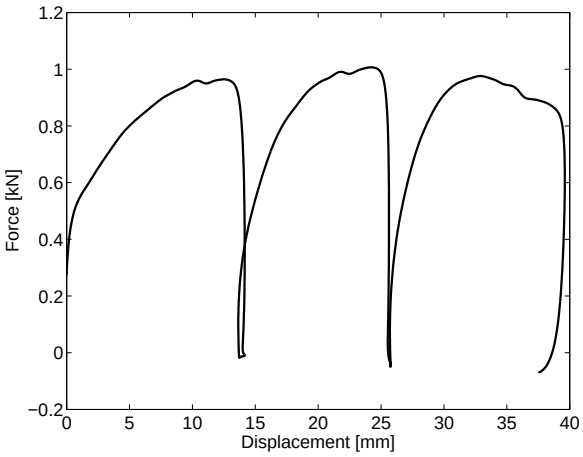

Figure F.35: *Force - displacement (top horizontal transducer) for test 3.*

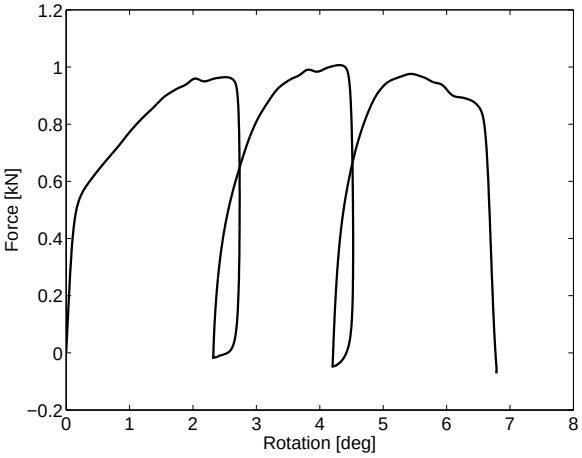

Figure F.36: *Force - Rotation of bucket for test 3.*

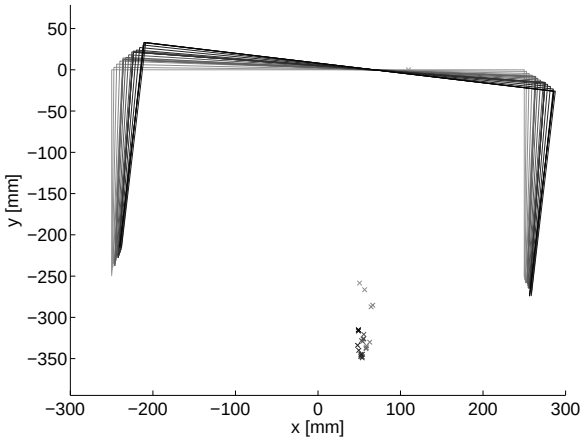

Figure F.37: *Development of rotation point for test 3.*

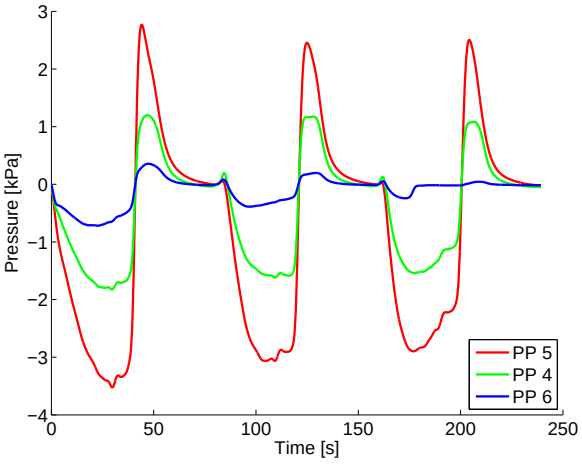

Figure F.38: *Pore pressures outside bucket skirt, test 3.*

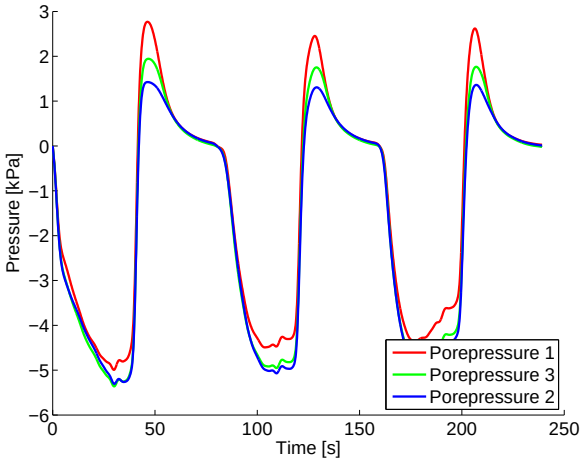

Figure F.39: *Pore pressures inside bucket skirt, test 3.*

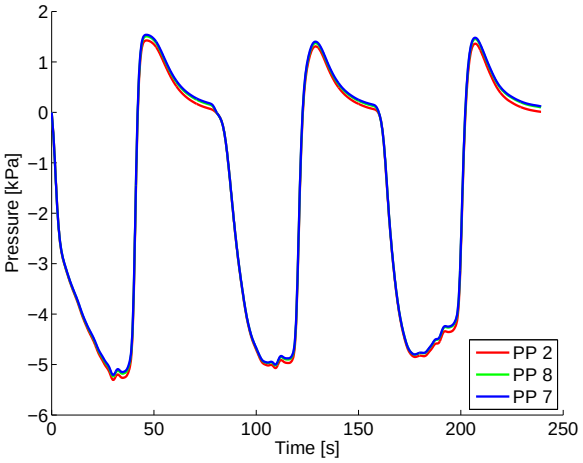

Figure F.40: *Pore pressures under bucket lid, test 3.*

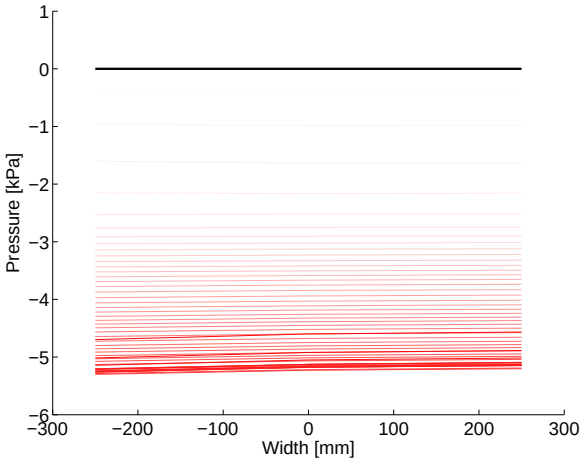

Figure F.41: *Pore pressure development under bucket lid, test 3.*

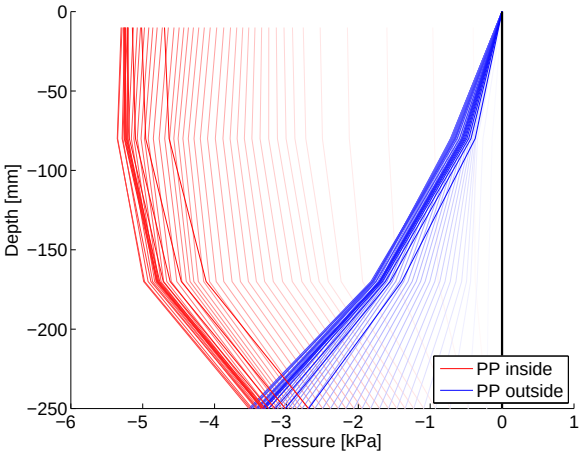

Figure F.42: *Pore pressure development along bucket skirt, test 3.*

F.4 Test 4

Monotonic Loading		**Test 4**
Sand:	Hydrostatic pressure in tank:	Date:
Aalborg University sand no. 1	2 bar	09.05.2012
Test ID:	Displacement per sequence:	Performed by:
Monotonicbucket04	40 mm	ÅS & LM
Bucket diameter:	Number of sequences:	
500 mm	3	
Skirt height:	Time per sequence:	
250 mm	4 s	

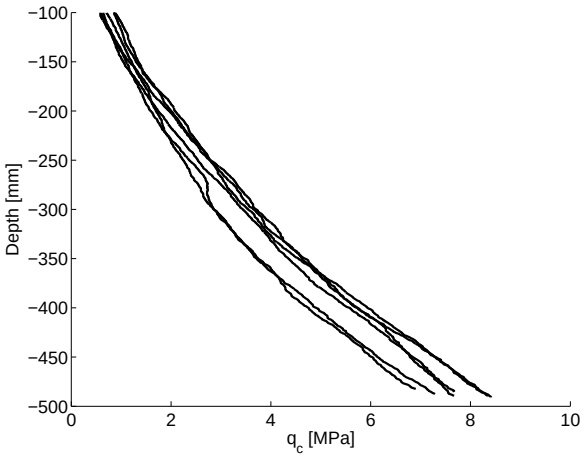

Figure F.43: *q_c versus depth for test 4.*

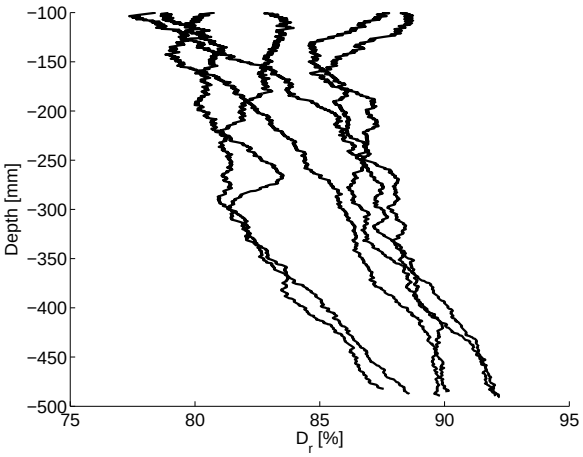

Figure F.44: *D_r versus depth for test 4.*

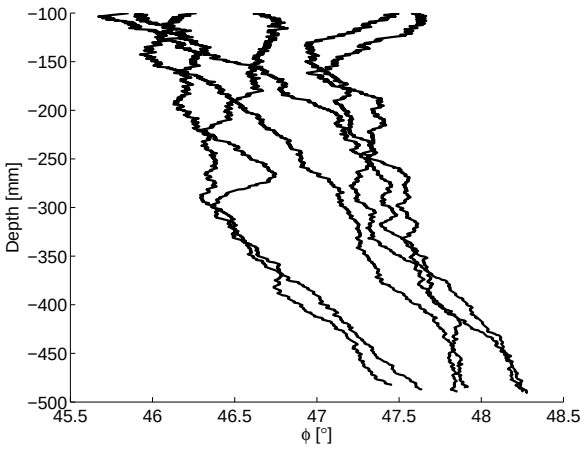

Figure F.45: *ϕ versus depth for test 4.*

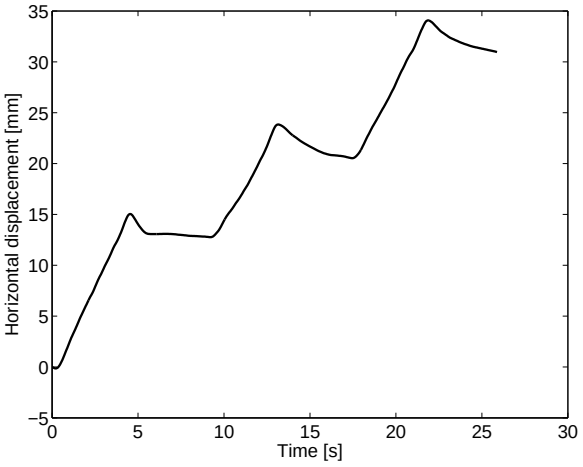

Figure F.46: *Horizontal displacement of center bucket lid versus time for test 4.*

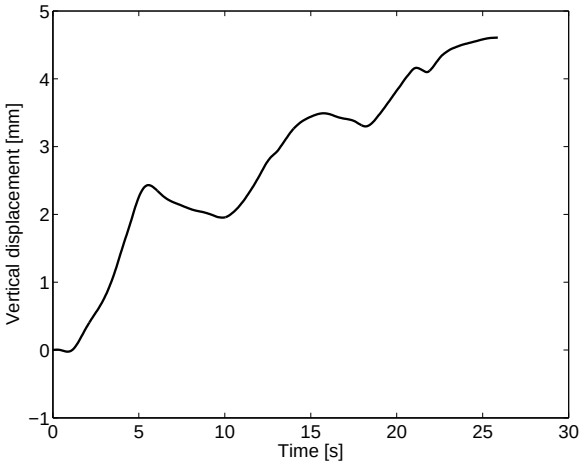

Figure F.47: *Vertical displacement of center bucket lid versus time for test 4.*

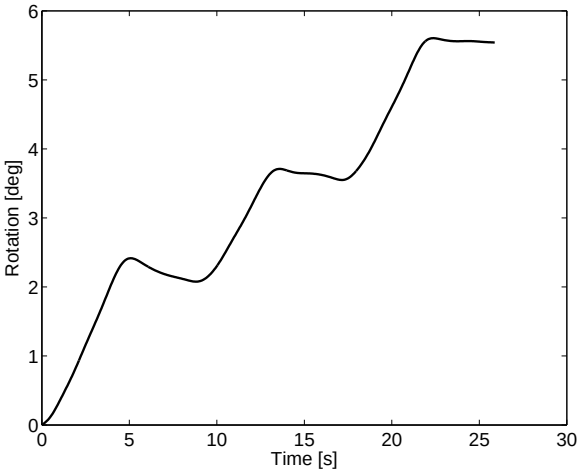

Figure F.48: *Rotation of bucket versus time for test 4.*

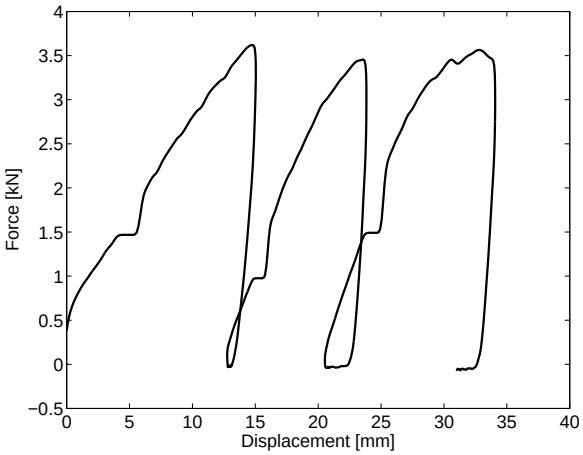

Figure F.49: *Force - displacement (top horizontal transducer) for test 4.*

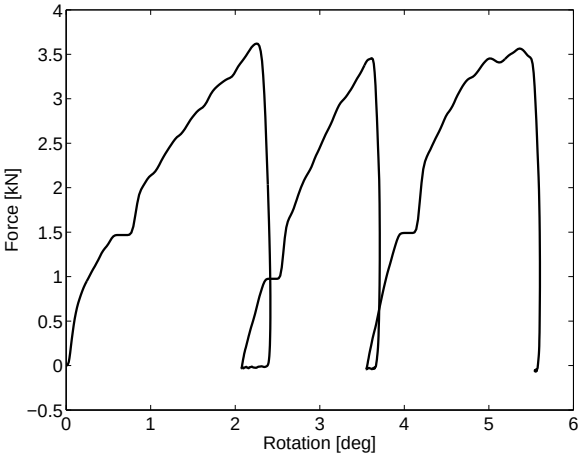

Figure F.50: *Force - Rotation of bucket for test 4.*

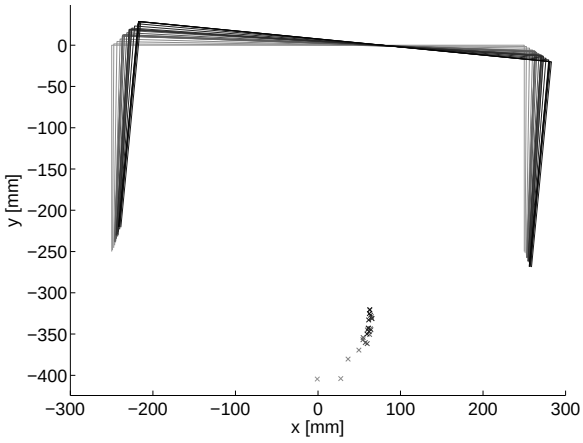

Figure F.51: *Development of rotation point for test 4.*

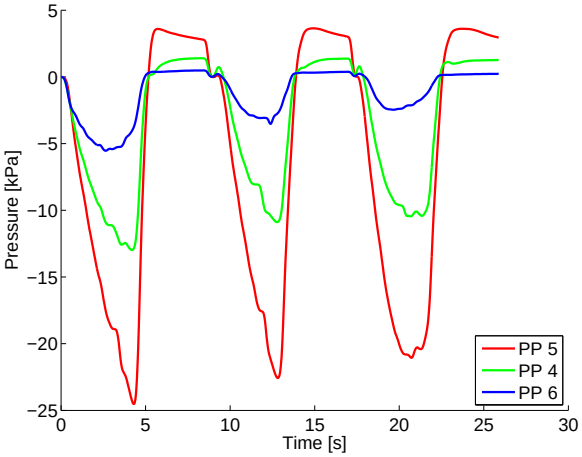

Figure F.52: *Pore pressures outside bucket skirt, test 4.*

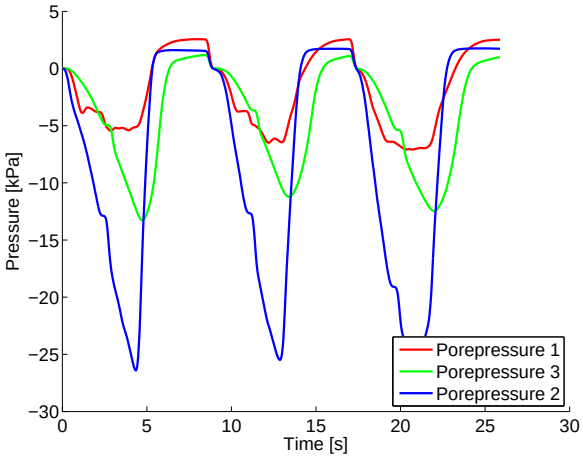

Figure F.53: *Pore pressures inside bucket skirt, test 4.*

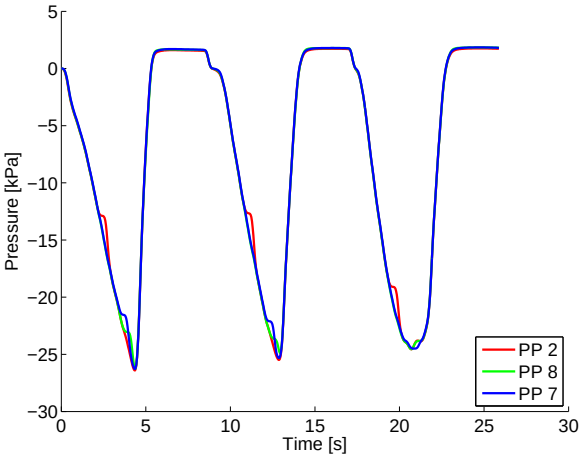

Figure F.54: *Pore pressures under bucket lid, test 4.*

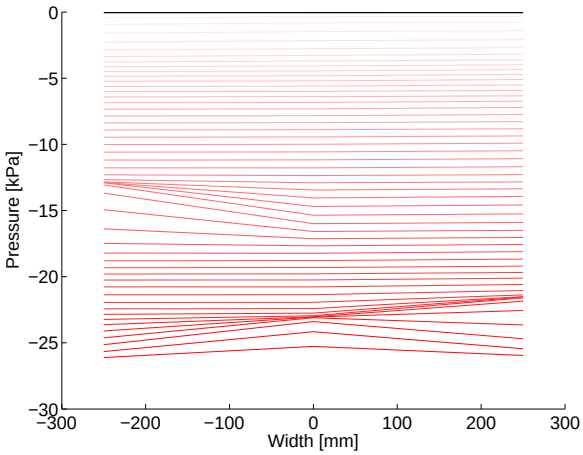

Figure F.55: *Pore pressure development under bucket lid, test 4.*

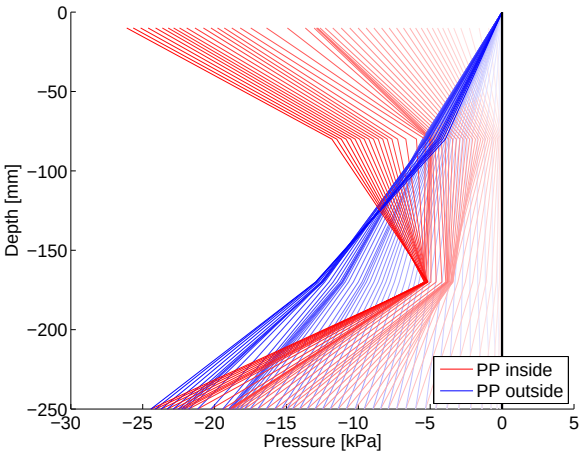

Figure F.56: *Pore pressure development along bucket skirt, test 4.*

Appendix **G**

Results from permeability tests

In the following chapter, the results from the permeability tests for both Aalborg University Sand no. 1, and Frederikshavn Sand 103-47 are presented. The results are presented in numbered enclosures for each prepared specimen.

G.1 Equipment

In the presented enclosures, the chosen cylinder, filterstone and spring are denoted with a letter or a number. The filterstone notation, μm, indicates the pore diameter. The chosen filterstone for both sand types of sand, 25 μm, are considered as *fine*.

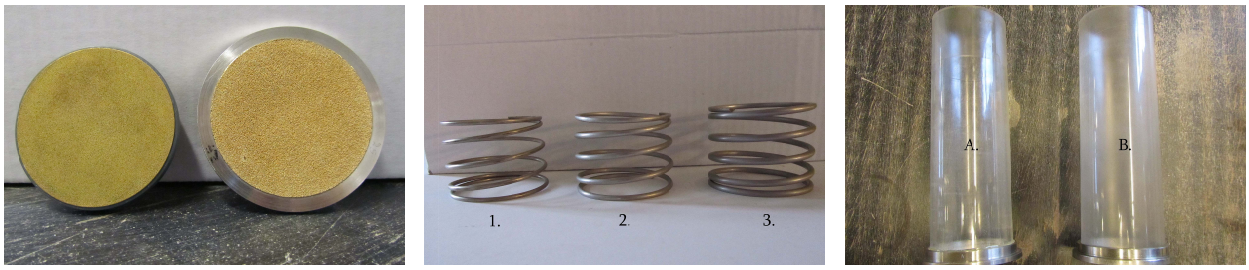

(a) 25 μm filterstone. (b) Accessible springs. 1 to 3, soft to stiff. (c) Permeameter cylinders.

Figure G.1: *Equipment for permeability test.*

Furthermore, the stiff spring, no. 3, were applied in all experiments, save the test presented in enclosure 1.
The permeameter cylinders A and B, have only minor geometrical differences. Still, theses differences could be enought to undermine the consistency of the results. Therefore only cylinder B were used in the experiments. Pictures of the filterstones, springs and cylinders are presented in Figure G.1.

G.2 Enclosures for Aalborg University Sand no. 1

The following section contains enclosures 1 - 10, where experiments on same sample with different standpipe are denoted *a* and *b*. This results in a total of 12 enclosures for the present sand, since two of the sample experiments were performed with two different standpipes.

Permeabilitytest on Aalborg University Sand no. 1, at D_r = 29.62%.

Soil type	Preparation method	Specimen data			Permeameter equipment
Aalborg University	Tamped by punner	Length	[mm]	198	Cylinder B
Sand no. 1		Diameter	[mm]	70	Filterstone 25 μm
		Void ratio	[-]	0.766	Spring no. 2
		Saturation	[-]	1.01	

Test setup	Standpipe diameter, D	[mm]	40
	Initial hydraulic head, h_0	[mm]	200
	Intermediate hydraulic head, h_1	[mm]	1265
	Final hydraulic head, h_2	[mm]	800

Test	Unit	1	2	3	Results
Temperature, T_1	[°C]	22.8	23.0	23.1	⇓
Temperature, T_2	[°C]	22.6	22.9	23.0	23.0
Flowtime h_0 - h_1, t_1	$[s]$	199	197	196	196.5
Flowtime h_1 - h_2, t_2	$[s]$	198	197	197	197
Kinematic viscosity, ν_T	$10^{-6}[m^2/s]$				0.9352
Density of water, ρ_w	$[g/cm^3]$				0.997
Hydraulic conductivity, k_T	$10^{-4}[m/s]$				1.5207
Permeability, K	$10^{-12}[m^2]$				14.488

Comments: At least two small pockets of air close to the plexiglass. Sample should have been compacted some more. Gap development between sand and top filter while filling stand pipe with water. Water/air pockets were reduced during testing. Gap between sand and top filter increased. One of two possibilities; top filter moved due to soft spring, or sand compacted. Our guess is on the latter, hence H is reduced by 1 mm in the ID and e calculations.

Test ID	PermAAU1-30%
Executed by	ÅS & LM
Evaluated by	ÅS & LM
Period	March 2012
Enclosure No.	1

Permeabilitytest on Aalborg University Sand no. 1, at D_r = 40.93%.

Soil type	Preparation method	Specimen data			Permeameter equipment
Aalborg University Sand no. 1	Tamped by punner	Length	[mm]	199	Cylinder B
		Diameter	[mm]	70	Filterstone 25 μm
		Void ratio	[-]	0.732	Spring no. 3
		Saturation	[-]	1.01	

Test setup			
	Standpipe diameter, D	[mm]	40
	Initial hydraulic head, h_0	[mm]	200
	Intermediate hydraulic head, h_1	[mm]	1265
	Final hydraulic head, h_2	[mm]	800

Test	Unit	1	2	3	Results
Temperature, T_1	[°C]	23.4	23.4	23.5	⇓
Temperature, T_2	[°C]	23.3	23.3	23.0	23.4
Flowtime h_0 - h_1, t_1	$[s]$	232	229	229	229
Flowtime h_1 - h_2, t_2	$[s]$	229	228	228	228
Kinematic viscosity, ν_T	$10^{-6}[m^2/s]$				0.9270
Density of water, ρ_w	$[g/cm^3]$				0.997
Hydraulic conductivity, k_T	$10^{-4}[m/s]$				1.3094
Permeability, K	$10^{-12}[m^2]$				12.366

Comments:

Test ID	PermAAU1-40%
Executed by	ÅS & LM
Evaluated by	ÅS & LM
Period	March 2012
Enclosure No.	2

Permeabilitytest on Aalborg University Sand no. 1, at D_r = 50.11%.

Soil type	Preparation method	Specimen data			Permeameter equipment
Aalborg University	Tamped by punner	Length	[mm]	199	Cylinder B
Sand no. 1		Diameter	[mm]	70	Filterstone 25 μm
		Void ratio	[-]	0.703	Spring no. 3
		Saturation	[-]	0.99	

Test setup			
	Standpipe diameter, D	[mm]	40
	Initial hydraulic head, h_0	[mm]	200
	Intermediate hydraulic head, h_1	[mm]	1265
	Final hydraulic head, h_2	[mm]	800

Test	Unit	1	2	3	Results
Temperature, T_1	[°C]	20.7	20.7	20.8	⇓
Temperature, T_2	[°C]	20.3	20.4	20.5	20.6
Flowtime h_0 - h_1, t_1	$[s]$	281	278	276	277
Flowtime h_1 - h_2, t_2	$[s]$	278	276	275	275.5
Kinematic viscosity, ν_T	$10^{-6}[m^2/s]$				0.9899
Density of water, ρ_w	$[g/cm^3]$				0.998
Hydraulic conductivity, k_T	$10^{-4}[m/s]$				1.0831
Permeability, K	$10^{-12}[m^2]$				10.922

Comments:

Test ID	PermAAU1-50%
Executed by	ÅS & LM
Evaluated by	ÅS & LM
Period	March 2012
Enclosure No.	3

Permeabilitytest on Aalborg University Sand no. 1, at D_r = 60.49%.

Soil type	Preparation method	Specimen data			Permeameter equipment
Aalborg University Sand no. 1	Tamped by punner	Length	[mm]	199	Cylinder B
		Diameter	[mm]	70	Filterstone 25 μm
		Void ratio	[-]	0.671	Spring no. 3
		Saturation	[-]	1.168	

Test setup			
	Standpipe diameter, D	[mm]	40
	Initial hydraulic head, h_0	[mm]	200
	Intermediate hydraulic head, h_1	[mm]	1265
	Final hydraulic head, h_2	[mm]	800

Test	Unit	1	2	3	Results
Temperature, T_1	[°C]	22.8	22.9	23.0	⇓
Temperature, T_2	[°C]	22.6	22.7	22.8	22.9
Flowtime h_0 - h_1, t_1	$[s]$	309	299	299	299
Flowtime h_1 - h_2, t_2	$[s]$	298	300	300	300
Kinematic viscosity, ν_T	$10^{-6}[m^2/s]$				0.9385
Density of water, ρ_w	$[g/cm^3]$				0.998
Hydraulic conductivity, k_T	$10^{-4}[m/s]$				0.9990
Permeability, K	$10^{-12}[m^2]$				9.5508

Comments:

Test ID	PermAAU1-60%
Executed by	ÅS & LM
Evaluated by	ÅS & LM
Period	March 2012
Enclosure No.	4

Permeabilitytest on Aalborg University Sand no. 1, at D_r = 70.56%.

Soil type	Preparation method	Specimen data			Permeameter equipment
Aalborg University	Tamped by punner	Length	[mm]	199	Cylinder B
Sand no. 1		Diameter	[mm]	70	Filterstone 25 μm
		Void ratio	[-]	0.640	Spring no. 3
		Saturation	[-]	1.00	

Test setup			
	Standpipe diameter, D	[mm]	40
	Initial hydraulic head, h_0	[mm]	200
	Intermediate hydraulic head, h_1	[mm]	1265
	Final hydraulic head, h_2	[mm]	800

Test	Unit	1	2	3	Results
Temperature, T_1	[°C]	24.7	25.0	25.0	⇓
Temperature, T_2	[°C]	24.4	24.8	24.8	24.9
Flowtime h_0 - h_1, t_1	$[s]$	343	331	328	329.5
Flowtime h_1 - h_2, t_2	$[s]$	336	329	329	329
Kinematic viscosity, ν_T	$10^{-6}[m^2/s]$				0.8954
Density of water, ρ_w	$[g/cm^3]$				0.997
Hydraulic conductivity, k_T	$10^{-4}[m/s]$				0.9087
Permeability, K	$10^{-12}[m^2]$				8.2889

Comments:

Test ID	PermAAU1-70%
Executed by	ÅS & LM
Evaluated by	ÅS & LM
Period	March 2012
Enclosure No.	5

Permeabilitytest on Aalborg University Sand no. 1, at D_r = 79.58%.

Soil type	Preparation method	Specimen data			Permeameter equipment
Aalborg University Sand no. 1	Tamped by punner	Length	[mm]	199	Cylinder B
		Diameter	[mm]	70	Filterstone 25 μm
		Void ratio	[-]	0.612	Spring no. 3
		Saturation	[-]	1.10	

Test setup			
	Standpipe diameter, D	[mm]	40
	Initial hydraulic head, h_0	[mm]	200
	Intermediate hydraulic head, h_1	[mm]	1265
	Final hydraulic head, h_2	[mm]	800

Test	Unit	1	2	3	Results
Temperature, T_1	[°C]	25.2	25.2	25.3	⇓
Temperature, T_2	[°C]	24.9	25.0	25.1	25.2
Flowtime h_0 - h_1, t_1	$[s]$	369	364	357	360.5
Flowtime h_1 - h_2, t_2	$[s]$	365	362	351	356.5
Kinematic viscosity, ν_T	$10^{-6}[m^2/s]$				0.8903
Density of water, ρ_w	$[g/cm^3]$				0.997
Hydraulic conductivity, k_T	$10^{-4}[m/s]$				0.8346
Permeability, K	$10^{-12}[m^2]$				7.5698

Comments: First test performed. Air bubbles rose up inside the sample under saturation. Flushed out the water, washed the o-rings, and re-installed the sample. Saturation went without problems this time.

t_1 and t_2 did not converge toward a stable result when pipe no. 4 were used. Three more tests were performed on this sample with standpipe no. 3, with the result presented in enclosure 6b.

Test ID	PermAAU1-80%a
Executed by	ÅS & LM
Evaluated by	ÅS & LM
Period	March 2012
Enclosure No.	6a

Permeabilitytest on Aalborg University Sand no. 1, at D_r = 79.58%.

Soil type	Preparation method	Specimen data			Permeameter equipment
Aalborg University	Tamped by punner	Length	[mm]	199	Cylinder B
Sand no. 1		Diameter	[mm]	70	Filterstone 25 μm
		Void ratio	[-]	0.612	Spring no. 3
		Saturation	[-]	1.10	

Test setup	Standpipe diameter, D	[mm]	20
	Initial hydraulic head, h_0	[mm]	200
	Intermediate hydraulic head, h_1	[mm]	1265
	Final hydraulic head, h_2	[mm]	800

Test	Unit	1	2	3	Results
Temperature, T_1	[°C]	25.0	25.0	24.4	⇓
Temperature, T_2	[°C]	24.0	24.0	24.0	24.4
Flowtime h_0 - h_1, t_1	$[s]$	100	100	100	100
Flowtime h_1 - h_2, t_2	$[s]$	102	101	100	100.5
Kinematic viscosity, ν_T	$10^{-6}[m^2/s]$				0.9065
Density of water, ρ_w	$[g/cm^3]$				0.997
Hydraulic conductivity, k_T	$10^{-4}[m/s]$				0.7461
Permeability, K	$10^{-12}[m^2]$				6.890

Comments: Second test run for sample at D_r = 79.58%, with standpipe no. 3, D = 20 mm. Permeability, K, differs from results from experiment with standpipe no. 4. Assuming quasi static conditions for both experiments, the reason for deviating results should be that the flow time did not stabilize for experiments with standpipe no. 4. Results from the current enclosure (6b) are chosen to represent the permeability for the sample at D_r = 79.58 %.

Test ID	PermAAU1-80%b
Executed by	ÅS & LM
Evaluated by	ÅS & LM
Period	March 2012
Enclosure No.	6b

Permeabilitytest on Aalborg University Sand no. 1, at D_r = 87.48%.

Soil type	Preparation method	Specimen data			Permeameter equipment
Aalborg University Sand no. 1	Tamped by punner	Length	[mm]	199	Cylinder B
		Diameter	[mm]	70	Filterstone 25 μm
		Void ratio	[-]	0.587	Spring no. 3
		Saturation	[-]	1.00	

Test setup			
	Standpipe diameter, D	[mm]	40
	Initial hydraulic head, h_0	[mm]	200
	Intermediate hydraulic head, h_1	[mm]	1265
	Final hydraulic head, h_2	[mm]	800

Test	Unit	1	2	3	Results
Temperature, T_1	[°C]	23.2	23.2	23.3	⇓
Temperature, T_2	[°C]	22.6	22.7	22.8	23.0
Flowtime h_0 - h_1, t_1	$[s]$	470	435	432	433.5
Flowtime h_1 - h_2, t_2	$[s]$	451	431	430	430.5
Kinematic viscosity, ν_T	$10^{-6}[m^2/s]$				0.9352
Density of water, ρ_w	$[g/cm^3]$				0.998
Hydraulic conductivity, k_T	$10^{-4}[m/s]$				0.6926
Permeability, K	$10^{-12}[m^2]$				6.5985

Comments: Large difference in flowtime between the first and second test. Could be due to unsatisfactory saturation.

Test ID	PermAAU1-88%
Executed by	ÅS & LM
Evaluated by	ÅS & LM
Period	March 2012
Enclosure No.	7

Permeabilitytest on Aalborg University Sand no. 1, at D_r = 90.79%.

Soil type	Preparation method	Specimen data			Permeameter equipment
Aalborg University	Tamped by punner	Length	[mm]	199	Cylinder B
Sand no. 1		Diameter	[mm]	70	Filterstone 25 μm
		Void ratio	[-]	0.577	Spring no. 3
		Saturation	[-]	1.03	

Test setup			
	Standpipe diameter, D	[mm]	40
	Initial hydraulic head, h_0	[mm]	200
	Intermediate hydraulic head, h_1	[mm]	1265
	Final hydraulic head, h_2	[mm]	800

Test	Unit	1	2	3	Results
Temperature, T_1	[°C]	23.9	23.9	23.9	⇓
Temperature, T_2	[°C]	23.5	23.6	23.6	23.8
Flowtime h_0 - h_1, t_1	$[s]$	436	427	422	424.5
Flowtime h_1 - h_2, t_2	$[s]$	436	428	423	425.5
Kinematic viscosity, ν_T	$10^{-6}[m^2/s]$				0.9190
Density of water, ρ_w	$[g/cm^3]$				0.997
Hydraulic conductivity, k_T	$10^{-4}[m/s]$				0.7040
Permeability, K	$10^{-12}[m^2]$				6.5904

Comments: Lower flowtime than registered at D_r = 87.48%.

Test ID	PermAAU1-91%a
Executed by	ÅS & LM
Evaluated by	ÅS & LM
Period	March 2012
Enclosure No.	8a

Permeabilitytest on Aalborg University Sand no. 1, at D_r = 90.79%.

Soil type	Preparation method	Specimen data			Permeameter equipment
Aalborg University Sand no. 1	Tamped by punner	Length	[mm]	199	Cylinder B
		Diameter	[mm]	70	Filterstone 25 μm
		Void ratio	[-]	0.577	Spring no. 3
		Saturation	[-]	1.03	

Test setup			
	Standpipe diameter, D	[mm]	20
	Initial hydraulic head, h_0	[mm]	200
	Intermediate hydraulic head, h_1	[mm]	1265
	Final hydraulic head, h_2	[mm]	800

Test	Unit	1	2	3	Results
Temperature, T_1	[°C]	24.3	24.3	24.3	⇓
Temperature, T_2	[°C]	23.8	24.0	24.1	24.2
Flowtime h_0 - h_1, t_1	$[s]$	102	101	101	101
Flowtime h_1 - h_2, t_2	$[s]$	101	101	101	101
Kinematic viscosity, ν_T	$10^{-6}[m^2/s]$				0.9909
Density of water, ρ_w	$[g/cm^3]$				0.997
Hydraulic conductivity, k_T	$10^{-4}[m/s]$				0.7406
Permeability, K	$10^{-12}[m^2]$				6.8655

Comments: Higher K than same sample with standpipe no. 4.

Test ID	PermAAU1-91%b
Executed by	ÅS & LM
Evaluated by	ÅS & LM
Period	March 2012
Enclosure No.	8b

Permeabilitytest on Aalborg University Sand no. 1, at D_r = 96.64%.

Soil type	Preparation method	Specimen data			Permeameter equipment
Aalborg University	Tamped by punner	Length	[mm]	199	Cylinder B
Sand no. 1		Diameter	[mm]	70	Filterstone 25 μm
		Void ratio	[-]	0.559	Spring no. 3
		Saturation	[-]	0.995	

Test setup	Standpipe diameter, D	[mm]	20
	Initial hydraulic head, h_0	[mm]	200
	Intermediate hydraulic head, h_1	[mm]	1265
	Final hydraulic head, h_2	[mm]	800

Test	Unit	1	2	3	Results
Temperature, T_1	[°C]	22.5	22.5	22.6	⇓
Temperature, T_2	[°C]	22.4	22.3	22.3	22.5
Flowtime h_0 - h_1, t_1	$[s]$	102	101	101	101
Flowtime h_1 - h_2, t_2	$[s]$	101	101	101	101
Kinematic viscosity, ν_T	$10^{-6}[m^2/s]$				0.9477
Density of water, ρ_w	$[g/cm^3]$				0.998
Hydraulic conductivity, k_T	$10^{-4}[m/s]$				0.5305
Permeability, K	$10^{-12}[m^2]$				5.1216

Comments: Some entrapped air close to the cylinder wall seen after saturation. Flushed out during the first test. Test only performed with standpipe no. 3, D = 20 mm.

Test ID	PermAAU1-97%
Executed by	ÅS & LM
Evaluated by	ÅS & LM
Period	March 2012
Enclosure No.	9

Permeabilitytest on Aalborg University Sand no. 1, at D_r = 97.68%.

Soil type	Preparation method	Specimen data			Permeameter equipment
Aalborg University Sand no. 1	Tamped by punner	Length	[mm]	199	Cylinder B
		Diameter	[mm]	70	Filterstone 25 μm
		Void ratio	[-]	0.556	Spring no. 3
		Saturation	[-]	1.03	

Test setup			
	Standpipe diameter, D	[mm]	40
	Initial hydraulic head, h_0	[mm]	200
	Intermediate hydraulic head, h_1	[mm]	1265
	Final hydraulic head, h_2	[mm]	800

Test	Unit	13	14	15	Results
Temperature, T_1	[°C]	23.5	23.7	23.9	⇓
Temperature, T_2	[°C]	23.3	23.4	23.5	23.6
Flowtime h_0 - h_1, t_1	$[s]$	485	484	483	483.5
Flowtime h_1 - h_2, t_2	$[s]$	484	483	482	482.5
Kinematic viscosity, ν_T	$10^{-6}[m^2/s]$				0.9216
Density of water, ρ_w	$[g/cm^3]$				0.997
Hydraulic conductivity, k_T	$10^{-4}[m/s]$				0.6195
Permeability, K	$10^{-12}[m^2]$				5.8162

Comments: Day one: Ran tests over and over again, 9 in total, with flowtime decreasing with approximately by 10 seconds for each test performed. Looked as if the sample had a hard time reaching complete saturation at such low void ratio. The specimen were left in the apparatus overnight. Testing proceeded the following day, where in total 6 tests were performed. After test no. 15 the flowtime were considered stable enough.

Test ID	PermAAU1-98%
Executed by	ÅS & LM
Evaluated by	ÅS & LM
Period	March 2012
Enclosure No.	10

G.3 Enclosures for Frederikshavn Sand 103-47

The following section contains enclosures 11 - 18, resulting in a total of 8 enclosures for the present sand. The permeability of the Frederikshavn sand is considerably higher than the Baskarp sand.

Permeability test on Frederikshavn sand 103-47, at D_r = 56.42%.

Soil type	Preparation method	Specimen data			Permeameter equipment
Frederikshavnsand 103-47	Tamped by punner	Length	[mm]	190	Cylinder B
		Diameter	[mm]	70	Filterstone 25 μm
		Void ratio	[-]	0.773	Spring no. 3
		Saturation	[-]	1.08	

Test setup			
	Standpipe diameter, D	[mm]	40
	Initial hydraulic head, h_0	[mm]	200
	Intermediate hydraulic head, h_1	[mm]	1265
	Final hydraulic head, h_2	[mm]	800

Test	Unit	1	2	3	Results
Temperature, T_1	[°C]	20.9	20.8	20.7	⇓
Temperature, T_2	[°C]	20.9	20.7	20.7	20.7
Flowtime h_0 - h_1, t_1	$[s]$	203	200	200	200
Flowtime h_1 - h_2, t_2	$[s]$	202	199	199	199
Kinematic viscosity, ν_T	$10^{-6}[m^2/s]$				0.9869
Density of water, ρ_w	$[g/cm^3]$				0.998
Hydraulic conductivity, k_T	$10^{-4}[m/s]$				1.4248
Permeability, K	$10^{-11}[m^2]$				14.325

Comments: Sample reduced volume after saturation. Gap between top filter and sand. Sample reduced height by 9 mm during test. Target D_r 30%, but ended up at 56% after sample height reduction. Got stable flowtimes, but do not completely trust the results.

Test ID	Permfred-56%
Executed by	ÅS & LM
Evaluated by	ÅS & LM
Period	March 2012
Enclosure No.	11

Permeability test on Frederikshavn sand 103-47, at D_r = 62.12%.

Soil type	Preparation method	Specimen data			Permeameter equipment
Frederikshavnsand	Tamped by punner	Length	[mm]	199	Cylinder B
103-47		Diameter	[mm]	70	Filterstone 25 μm
		Void ratio	[-]	0.753	Spring no. 3
		Saturation	[-]	1.00	

Test setup			
	Standpipe diameter, D	[mm]	40
	Initial hydraulic head, h_0	[mm]	200
	Intermediate hydraulic head, h_1	[mm]	1265
	Final hydraulic head, h_2	[mm]	800

Test	Unit	1	2	3	Results
Temperature, T_1	[°C]	21.7	21.7	21.6	⇓
Temperature, T_2	[°C]	21.7	21.6	21.6	21.6
Flowtime h_0 - h_1, t_1	$[s]$	237	232	233	232.5
Flowtime h_1 - h_2, t_2	$[s]$	236	231	232	231.5
Kinematic viscosity, ν_T	$10^{-6}[m^2/s]$				0.9663
Density of water, ρ_w	$[g/cm^3]$				0.998
Hydraulic conductivity, k_T	$10^{-4}[m/s]$				1.2896
Permeability, K	$10^{-12}[m^2]$				12.695

Comments:

Test ID	PermFred-62%
Executed by	ÅS & LM
Evaluated by	ÅS & LM
Period	March 2012
Enclosure No.	12

Permeability test on Frederikshavn sand 103-47, at D_r = 66.94%.

Soil type	Preparation method	Specimen data			Permeameter equipment
Frederikshavnsand 103-47	Tamped by punner	Length	[mm]	199	Cylinder B
		Diameter	[mm]	70	Filterstone 25 μm
		Void ratio	[-]	0.736	Spring no. 3
		Saturation	[-]	1.10	

Test setup			
	Standpipe diameter, D	[mm]	40
	Initial hydraulic head, h_0	[mm]	200
	Intermediate hydraulic head, h_1	[mm]	1265
	Final hydraulic head, h_2	[mm]	800

Test	Unit	1	2	3	Results
Temperature, T_1	[°C]	23.4	23.4	23.5	⇓
Temperature, T_2	[°C]	23.2	23.2	23.3	23.4
Flowtime h_0 - h_1, t_1	$[s]$	229	228	228	228
Flowtime h_1 - h_2, t_2	$[s]$	228	228	227	227.5
Kinematic viscosity, ν_T	$10^{-6}[m^2/s]$				0.9276
Density of water, ρ_w	$[g/cm^3]$				0.997
Hydraulic conductivity, k_T	$10^{-4}[m/s]$				1.3137
Permeability, K	$10^{-12}[m^2]$				12.414

Comments:

Test ID	PermFred-67%
Executed by	ÅS & LM
Evaluated by	ÅS & LM
Period	March 2012
Enclosure No.	13

Permeability test on Frederikshavn sand 103-47, at D_r = 71.78%.

Soil type	Preparation method	Specimen data			Permeameter equipment
Frederikshavnsand	Tamped by punner	Length	[mm]	199	Cylinder B
103-47		Diameter	[mm]	70	Filterstone 25 μm
		Void ratio	[-]	0.719	Spring no. 3
		Saturation	[-]	1.00	

Test setup			
	Standpipe diameter, D	[mm]	40
	Initial hydraulic head, h_0	[mm]	200
	Intermediate hydraulic head, h_1	[mm]	1265
	Final hydraulic head, h_2	[mm]	800

Test	Unit	1	2	3	Results
Temperature, T_1	[°C]	20.4	20.6	20.9	⇓
Temperature, T_2	[°C]	20.4	20.5	20.6	20.7
Flowtime h_0 - h_1, t_1	$[s]$	271	266	265	265.5
Flowtime h_1 - h_2, t_2	$[s]$	270	265	264	264.5
Kinematic viscosity, ν_T	$10^{-6}[m^2/s]$				0.9887
Density of water, ρ_w	$[g/cm^3]$				0.998
Hydraulic conductivity, k_T	$10^{-4}[m/s]$				1.1291
Permeability, K	$10^{-12}[m^2]$				11.372

Comments:

Test ID	PermFred-72%
Executed by	ÅS & LM
Evaluated by	ÅS & LM
Period	March 2012
Enclosure No.	14

Permeability test on Frederikshavn sand 103-47, at D_r = 79.80%.

Soil type	Preparation method	Specimen data			Permeameter equipment
Frederikshavnsand 103-47	Tamped by punner	Length	[mm]	199	Cylinder B
		Diameter	[mm]	70	Filterstone 25 μm
		Void ratio	[-]	0.691	Spring no. 3
		Saturation	[-]	0.98	

Test setup			
	Standpipe diameter, D	[mm]	40
	Initial hydraulic head, h_0	[mm]	200
	Intermediate hydraulic head, h_1	[mm]	1265
	Final hydraulic head, h_2	[mm]	800

Test	Unit	1	2	3	4	Results
Temperature, T_1	[°C]	21.8	21.9	22.1	22.3	⇓
Temperature, T_2	[°C]	21.3	21.6	21.8	22.0	22.1
Flowtime h_0 - h_1, t_1	$[s]$	286	282	281	281	281
Flowtime h_1 - h_2, t_2	$[s]$	282	281	279	279	279
Kinematic viscosity, ν_T	$10^{-6}[m^2/s]$					0.9558
Density of water, ρ_w	$[g/cm^3]$					0.998
Hydraulic conductivity, k_T	$10^{-4}[m/s]$					1.0686
Permeability, K	$10^{-12}[m^2]$					10.405

Comments:

Test ID	PermFred-80%
Executed by	ÅS & LM
Evaluated by	ÅS & LM
Period	March 2012
Enclosure No.	15

Permeability test on Frederikshavn sand 103-47, at D_r = 85.78%.

Soil type	Preparation method	Specimen data			Permeameter equipment
Frederikshavnsand	Tamped by punner	Length	[mm]	199	Cylinder B
103-47		Diameter	[mm]	70	Filterstone 25 μm
		Void ratio	[-]	0.670	Spring no. 3
		Saturation	[-]	1.00	

Test setup			
	Standpipe diameter, D	[mm]	40
	Initial hydraulic head, h_0	[mm]	200
	Intermediate hydraulic head, h_1	[mm]	1265
	Final hydraulic head, h_2	[mm]	800

Test	Unit	1	2	3	Results
Temperature, T_1	[°C]	21.7	21.7	21.8	⇓
Temperature, T_2	[°C]	21.4	21.4	21.5	21.6
Flowtime h_0 - h_1, t_1	$[s]$	331	329	329	329
Flowtime h_1 - h_2, t_2	$[s]$	329	328	327	327.5
Kinematic viscosity, ν_T	$10^{-6}[m^2/s]$				0.9663
Density of water, ρ_w	$[g/cm^3]$				0.998
Hydraulic conductivity, k_T	$10^{-4}[m/s]$				0.9115
Permeability, K	$10^{-12}[m^2]$				8.9730

Comments:

Test ID	PermFred-86%
Executed by	ÅS & LM
Evaluated by	ÅS & LM
Period	March 2012
Enclosure No.	16

Permeability test on Frederikshavn sand 103-47, at D_r = 91.76%.

Soil type	Preparation method	Specimen data			Permeameter equipment
Frederikshavnsand 103-47	Tamped by punner	Length	[mm]	199	Cylinder B
		Diameter	[mm]	70	Filterstone 25 μm
		Void ratio	[-]	0.650	Spring no. 3
		Saturation	[-]	1.00	

Test setup			
	Standpipe diameter, D	[mm]	40
	Initial hydraulic head, h_0	[mm]	200
	Intermediate hydraulic head, h_1	[mm]	1265
	Final hydraulic head, h_2	[mm]	800

Test	Unit	1	2	3	4	Results
Temperature, T_1	[°C]	21.3	21.4	21.5	21.6	⇓
Temperature, T_2	[°C]	21.0	21.2	21.3	21.4	21.5
Flowtime h_0 - h_1, t_1	$[s]$	359	349	348	347	347.5
Flowtime h_1 - h_2, t_2	$[s]$	355	347	346	345	345.5
Kinematic viscosity, ν_T	$10^{-6}[m^2/s]$					0.9699
Density of water, ρ_w	$[g/cm^3]$					0.998
Hydraulic conductivity, k_T	$10^{-4}[m/s]$					0.8635
Permeability, K	$10^{-12}[m^2]$					8.5315

Comments:

Test ID	PermFred-92%
Executed by	ÅS & LM
Evaluated by	ÅS & LM
Period	March 2012
Enclosure No.	17

Permeability test on Frederikshavn sand 103-47, at D_r = 101.47%.

Soil type	Preparation method	Specimen data			Permeameter equipment
Frederikshavnsand	Tamped by punner	Length	[mm]	199	Cylinder B
103-47		Diameter	[mm]	70	Filterstone 25 μm
		Void ratio	[-]	0.616	Spring no. 3
		Saturation	[-]	1.02	

Test setup			
	Standpipe diameter, D	[mm]	40
	Initial hydraulic head, h_0	[mm]	200
	Intermediate hydraulic head, h_1	[mm]	1265
	Final hydraulic head, h_2	[mm]	800

Test	Unit	1	2	3	Results
Temperature, T_1	[°C]	22.6	22.6	22.7	⇓
Temperature, T_2	[°C]	22.2	22.3	22.4	22.5
Flowtime h_0 - h_1, t_1	$[s]$	414	408	407	407.5
Flowtime h_1 - h_2, t_2	$[s]$	412	408	407	407.5
Kinematic viscosity, ν_T	$10^{-6}[m^2/s]$				0.9461
Density of water, ρ_w	$[g/cm^3]$				0.998
Hydraulic conductivity, k_T	$10^{-4}[m/s]$				0.7342
Permeability, K	$10^{-12}[m^2]$				7.0764

Comments: Ended up with a e that is higher than e_{min}, after severe tamping of specimen.

Test ID	PermFred-101%
Executed by	ÅS & LM
Evaluated by	ÅS & LM
Period	March 2012
Enclosure No.	18

Bibliography

Byrne and Houlsby, **2003**. B.W. Byrne and G.T. Houlsby. *Foundations for Offshore Wind Turbines*. Philosophical Transactions of the Royal Society, 10.1098/rsta.2003.1286, 2909–2930, 2003.

EWEA, **2010**. EWEA. *Wind Energy Factsheets*. The European Wind Energy Association, 2010.

Fisker and Kromann, **2004**. L.B. Fisker and K. Kromann. *Cyklisk Belastning af Boettefundament i Tryktank*. Speciale ved AAU, 2004.

Houlsby and Byrne, **2005a**. G.T. Houlsby and B.W. Byrne. *Design procedures for installation of suction caisson in sand*. ICE 158, Paper 13818, 135–144, 2005.

Houlsby and Byrne, **2005b**. G.T. Houlsby and B.W. Byrne. *Design procedures for installation of suction caisson in clay and other materials*. ICE 158, Paper 13817, 75–82, 2005.

Houlsby, Ibsen, and Byrne, **2005**. G.T. Houlsby, L.B. Ibsen, and B.W. Byrne. *Suction caissons for wind turbines*. Frontiers in Offshore Geotechnics: ISFOG 2005, Taylor & and Francis Group, London, ISBN 978-0-415-58480-7, 75–93, 2005.

Ibsen and Lade, **1998**. L.B. Ibsen and P.V. Lade. *The Strength and Deformation Characteristics of Sand Beneath Vertical Breakwaters Subjected to Wave Loading*. AAU Geotechnical Engineering Papers, Soil Mechanics Paper No 23(ISSN 1398-6465 R 9805), 1998.

Ibsen and Thilsted, **2011**. L.B. Ibsen and C.L. Thilsted. *Numerical study of piping limits for suction installation of offshore skirted foundations and anchors in layered sand*. Frontiers in Offshore Geotechnics II, ISBN 978-0-415-58480-7, 421–426, 2011.

Ibsen, Liingaard, and Nielsen, **2005**. L.B. Ibsen, M. Liingaard, and S.A. Nielsen. *Bucket Foundations, a status*. Conference Proceedings Copenhagen Offshore Wind 2005, 2005.

Ibsen, Hanson, Hjort, and Thaarup, **2009**. L.B. Ibsen, M. Hanson, T. Hjort, and M. Thaarup. *MC - Parameter Calibration for Baskarp Sand No. 15*, 2009.

J.R Hedegaard, **1993**. M.B. Jensen J.R Hedegaard. *Klassifikationsforsoeg med Baskarp-sand No 15*, 1993.

Krohn, Morthorst, and Awerbuch, **2009**. S. Krohn, P.E. Morthorst, and s. Awerbuch. *The Economics of Wind Energy*. EWEA, 2009.

Lesny, **2010**. K. Lesny. *Foundations for Offshore Wind Turbines*. ISBN 978-3-86797-042-6, Tools for Planning and Design. VGE Verlag GmbH, 2010.

Pedersen and Kristensen, **2007**. T.S. Pedersen and L.K. Kristensen. *Bøttefundamenters styrke og deformationsegenskaber ved cyclisk belastning*. Speciale ved AAU, 2007.

Randolph and Gouvernec, **2011**. M. Randolph and S. Gouvernec. *Offshore Geotechnical Enigineering*. ISBN 978-0-415-47744-4. Spoon Press, 2011.

Sawin, Martinot, and Adib, **2011**. J.L. Sawin, E. Martinot, and R. Adib. *Renewables 2011, Global Status Report*. Renewable Energy Policy Network for the 21th Century, 2011.

Wilkes, Moccia, and Dragan, **2012**. J. Wilkes, J. Moccia, and M. Dragan. *Wind in Power, 2011 European statistics*. The European Wind Energy Association, 2012.

W.P. Lund, **1998**. K.P. Jakobsen W.P. Lund. *Permeability Test on Silkeborg Sand No. 0000*, 1998.

www.hornsrev.dk. www.hornsrev.dk. *Newsletter on the Horns Rev Project*. URL: `http://www.hornsrev.dk/Engelsk/nyheder/nyh_nov_02/uk-nov_02.htm`.